ANKARA YILDIRIM BEYAZIT UNIVERSITY

GRADUATE SCHOOL OF NATURAL AND APPLIED SCIENCES



EFFECT OF GRAPHENE ADDITION AND HEAT TREATMENT ON MICROSTRUCTURE AND TRIBOLOGICAL PROPERTIES OF NI-P ELECTROLESS COATING

M.Sc. Thesis by

Hatice GÜNDÜZ

Department of Mechanical Engineering

January 2022

ANKARA

EFFECTS OF GRAPHENE ADDITION AND HEAT TREATMENT ON MICROSTRUCTURE AND TRIBOLOGICAL PROPERTIES OF NI-P ELECTROLESS COATING

A Thesis Submitted to

The Graduate School of Natural and Applied Sciences of

Ankara Yıldırım Beyazıt University

In Partial Fulfillment of the Requirements for the Degree of Master of Science in Mechanical Engineering, Department of Mechanical Engineering

by

Hatice GÜNDÜZ

January, 2022

ANKARA

M. Sc. THESIS EXAMINATION RESULT FORM

We have read the thesis entitled "**EFFECTS OF GRAPHENE ADDITION AND HEAT TREATMENT ON MICROSTRUCTURE AND TRIBOLOGICAL PROPERTIES OF NI-P ELECTROLESS COATING"** completed by **HATİCE GÜNDÜZ** under the supervision of **PROF. DR. FAHRETTİN ÖZTÜRK** and we certify that in our opinion it is fully adequate, in scope and in quality, as a thesis for degree of Master Science.

Prof. Dr. Fahrettin ÖZTÜRK

Supervisor

Assoc. Prof. Elmas SALAMCI

Jury Member

Ass. Prof. Yasin SARIKAVAK

Jury Member

Prof. Dr. Sadettin ORHAN

Director

Graduate School of Natural and Applied Sciences

ETHICAL DECLARATION

I hereby declare that, in this thesis which has been prepared in accordance with the Thesis Writing Manual of Graduate School of Natural and Applied Science,

- All data, information and documents are obtained in framework of academic and ethical rules,
- All information, documents and assessments are presented in accordance with scientific ethics and morals.
- All the materials that have been utilized are fully cited and referenced,
- No change has been made on the utilized materials,
- All the works presented original, and in any contrary case of above statements, I accept to renounce all my legal rights.

Date: **Signature:**

28/01/2022 **Name & Surname: Hatice GÜNDÜZ**

ACKNOWLEDGMENTS

I would like to thank my thesis advisor Prof. Dr. Fahrettin ÖZTÜRK, who has guided me throughout my graduate education with his invaluable knowledge and experience. I would also like to express my gratitude to my co-advisor Assoc. Prof. Ramazan KARSLIOĞLU, for he has always been supportive throughout my thesis work.

I would like to thank the thesis defense jury members Assoc. Prof. Elmas Salamcı and Ass. Prof. Yasin Sarıkavak for their valuable advice and guidance.

I would like to extend my thanks to Research Assistant Aysun Güven, who shared all her knowledge with me during my studies and provided me with psychological academic support.

I would like to thank AYBU Scientific Research and Projects Unit for its financial contribution to project number FYL-2021-2229.

I would especially like to express my gratitude to my sisters, my brother, and my friends for their support, even though I neglected them throughout my graduate study.

Most importantly, I owe a debt of gratitude to my parents Halime and Selami Gündüz, who have always been by my side since the day I was born, who have never spared their love and support. Thank you both for giving me the strength to follow my dreams. I am so lucky to have them.

2022, 28 January **Hatice GÜNDÜZ**

EFFECTS OF GRAPHENE ADDITION AND HEAT TREATMENT ON MICROSTRUCTURE AND TRIBOLOGICAL PROPERTIES OF NI-P ELECTROLESS COATING

ABSTRACT

Titanium and its alloys are widely used in many industries, especially in aerospace, because it combines features such as high strength, considerable corrosion resistance, and low density. Despite these important properties, the low wear resistance of titanium and its alloys is undesirable for engineering applications, so various surface enhancement methods are used to improve the weak tribological properties of titanium. In this study, nanoparticle reinforced graphene-nickel-phosphorous (Gr-Ni-P) coatings are produced by electroless coating technique. The purpose of this study is to investigate the effects of the Gr-Ni-P coating on the tribological properties of titanium alloy. In addition, the effect of heat treatment on microstructure and tribological properties is investigated. Microstructural properties are analyzed with Scanning Electron Microscope (SEM), X-Ray Diffractometer (XRD), X-Ray Photon Spectrometry (XPS), and Raman Spectroscopy. Tribological and mechanical properties are also investigated by a reciprocating ball on plate method and microhardness test device.

Results indicate that graphene addition and heat treatment significantly affect the performance of the coating and improve microstructure and tribological properties. The microhardness results are the highest for the coated sample with the heat-treated. It is also seen that the heat treatment has a positive effect on wear in both the coated and the uncoated samples. The dominant wear mechanism is adhesive and abrasive in uncoated samples, while delamination in coated samples.

Keywords: Graphene; nanocomposite; nickel matrix coatings; titanium coating; electroless nickel coating; Ni-P electroless coating.

GRAFEN İLAVESİ VE ISIL İŞLEMİNİN NI-P AKIMSIZ KAPLAMANIN MİKRO YAPISI VE TRİBOLOJİK ÖZELLİKLERİ ÜZERİNE ETKİSİ

ÖZ

Titanyum ve alaşımları, yüksek mukavemet, iyi korozyon direnci ve düşük yoğunluk gibi özellikleri bir araya getirdiği için, özellikle havacılık olmak üzere birçok endüstride yaygın olarak kullanılmaktadır. Bu iyi özelliklere rağmen, titanyum ve alaşımlarının düşük aşınma direnci mühendislik uygulamaları için istenmeyen bir durumdur. Titanyumun zayıf tribolojik özelliklerini iyileştirmek için birçok yüzey iyileştirme yöntemi kullanılmaktadır. Bu çalışmada, akımsız kaplama tekniği ile nano parçacık takviyeli grafen-nikel-fosfor (Gr-Ni-P) kaplamalar üretilmiştir. Bu çalışmanın amacı, Gr-Ni-P kaplamanın titanyum alaşımının tribolojik özellikleri üzerindeki etkilerini araştırmaktır. Ayrıca ısıl işlemin mikro yapı ve tribolojik özelliklere etkisi araştırılmıştır. Mikro yapısal özellikler Taramalı Elektron Mikroskobu (SEM), X-Işını Difraktometresi (XRD), X-Işını Foton Spektrometresi (XPS) ve Raman Spektroskopisi ile analiz edilmiştir. Tribolojik ve mekanik özellikler de plaka üzerinde pistonlu bilye yöntemi ve mikro sertlik test cihazı ile araştırılmıştır.

Sonuçlar, grafen ilavesinin ve ısıl işlemin kaplamanın performansını güçlü bir şekilde etkilediğini, mikro yapıyı ve tribolojik özellikleri iyileştirdiğini göstermektedir. Mikro sertlik sonuçları, ısıl işlemle kaplanmış numune için en yüksektir. Ayrıca ısıl işlemin hem kaplanmış hem de kaplanmamış numunelerde aşınma üzerinde olumlu etkisi olduğu görülmektedir. Kaplamasız numunelerde baskın aşınma mekanizması yapışkan ve aşındırıcı iken kaplanmış numunelerde delaminasyondur.

Anahtar Kelimeler: Grafen; nano kompozit, nikel matrisli kaplamalar; titanyum kaplama; akımsız nikel kaplama; Ni-P akımsız kaplama.

CONTENTS

M. Sc. THESIS EXAMINATION RESULT FORM ii
ETHICAL DECLARATION iii
ACKNOWLEDGMENTS iv
ABSTRACT v
ÖZ vi
NOMENCLATURE x
LIST OF TABLES xi
LIST OF FIGURES xii
CHAPTER 1 1
INTRODUCTION 1
CHAPTER 2 4
METAL MATRIX NANOCOMPOSITES 4
2.1. Metal Matrix Composites 4
2.1.1. Matrix Materials in Metal Matrix Composites 5
2.1.2. Reinforcing Materials in Metal Matrix Composites 6
2.1.3. Production of Metal Matrix Composites 6
2.2. Metal Matrix Nano Composite Materials 7
2.2.1. Powder Metallurgy 8
2.2.2. Thermal Spray 9
2.2.3. Cold Spray Forming 10
2.2.4. In Situ 11
2.2.5. Electroplating Process 12
2.2.5.1. Electrodeposition 12
2.2.5.2 Electroless Deposition 13
CHAPTER 3 14
ELECTROLESS NI-P NANOCOMPOSITE COATINGS 14
3.1 Electroless Nickel Coatings 14
3.1.1 Basic Components of Electroless Nickel Coating Bath 17
3.1.1.1. The Nickel Source 17
3.1.1.2. Reducing Agents 17
3.1.1.3. Complexing Agents 18
3.1.1.4. Stabilizers/Inhibitors 18

3.1.1.5. Energy 19
3.1.2 Main Categories of Electroless Nickel Plating 19
3.2 Electroless Nickel-Phosphorus Deposits 20
3.2.1. Effective Parameters for Electroless Ni-P Process 21
3.2.1.1. Effect of Temperature 21
3.2.1.2. Effect of Bath pH 22
3.2.1.3. Effect of Bath Composition 23
3.2.2. Properties of Electroless Ni-P Process 25
3.2.2.1 Hardness 26
3.2.2.2 Heat Treatment 27
3.2.2.3 Adhesion Properties 28
3.2.2.3 Tribological Behavior 29
3.2.2.3.1 Test Methods 29
3.2.2.3.1 Wear Resistance 30
3.3 Electroless Composite Coatings 32
3.3.1 History of Electroless Composite Coatings 32
3.3.2 Bath Composition 32
3.4 Graphene 34
3.4.1 Properties of Graphene 35
3.5 Titanium and Titanium Alloys 36
3.5.1 General Properties of Titanium 36
3.5.2. The Classification of Titanium Alloys 37
3.6 A Brief Review on Graphene Reinforced Nickel Matrix Composite Coatings 42
CHAPTER 4 47
EXPERIMENTAL METHOD 47
4.1. Preparation of the Experiment Setup 47
4.1.1. Preparation of Substrates 47
4.1.2 Preparation of Graphene-Reinforced Electroless Ni-P Coating Bath 50
4.2 Experimental Processes Applied to the Samples After Coating Process 50
4.2.1 Heat Treatment 50
4.2.2 Abrasion Test 51
4.3. Characterization of Coating Layer 53

4.3.1. Surface Preparation of Samples for Optical Microscope and SEM Analysis 53
4.3.2. Coating Thickness Analysis 54
4.3.3. Scanning Electron Microscopy (SEM) Analysis 54
4.3.4. X-Ray Diffractometer (XRD) Analysis 55
4.3.5. X-Ray Photoelectron Spectroscopy (XPS) Analysis 56
4.3.6 Raman Spectroscopy Analysis 56
4.3.7 Microhardness Analysis 57
CHAPTER 5 59
RESULTS AND DISCUSSION 59
5.1 Structural Analysis 60
5.1.1 SEM Analyses 60
5.1.2 XRD Results 65
5.1.3. Coating Thickness Results 67
5.1.4 XPS Results 69
5.1.5 Raman Spectrum of Composite Coating 71
5.2 Tribological Behavior of the Substrates 72
5.2.1 Microhardness Measurement Results 72
5.2.2 Wear Mechanisms 74
5.2.3 EDS Analysis of Wear Scratches 78
5.2.4 Wear Scratch Widths 83
5.2.5 Specific Wear Rates 84
CHAPTER 6 86
CONCLUSION 86
REFERENCES 88
CURRICULUM VITAE 100

NOMENCLATURE

Å: Angstrom

cm: Centimeter

EN: Electroless Nickel Coating

eV: Electron Volt

EDS: Energy-Dispersive X-Ray Spectroscopy

D: Dimension

g: Gram

Gr: Graphene

GNP: Graphene Nano Particle

Hz: Hertz

L: Liter

mm: Millimeter

min: Minute

MMC: Metal Matrix Composite

MMNC: Metal Matrix Nanocomposite

N: Newton

Ni-P: Nickel-Phosphorus

N-B: Nickel-Boron

SEM: Scanning Electron Microscope

XPS: X-Ray Photoelectron Spectroscopy

XRD: X-Ray Diffraction

°C: Celsius Degree

θ: Bragg Angle

Gr-Ni-P: Graphene-Nickel-Phosphorous

LIST OF TABLES

Table 2.1 Classification of composite materials [9] 4
Table 2.2 Commonly used matrix materials [8] 6
Table 3.1 Properties of electroless nickel plating [38] 15
Table 3.2 Popular reducing agents and remarks 17
Table 3.3 Bath components of electroless Ni-P [54] 21
Table 3.4 Coating properties according to phosphorus content [62] 26
Table 3.5 Electroless composite coating bath components and functions [65] 33
Table 3.6 Properties of graphene [75] 36
Table 3.7 Physical-mechanical properties and chemical contents of Ti-6Al-4V [85] 41
Table 4.1 Wear test parameters 52

LIST OF FIGURES

Figure 2.1 Production methods of MMNC [19] 8

Figure 2.2 Method and problems of powder metallurgy [22] 9

Figure 2.3 Thermal spray process and its problems [22] 10

Figure 2.4 Cold spray setup [25] 11

Figure 2.5 Electrodeposition setup [29] 12

Figure 3.1 Difference between electroless and electrodeposition [52]……..15

Figure 3.2 Primary uses for electroless nickel coatings [41] 16

Figure 3.3 Types of electroless nickel coatings [51] 20

Figure 3.4 Effect of temperature on deposition rate [57] 22

Figure 3.5 Effect of pH [57] 23

Figure 3.6 Effect of nickel chloride concentration on the deposition rate of electroless [60] 24

Figure 3.7 Dependence of deposition rate in an acetate-containing solution on the Ni_2^+/ H_2PO_2−ratio [60] 25

Figure 3.8 Hardness for different temperatures at 1h (wt. % P) I: 12%; II: 8.8%; III: 6.7%; IV:6,3% [66] 28

Figure 3.9 Common tribo-testing methods (a) Pin-on-disc, (b) Ball-on-plate, (c) Pin-on-plate, (d) Roller-on-plate [68] 30

Figure 3.10 Effect of P content on wear resistance [66] 31

Figure 3.11 Effect of heat treatment on the wear resistance [47] 31

Figure 3.12 Carbon allotropes [71] 34

Figure 3.13 Three-dimensional phase diagram to classify Ti alloys [76] 39

Figure 3.14 The microstructure of the synthesized Ni/graphene composites, a) SEM image of Ni-graphene sheet, b) EDS of marked region in image a, c) Higher magnification of Ni-P graphene sheets, d) EDS of marked region in image c. 43

Figure 3.15 Microstructure of coating, a) Nickel coating b) Graphene reinforced nickel plating 44

Figure 3.16 XRD patterns of Ni-P and G-NiP coating: a) Code posited, b) Heat-treated 45

Figure 4.1 Ti-6Al-4V substrate and microstructure of the substrate……...48

Figure 4.2 Surface preparation of substrate a) Cleaning, b) Soaking, and c) Zincating 49

Figure 4.3 Heat treatment of substrates 51

Figure 4.4 Device and schematic view of reciprocating wear mechanism [19] 52

Figure 4.5 a) Mounting device, **b)** Sanding device 53
Figure 4.6 Coating thickness measuring device 54
Figure 4.7 SEM device 55
Figure 4.8 Raman spectrometer device 57
Figure 4.9 Microhardness test device 58
Figure 5.1 SEM analysis of Ti-6Al-4V substrate 60
Figure 5.2 SEM analysis of Gr-Ni-P composite coating 61
Figure 5.3 SEM analysis of heat-treated Ti-6Al-4V substrate 62
Figure 5.4 SEM analysis of heat-treated composite 62
Figure 5.5 EDS analysis of a Ti-6Al-4V sample 63
Figure 5.6 EDS analysis of a heat-treated Ti-6Al-4V sample 64
Figure 5.7 EDS analysis of a composite coated sample 64
Figure 5.8 EDS analysis of a heat-treated composite sample 64
Figure 5.9 Ti-6Al-4V XRD patterns 66
Figure 5.10 Nanocomposite coating XRD patterns 66
Figure 5.11 A section of Ti-6Al-4V substrate 67
Figure 5.12 A section of Ni-P-Gr coating 67
Figure 5.13 Composite coating XPS 69
Figure 5.14 Composite coating wear scarf XPS 70
Figure 5.15 C1s and Ni 2p3/2 regions of high-resolution XPS spectra obtained with carbon and Ni in the Ni-graphene nanocomposite coating: a) C1s on surface b) C1s on scratch c) Ni2p on surface d) Ni2p on scratch. 70
Figure 5.16 Raman spectroscopy of composite coating: a) Coated surface b) Coated scratch c) Coated heat-treated surface d) Coated heat-treated scratch 71
Figure 5.17 Average microhardness values 73
Figure 5.18 Wear traces of Ti-6Al-4V substrates a) Non-heat-treated and b) Heat-treated. 75
Figure 5.19 Wear traces of composite coating substrates: a) Non-heat-treated and b) Heat-treated 76
Figure 5.20 High magnification SEM photograph of heat-treated composite wear mark 77
Figure 5.21 EDS mapping of a non-heat-treated Ti-6Al-4V sample 78
Figure 5.22 EDS mapping of a heat-treated Ti-6Al-4V sample 79
Figure 5.23 EDS mapping of a non-heat-treated composite sample 80
Figure 5.24 EDS mapping of a heat-treated composite sample 81

Figure 5.25 SEM morphologies of the wear tracks of substrates: a) Ti-6Al-4V b) Heat-treated Ti-6Al-4V c) Composite coating d) Heat-treated composite coating. 83

Figure 5.26 The wear scar generated by reciprocating sliding motion of the ball on a flat specimen; a) 2D view of the wear scar [116] b) 3D view of the wear scar [117]. 84

Figure 5.27 Specific wear rates 85

CHAPTER 1

INTRODUCTION

The materials community is endeavoring to produce materials with different mechanical, chemical, and physical properties to enhance the properties of the materials. However, it is quite difficult to meet all the requirements of industry. Therefore, many new processes have been explored.

Composite is a material formed by the combination of more than one natural or synthetic component. Metal matrix composites are materials that encompass many properties such as high elastic modulus, abrasion resistance, strength, and high temperature. They are widely produced and used in a variety of fields in recent years. These composites can be used at higher temperatures, having greater strength than the matrix metal and combining the high toughness properties of metals with the compressive and abrasion resistance properties of ceramics. Indeed, research has shown that 75% of machine damage is caused by wear on the rubbing surfaces [1]. Therefore, various metal matrix composite materials with high abrasion resistance have been produced to prolong the life of the parts. Particle-reinforced composites have superior isotropic, physical, and mechanical properties to fiber-reinforced composites. Particles, which are quite hard compared to the matrix metal, provide especially better wear properties to the composite they reinforce [1].

Nanostructured materials, which have proven to be superior to microstructure materials, can be 1D, 2D, 3D, or 4D in size and are characterized by an average grain size of 100 nm or less. The 2D nanomaterials can be used for electrical applications or coatings. Adding nanostructured reinforcement material to metal matrices improves the mechanical properties of the composite, making them suitable for high reliability and high-performance applications [2].

Nickel matrix composite materials are suitable to be used as solid lubricating materials because they have high wear resistance, strength, and hardness. Self-lubricating graphene nanoparticles are added to the coating to improve the mechanical properties of the nickel matrix. Graphene (Gr) is a reinforcing material consisting of a single layer of carbon, also defined as 2-dimensional (2D), and sp2 hybridized carbon structure. It attracts a lot of attention due to its basic properties and application areas. In fact, their extraordinary strength and lightness make nano-sized graphene particles a preferable material for ultra-high-strength nanocomposites. Since its discovery in 2004, graphene nanoparticles have proved an ideal alternative in many fields from nanoelectronics to sensors. Thanks to its honeycomb-shaped hexagonal structure, graphene is endowed with numerous strengths such as being atomically thin, inert, wear-resistant, impermeable, and mechanically durable [3]. The addition of graphene, which is considered the strongest and thinnest material, to various matrices is expected to increase the reliability and performance of the composite, thus the cost-effectiveness, compared to other reinforcement materials. Like graphite, graphene exhibits self-lubricating properties when reinforced into metal matrices for tribological applications. However, unlike graphite, graphene can provide solid lubricant properties and reduce wear regardless of the area in which the composite is used [4].

Titanium, on the other hand, has excellent mechanical and physical properties such as high strength, low weight, and remarkable corrosion resistance, so it is used in many industries, especially in aerospace. Still, titanium and its alloys are insufficient in environments with friction and wear. This material has weak tribological properties because of its electron arrangement, crystalline structure, and lack of lubricants [5], so several surface enhancement processes are applied to compensate for this weakness.

The purpose of this study, supported by the AYBU Scientific Research and Projects Unit with the project code FYL-2021-2229, was to investigate the effects of electroless Ni-P coating with graphene nanoparticle reinforcement on the weak tribological properties of titanium alloy. In addition, the effect of heat treatment on microstructure and tribological properties of the uncoated and the coated titanium alloys was investigated. It was found that graphene-reinforced Ni-P matrix nanocomposite coating could be successfully applied on titanium alloy substrate. Microstructural

properties of heat-treated and non-heat-treated, non-coated, and nanocomposite layers were also investigated by Scanning Electron Microscopy (SEM), X-Ray Diffractometer (XRD), X-Ray Photon Spectrometry (XPS), and Raman Spectroscopy. In addition, tribological and mechanical properties were analyzed by a reciprocating ball on plate testing and microhardness test device. It was concluded that graphene addition and heat treatment remarkably improved the microstructure and tribological properties.

CHAPTER 2

METAL MATRIX NANOCOMPOSITES

2.1. Metal Matrix Composites

Composite materials are materials produced by combining component materials with different properties and shapes to obtain entirely new properties [6]. They are generally produced by dispersing one or more discontinuous phases in a continuous phase. While the continuous phase is called the matrix, the discontinuous phase is generally called the reinforcing material named fiber because it has better properties than the continuous phase [7]. The matrix material functions to preserve the formal integrity of the material and to hold the reinforcements together. On the other hand, reinforcement materials are used to improve the desired properties of the matrix material [8].

Composite materials can meet the requirements of advanced technology as they have superior properties than each component used in their production and be widely used in different industries such as transportation, aerospace, defense, construction, and energy. They are classified according to reinforcement and matrix elements as indicated in Table 2.1 [9].

Table 2.1 Classification of composite materials [9]

Composite Materials	
Matrix Types	**Reinforcement Types**
Polymeric Matrix	Whisker-Reinforced
Ceramic Matrix	Fiber-Reinforced
Metal Matrix	Particle-Reinforced

Composite materials that use metal as a matrix material according to the area of the use are called Metal Matrix Composite (MMC). MMCs were first developed in the early 1960s upon discovery that they could be used at higher temperatures and provide greater specific strength than the materials in their composition. When compared with

the metal and monolithic materials they replace, the MMCs show superior properties such as usability at high temperature, high strength, low density, reproducibility, high thermal and electrical conductivity, high specific module, high specific strength, high elasticity modulus/density ratios, and low coefficient of thermal expansion [8].

Despite its superior properties, the metal matrix composites have some limitations. They have lower ductility, their production systems and equipment are more costly, and since they are newly developing materials, companies and manufacturers are less familiar about them [8].

2.1.1. Matrix Materials in Metal Matrix Composites

In composite materials, the matrix element should ideally have features such as lightness, corrosion resistance, fracture toughness, and compatibility with the reinforcement element. It should protect the reinforcement member against wear and corrosion while transferring the load to the reinforcement member. Indeed, matrices determine the compression, shear, creep, yield, dielectric, and thermomechanical properties of the composite material [10].

Matrix materials commonly used in composite structures are light metals and alloys with properties such as high strength, low density, favorable mechanical properties, and light weight. Another characteristic feature of such materials is their high corrosion resistance against the atmosphere. In this context, nickel (Ni), aluminum (Al), zinc (Zn), magnesium (Mg), titanium (Ti), copper (Cu) or alloys of these metals are used as matrix material in metal matrix composite structures [11]. Some mechanical properties of these commonly used matrix materials are given in Table 2.2.

Table 2.2 Commonly used matrix materials [8]

Metal	Yield Strength (MPa)	Specific Strength (Nm/kg)	Density (g/cm)
Nickel	148	16.6	8.9
Aluminum	30	11.1	2.7
Magnesium	69	39.6	1.74
Titanium	140	31	4.51
Copper	69	7.7	8.93

2.1.2. Reinforcing Materials in Metal Matrix Composites

Reinforcing materials in metal matrix composites have an important place in the formation of composites that have suitable mechanical properties for the areas of the use. While metal matrix composites are reinforced in two ways as continuous and discontinuous according to their application areas, they are classified further into four groups as *particles, continuous fibers, whiskers,* and *discontinuous fibers*. The most widely used form in industry is *particles* because it is more practical than long fibers and has a composite structure that does not change depending on the direction [12]. Depending on the desired property, reinforcement elements in different forms such as whisker, fiber or particle are used as reinforcement elements such as silicon carbide (SiC), titanium nitride (TiN), graphite, aluminum nitride (AlN), silicon nitride (Si_3N_4), boron carbide (B_4C), titanium diboride (TiB_2), graphene, aluminum oxide (Al_2O_3), and boron (B) [13-15].

2.1.3. Production of Metal Matrix Composites

The appropriate method of producing MMCs depends on what is expected of the composite material. Most importantly, to the following should be considered in the production of metal matrix composites [8]:

- Temperature range
- Possible chemical reactions between matrix-reinforcement
- Shape of reinforcement material
- Matrix-reinforcing material compatibility
- Dimensional properties required from the product

- Matrix-reinforcement additional processing requirement
- Matrix-reinforcement to ensure full interfacial bonding
- Metal matrix composites consisting of a metal matrix and a reinforcing material

2.2. Metal Matrix Nano Composite Materials

Nano technology aims to obtain large structures with renewed molecular structure by working at the molecular level. The properties of the materials vary along the macro and nano scales. Metal matrix nanocomposites are formed by dispersing particles of nano size in the metal matrix [16].

The reinforcement of nano sized particles into the matrix significantly improves the properties of the material, and the benefit is maximized if the nanoparticle is homogeneously dispersed in the matrix [17]. These nano composite coatings become useful in the developing technology with features such as wear resistance and high hardness [18].

To produce metal matrix nanocomposites (MMNC), ceramic second phase particles such as boride, carbide, oxide, and nitride are reinforced into matrix materials such as aluminum, nickel, copper, and titanium, thereby imparting improved mechanical properties to the matrix material. Metal matrix nanocomposites combine properties such as high strength of nanoparticles with the toughness and high ductility of metallic materials. They are produced by methods such as powder metallurgy, mechanical alloying, electrodeposition, and thermal spray [19], which are shown in Figure 2.1.

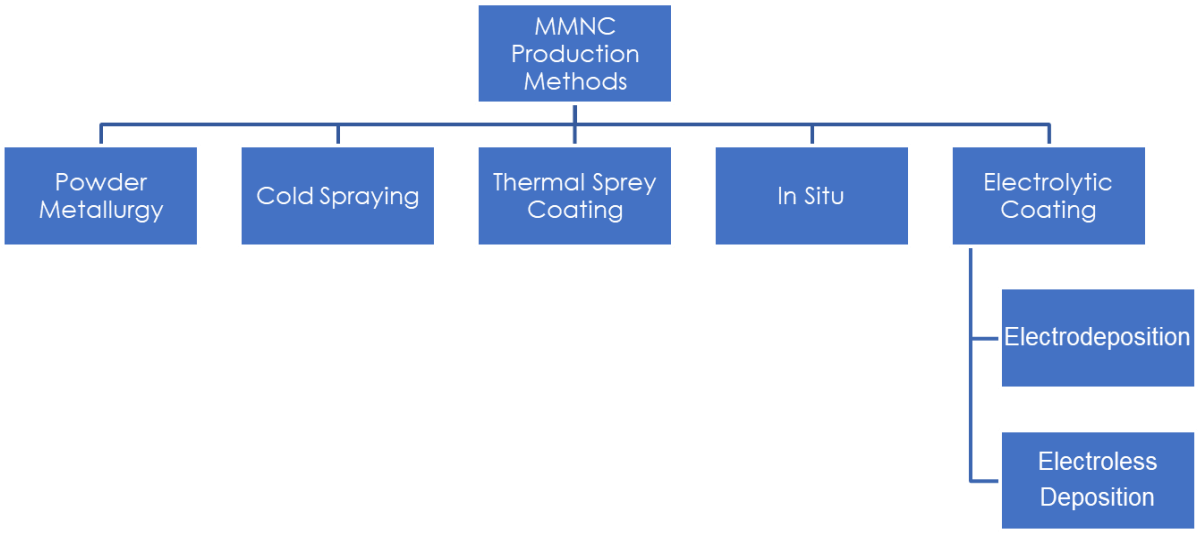


Figure 2.1 Production methods of MMNC [19]

2.2.1. Powder Metallurgy

Powder metallurgy is the most preferred metal matrix composite production as it ensures geometric stability during production. It follows the steps of powder preparation, cold molding, and sintering [20]. The powder metallurgy method uses graphene powder and metal matrix powder for the mixtures, which are then used for the consolidation process to produce composite material [21].

The powder metallurgy method generally consists of two simple and workable steps, powder mixing and sintering, so it is frequently used in the production of composite materials. The powder mixing step has an important effect on dispersion of graphene. Powder is generally mixed with ball milling method, which inflicts large deformation during the powder mixing process, repeated fracture, and welding intervention between the graphene and the metal matrix. This method causes fracture of graphene powders, aggravating the degree of defect and undermining the strengthening effect. The solvent mixing method, on the other hand, disperses the graphene homogeneously in the solvent under ultrasonic agitation using deionized water or organic solvents. Composite powder can be obtained by the freeze-drying method. However, this method causes poor bonding strength between graphene and metal, so graphene can easily Thus, composite materials produced in the powder metallurgy method

inevitably form macro-defects such as pores. These defects affect the thermal-electrical conductivity and strength of graphene-reinforced metal matrix composites. Figure 2.2 presents the powder metallurgy method and related problems [22].

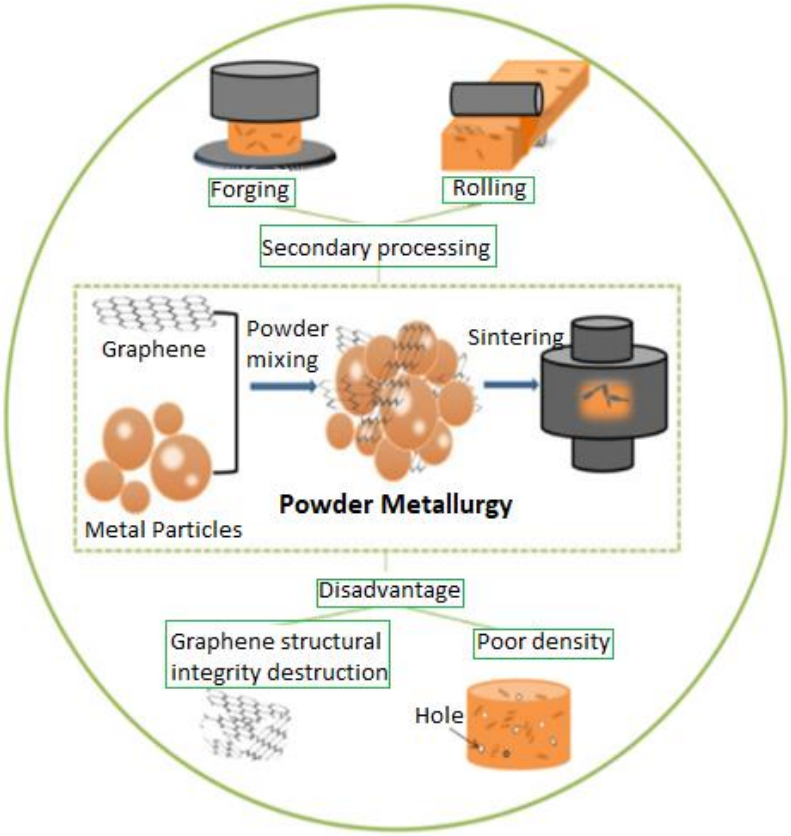


Figure 2.2 Method and problems of powder metallurgy [22]

2.2.2. Thermal Spray

Thermal spray (TS) is used to prepare surface coatings on industrial components such as anti-rust coatings in automotive and thermal barrier coating in aerospace [23]. In the TS process, the order of steps are as follows: droplet formation, droplet spraying, atomizing droplet deposition, and cooling on substrate. As seen in Figure 2.3, coating thickness and quality are greatly affected by discharge port size and the nozzle travel speed. The same figure shows the graphene reinforced metal matrix nanocomposites production process by the thermal spray method, wherein graphene nano-powders were melted in the combustion chamber and accelerated to high velocity and deposited on the substrate layer [22].

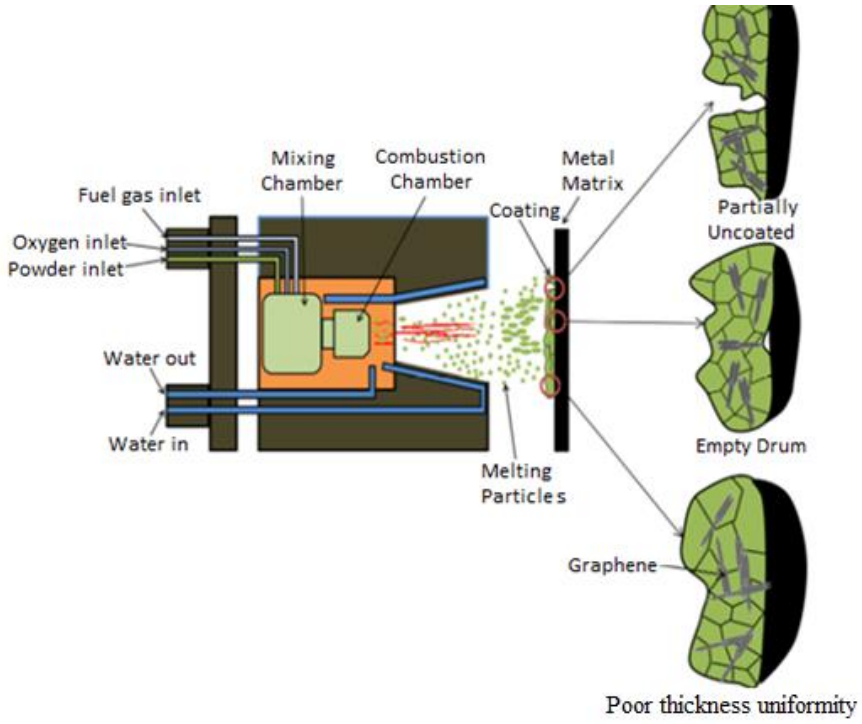


Figure 2.3 Thermal spray process and its problems [22]

2.2.3. Cold Spray Forming

Cold spray technology is a surface modification technology developed to increase the interaction between the substrate and the coating material. By means of the high-pressure air produces passing through the nozzle, the dust particles are escalated to subsonic velocities and are deposited by being crashed on the substrate. During the collision, the solid particles are plastically deformed and mechanically bonded to the substrate to form the coating. This method is used not only to create coatings, but also to obtain additive manufacturing producing metal matrix composites. Homogeneous distribution of reinforcement material depends on premixing. Strength, density, and activity characteristics of the MMC, or the coatings, depend on the materials. Yin et al. [24] homogeneously dispersed GNP/copper prepared by ball milling and produced graphene nano particle reinforced copper matrix composite coatings with lower friction coefficient by the cold spray method. However, due to the easy deformation of the solid particles during the cold spraying process, agglomeration of the

reinforcement materials occurred, and the material structures were damaged. The cold spray setup is shown in Figure 2.4.

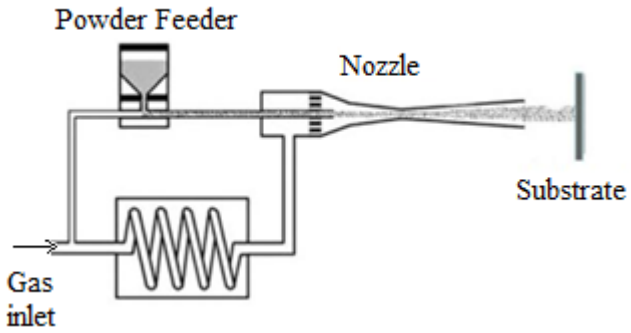


Figure 2.4 Cold spray setup [25]

2.2.4. In Situ

In situ MMNCs containing reinforcement phases synthesized in the metal matrix by elements or chemical reactions between elements and compounds during composite production have been developed. One reason to do so was to establish homogeneous dispersion of the reinforcement phase in the matrix to provide optimum mechanical properties. The advantages of metal matrix nanocomposites produced in situ over conventional MMC are as follows [26]:

(a) Thermodynamically stable formation of reinforcement phases in the matrix, which decreases the deterioration rate in high-temperature processes

(b) Clean reinforcement-matrix interface as a result of strong interfacial bonding

(c) More homogeneous and fine-dimensional reinforcement phases, which provide better mechanical properties

The great potential of in situ MMNCs for wide applications has resulted in the development of various production techniques over the past decade. Using these

methods, in situ nanocomposites can be produced in a wide range of matrices (e.g. titanium, aluminum, iron, nickel, and copper) and second phase particles (e.g. oxides, borides, nitrides, carbides).

2.2.5. Electroplating Process

2.2.5.1. Electrodeposition

Electrodeposition is the process of coating a thin layer of plating metal on the surface of different conductive materials by electrochemical reduction of plating metal ions from a solution containing an electrolyte. A typical setup for small scale electrodeposition is shown in Figure 2.5. Improving the properties of metal surfaces through the production of metallic nano crystalline coatings [27], this technology is used in many industries, including jewelry, automotive, household appliances, and aerospace. The methods of pulse current (PC), direct current (DC), and pulse-reverse current (PRC) have been used to make metallic coatings by electrodeposition method. Of them, PC and PRC methods have received more attention recently as mechanical properties and corrosion have been improved. In many studies, higher wear resistance and hardness have been obtained from the DC coatings with the PRC and the PC methods [28].

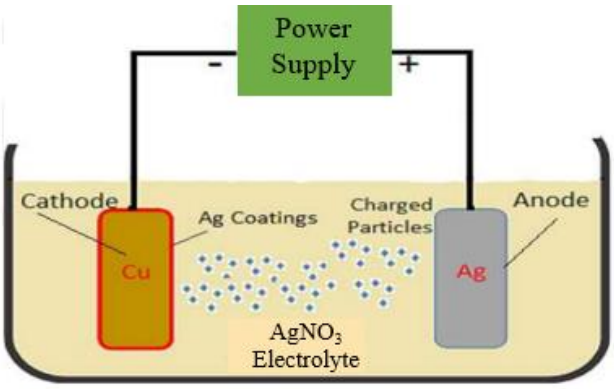


Figure 2.5 Electrodeposition setup [29]

2.2.5.2 Electroless Deposition

Electroless plating is a chemical reduction process based on the catalytic reduction of the metal cation in a chemical reduction medium. The metal deposition takes place without the need for an external electrical source. This is the main difference from the electrodeposition process, which requires electrical energy to reduce metal ions [30]. Various metals such as gold, palladium, nickel, copper, platinum, and alloys include one or more of these metals, which are effectively plated by this process. Electroless coating has high levels of wear resistance, electrical resistance, hardness, corrosion resistance, and low porosity with a uniform precipitation layer even for complex shapes and geometric parts. With these properties, electroless coating is suitable for many industrial applications [31].

CHAPTER 3

ELECTROLESS NI-P NANOCOMPOSITE COATINGS

3.1 Electroless Nickel Coatings

In the first half of the twentieth century, Brenner and Riddell [32] developed an unprecedented method of plating which is named by these scientists as electroless coating. Electroless coating, also known as chemical or autocatalytic coating, is a non-galvanic plating process that any need for external electrical current and involves a series of simultaneous reactions in an aqueous solution. The most common electroless plating method is electroless nickel plating [33].

Electroless nickel coatings are formed by reducing nickel ions to nickel-metal by means of reducers on conductive substrates which are immersed in a nickel-containing aqueous solution bath. Nickel, which reacts with the boron or phosphorus atom, forms an alloy. The reduction process continues onto nickel, which also has a catalytic effect. Hence, such coatings are also referred to as autocatalytic coatings in the literature. The electroless coating process taking place in the bath solution, the electroless coating process reaches a uniform coating deposit on all parts regardless of shape. Thanks to this important feature, homogeneous coating thickness is obtained on most complex parts [34,35]. Figure 3.1 shows the difference between electroless and electroplating coatings, clearly demonstrating the uniformity of electroless nickel plating.

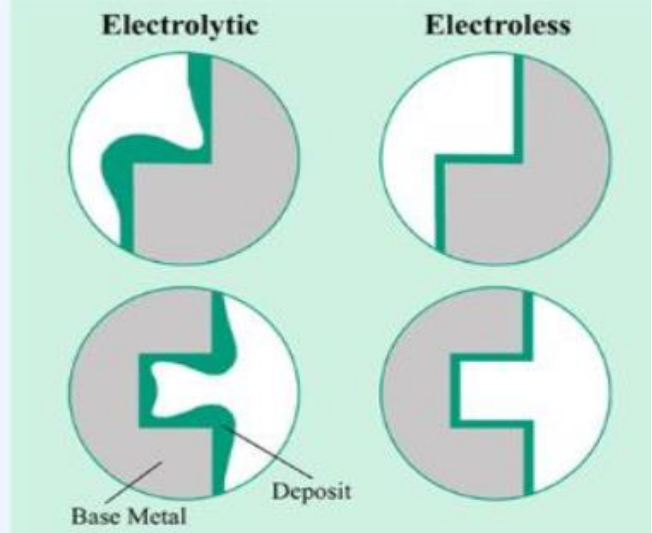


Figure 3.1 Difference between electroless and electrodeposition [52]

Electroless nickel coatings are suitable for hard chrome coating applications in industry with their high performance in terms of hardness, wear, and corrosion resistance. As chrome plating can harm the environment and human health, it makes sense to replace it by electroless nickel, which will not decrease the performance. When done so, the harmful effects are eliminated in the long run, and the effects of the change in this area are observed in various areas [36].

Electroless nickel coatings are preferred in many areas thanks to their high corrosion resistance, resistance to abrasion, lubricity, hardness, uniform coating thickness distribution, and solderability [37]. The properties and benefits of electroless nickel coatings are presented in the Table 3.1.

Table 3.1 Properties of electroless nickel plating [38]

Feature	Benefit
High hardness	Low wear characteristics
Excellent corrosion resistance	Good coating durability
Homogenous thickness	Elimination of post plate finish
Availability of low friction co-deposits	Self-lubricating coating
Remarkable chemical resistance	Protective coating function
Solderability/braze ability/weldability	Functionality in many applications

With their superior properties, electroless nickel coatings are used in a wide range of fields, and their application range is expanding every day. They are currently used in aerospace, automotive, chemistry, defense, medical, and dental industries, as well as in places where good resistance to abrasion and corrosion is desired [39]. Their primary use is shown in the Figure 3.2. Electroless coatings can be obtained on magnesium, cast iron, steel, aluminum, brass, bronze, titanium, and insulating materials (ceramics and plastics) [35,40].

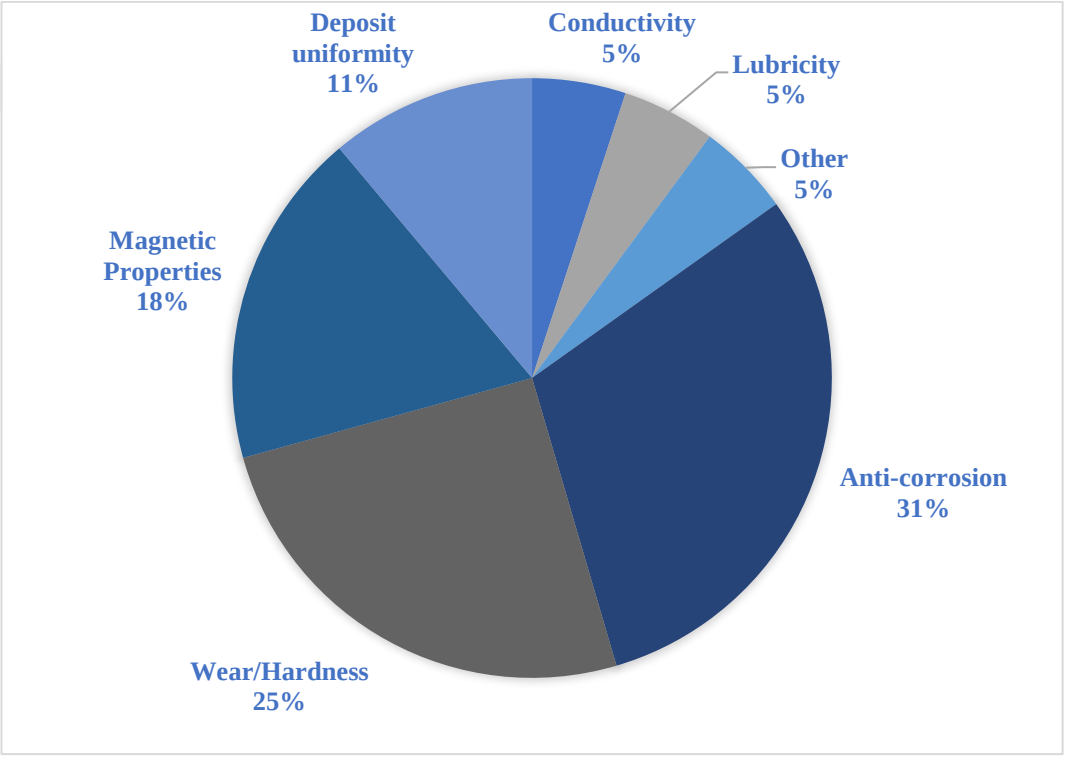


Figure 3.2 Primary uses for electroless nickel coatings [41]

Despite all these superior properties, electroless nickel coatings have various limitations such as brittleness, low coating speed, high chemical cost, pre-treatment requirement for some materials, and low weldability [42].

3.1.1 Basic Components of Electroless Nickel Coating Bath

At present, the most common catalytic plating method used is unquestionably electroless nickel plating. The major cause of its prevalent industrial and commercial use is the unique properties of EN deposits. The physical and chemical characteristics of an EN coating depend on its composition, which is related to the formulation and operating conditions of the aqueous solutions of the electroless nickel bath. The components that constitute electroless nickel bath are the nickel sources, reducing agents, complexing agents, stabilizers/inhibitors, and energy [43].

3.1.1.1. The Nickel Source

Soluble metal salts are used as the nickel ion source in solution in the electroless nickel plating process. Among them, which have different solubility, purity, and compatibility characteristics, the most common metal salt is nickel sulphate, which is preferred especially in corrosion resistant applications. The main metal salts used are nickel sulphate ($NiSO_4$), nickel acetate ($Ni(CH_3CO_2)_2$), nickel chloride ($NiCl_2$), nickel hypophosphite, and nickel sulfamate [43, 44].

3.1.1.2. Reducing Agents

In electroless plating baths, reducing agents are the most important substances besides the compounds used as the nickel ion source. The main task of reducers is to obtain nickel by reacting with ion sources. Reducers affect the chemical properties of the baths, the type of alloy to be used, and the chemical composition of the baths. The most popular reducing agents are presented in the Table 3.2 by deposit type and remarks [34, 45].

Table 3.2 Popular reducing agents and remarks

Deposit	Reducing agent	Remarks
Ni-P	Sodium hypophosphite (NaH_2PO_2)	Acid or alkaline bath (2-17 % P)
Ni-B	Sodium borohydride ($NaBH_4$) Amino borane (DMAB)	Acid or alkaline bath Alkaline bath (0.5-10 & B)
Pure Ni	Hydrazine (NH_2NH2)	Alkaline bath

3.1.1.3. Complexing Agents

During the electroless plating process, the dissolved nickel ions interact with water, and these ions make weak bonds. Such complex nickel ions, called free nickel ions, can precipitate in the bath solution, directly affecting the chemical balance of the solution and the coating quality. Sometimes, it even causes the plating solution to decompose and become unusable. In this case, complex formers, usually consisting of organic acids and their salts, are added to the bath solution to control the amount of free nickel and stabilize the bath [45].

Plating properties such as nickel-plating speed, internal stress, and phosphorus/boron content are affected by complex formers. Complexing agents have a low stability constant and increase the coating speed in the application. At the same time, these substances, which act as a buffer, prevent sudden pH drops caused by hydrogen ions released during the reduction process [43, 46]. Major complexing agents are acetate (CH_3COOH), ethylenediamine ($H_2NCH_2\,CH_2NH_2$), amino acetate (NH_2CH_2COOH), succinate ($HOOCCH_2\;CH_2COOH$), citrate ($HOOCCH_2\;(OH)C(COOH)COOH$), hydroxy acetate ($HOCH_2\;COOH$), pyrophosphate ($H_2O_3POPO_3H_2$), and malate ($HOOCCH_2\,CH(OH)COOH$) [46].

3.1.1.4. Stabilizers/Inhibitors

Electroless nickel plating bath may become unstable due to factors such as high concentration of the reducer and the consequent formation of a reducer-intense region in the bath, the local overheating of the bath, and the catalytic effect on the surface of the dust in the system. To eliminate these problems and minimize the risk, additives called inhibitors/stabilizers should be added to the electroless coating bath although the bath is well controlled and regular filtration and mixing is applied.

Three different types of inhibitors, namely sulfur compounds, oxyanions, and heavy metal ions, are used in electroless plating baths containing hypophosphite; organic sulfur compounds and metal inhibitors are used in boron hydride and amine boron baths. The use of stabilizer has the advantage of increasing coating speed and

brightness, yet the disadvantage of decreasing ductility, causing internal stress, and increasing porosity [43, 47].

3.1.1.5. Energy

Energy is required for catalytic reactions to take place, and for electroless nickel plating, this energy is supplied with the help of heat. Energy or heat, which is the most important parameter for coating to occur in an electroless coating solution, influences bath kinetics and coating speed. The indicator of the energy for the plating bath is temperature. In electroless nickel plating bath solutions, decomposition of the bath solution is likely to occur at temperatures above 100 °C, while the coating rate below 65 °C is very low [43].

3.1.2 Main Categories of Electroless Nickel Plating

Electroless nickel plating can be categorized into three main groups: alloy, composite, and metallic.

Alloy Coatings: Electroless alloy plating refers to the deposition of metal alloys on the studied substrate. The deposited alloy plating relies on the reducing agent. To produce ternary (e.g. Ni-P-B, Ni-W-P, Ni-Co-P) or quaternary (Ni–W–Cu–P) alloy coatings, metallic is added into the electroless bath. This coating process serves to manufacture stable and homogeneous plating for different industrial applications. The rapid deposition rate and manufacture quality in a substantial operation period at significantly low operating overheads are some major reasons why this method is applied [48]. Electroless depositions are oxidation-reduction reactions with the important reductant and oxidizer components in the bath solution [49].

Composite Coatings: When composite materials co-deposit in the alloy coating, the coating is called electroless composite plating. This type of coating is prepared with solid particles along with a normal electroless nickel plating bath so that the solid particles and nickel-P or nickel-B matrix constitute co-deposition. Electroless composite coatings have recently gained extensive acceptance in the preparation of this coating type. The most widely used solid particles are ZrO_2, SiC, C, PTFE, and Al_2O_3 [50].

Metallic Coatings: In optimal conditions, pure nickel coatings (electroless metallic coating) are a practicable alternative to electroplating as a hard-coating method. Its hardness, wear resistance, low friction, and corrosion properties allow for various applications. These types of electroless coatings are shown in Figure 3.3 [51].

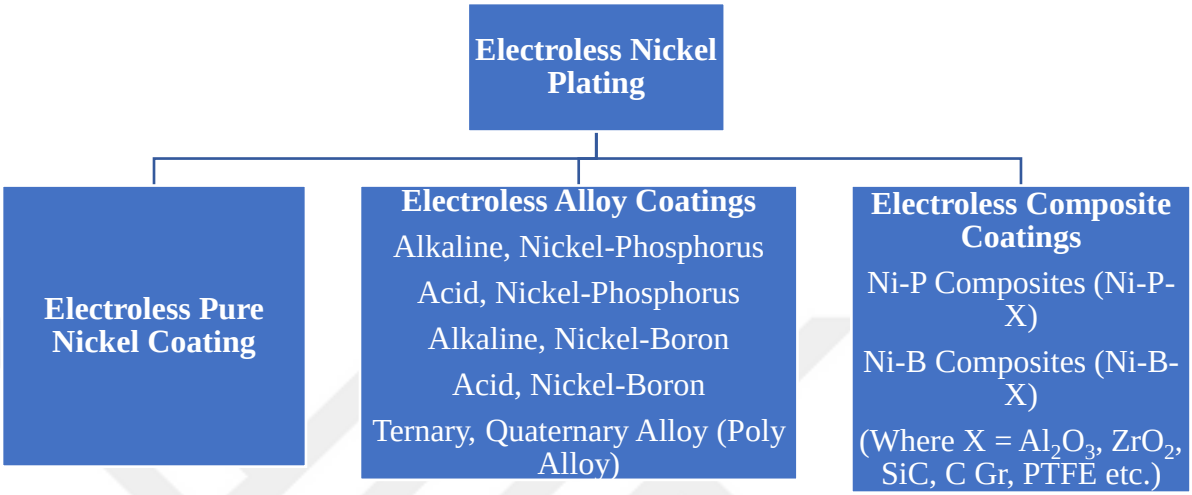


Figure 3.3 Types of electroless nickel coatings [51]

3.2 Electroless Nickel-Phosphorus Deposits

Electroless nickel-phosphorus plating is a coating containing phosphorus by 1-13%. The phosphorus content has a role in determining the coating properties. Indeed, the chemical and physical properties of the coating vary depending on the phosphorus content. For this reason, nickel-phosphorus coatings are divided into three groups according to the amount of phosphorus: low, medium, and high phosphorus coatings [53].

The properties of the coating obtained are influenced by the content of the bath and working conditions. Actually, electroless nickel-phosphorus coatings are largely dependent on bath components. Bath composition significantly affects the coating speed and deposit properties. The main materials found in the electroless Ni-P bath and their functions are summarized in Table 3.3 below.

Table 3.3 Bath components of electroless Ni-P [54]

Component	Functions	Examples
Metal ions	Source of metal	Nickel chloride, nickel acetates, nickel sulfate
Hypophosphite ions	Reducing agent	Sodium hypophosphite
Complexings	Form Ni complexes, prevent excess free Ni ion concentration, stabilize and prevent Ni phosphate precipitation, act as pH buffers	Monocarboxylic acids, hydrocarboxylic acids, dicarboxylic acids, ammonia, alkanolamines
Accelerators (exultants)	Active reducing agent and accelerator of deposition	Anions of some mono-and dicarboxylic acids, borates, fluorides
Buffers	For long-term pH control	Sodium salt of certain complexings, depending on pH range used
Stabilizers	Prevent solution breakdown by shielding catalytically active nuclei	Pb, As, Sn, Mo, Th or Cd ions, thiourea, etc.
pH regulators	Subsequent pH adjustment	Sulfuric and hydrochloric acids, soda, ammonia, caustic soda
Wetting agents	Increase wettability of surfaces to be coated	Ionic and nonionic surfactants

3.2.1. Effective Parameters for Electroless Ni-P Process

There are various effective parameters such as pH, temperature, nickel, and hypophosphite concentration. Additionally, the proportion of complexing agents which form in the electroless plating bath, can affect the microstructure, surface morphology, and deposition rate. Pre-treatment of the surface of the substrate material is as important as other parameters since the detraction of foreign contaminants like dust, oxides, and corrosion products is essential to obtain strong adhesion between coating and substrate. The eventual appearance of plating can be affected by mechanical defects and roughness of the substrate [55].

3.2.1.1. Effect of Temperature

The rate of deposition is influenced by an important parameter: bath temperature. The redox reactions which take place in the entire reaction require an external energy.

Indeed, the necessity of heat is valid for every type of bath. As the temperature increases, so does the deposition rate of coating, inasmuch as the entire reaction in the solutions is endothermic. The plating process in the bath solution with hypophosphite is carried out at 60-95°C. As shown in Figure 3.4, regardless of the bath alkalinity or acidity, an exponential relation exists between the deposition rate and the temperature. Acidic baths are carried out at 80°- 90°C whilst alkaline ones at lower temperatures, so when plastic is used as substrate, alkaline baths are preferred [56].

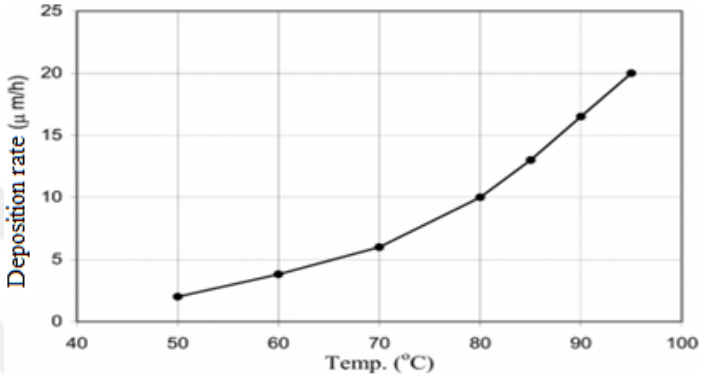


Figure 3.4 Effect of temperature on deposition rate [57]

3.2.1.2. Effect of Bath pH

In the electroless nickel platings, the pH of the bath is a critical parameter. When the pH of the bath solution increases, the nickel reduction accelerates. On the other hand, this increment delays the self-reduction of P from hypophosphite because of the hydroxide ions generated. For this reason, baths including high pH possess low phosphorus amounts. Nevertheless, because the deposition rate is preponderantly controlled by the nickel reduction reaction, ascending of the pH leads to ascending of the deposition rate. Figure 3.5 clearly demonstrates that not only the deposition rate but also the phosphorus content is affected by pH, the details of which are also reported by Riedel [58].

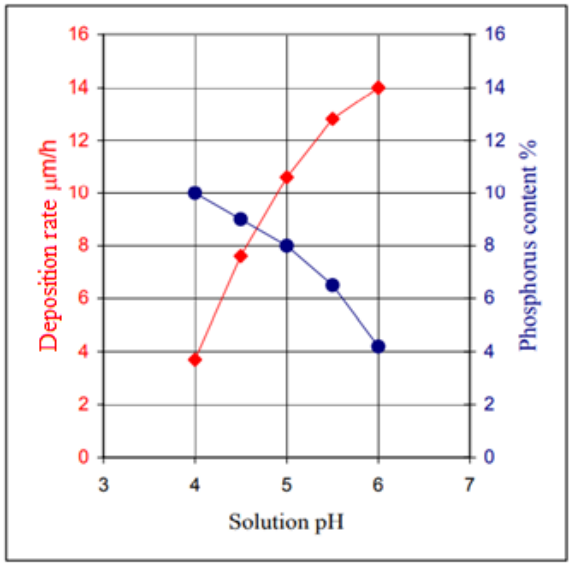


Figure 3.5 Effect of pH [57]

When the pH of the bath ascends, a series of differences occur. The deposition rate increases in a nearly linear fashion. Hypophosphite reaction modification from reduction to homogeneous occurs, so indigenous decomposition of bath solution and nickel deposition, as well as the solubility of nickel phosphate, decrease, which sometimes initiates decomposition and rough deposits. Finally, the phosphorus content decreases [58].

On the other hand, when the pH of the bath descends, the sedimentation of hydroxides and basic salts diminishes, hypophosphite's reducing power decreases, and more efficient buffering action of genres in the bath occurs [58].

3.2.1.3. Effect of Bath Composition

Various chemicals are present in different concentrations in the coating bath. Whilst the concentration of some of these chemicals descends, others ascend, and new products are formed as a result of chemical reactions. Throughout the process, the concentration of nickel decreases. If it does so to below 50%, the solution must be renewed. Similarly, when the concentration of stabilizers decreases, the balance of the bath will be disrupted, and nickel hydroxide precipitation will be inevitable [59].

According to Riedel, the deposition rate depends on two major factors which are Ni concentration and $Ni^{2+}/H_2PO_2^-$ ratio [58]. Hypophosphite concentration should be from 0.15 to 0.35 mol/L, and the optimal ratio of $Ni^{2+}/H_2PO_2^-$ should be maintained between 0.25 and 0.60, and prudentially between 0,30 and 0,45.

Nickel source, which includes nickel acetate, nickel chloride, nickel sulfate, etc., has an important role in identifying the characteristics of electroless Ni-P plating. Figure 3.6 demonstrates the relationship between the deposition rate of nickel phosphorus and nickel source concentration. Optimum nickel concentration is needed to obtain the peak for electroless Ni-P deposition rate in bath solution [43].

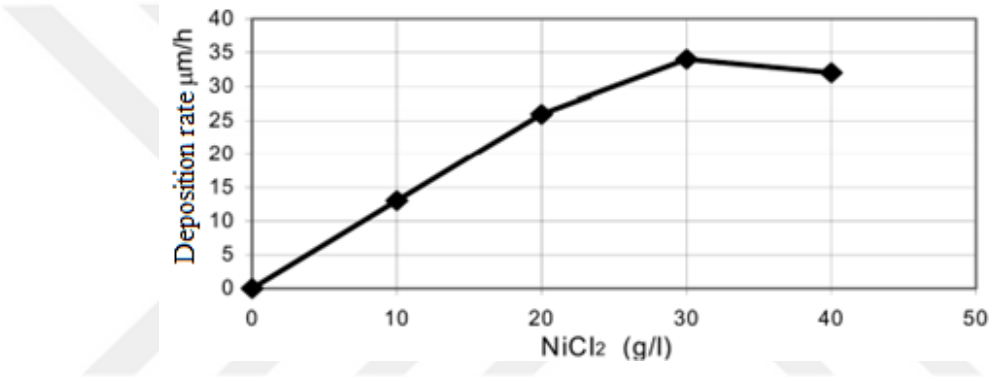


Figure 3.6 Effect of nickel chloride concentration on the deposition rate of electroless [60]

The rate of reduction is substantially affected by hypophosphite concentration variation. For nickel, it is improved by the increment in hypophosphite concentration, yet the surplus concentration of reducing elements can lead to a reduction in the bulk of the bath. This situation leads to the decomposition of the solution. As Figure 3.7 shows below, when the ratio $Ni^{2+}/H_2PO_2^-$ is approximately 0,45, the maximum deposition rate is acquired. When $Ni^{2+}/H_2PO_2^-$ ratio descends, the hypophosphite concentration ascends, thereby increasing the risk of decomposition for bath solution. When $Ni^{2+}/H_2PO_2^-$ ratio ascends, the rate of deposition descends, and the content of phosphorus of the deposit descends too [60].

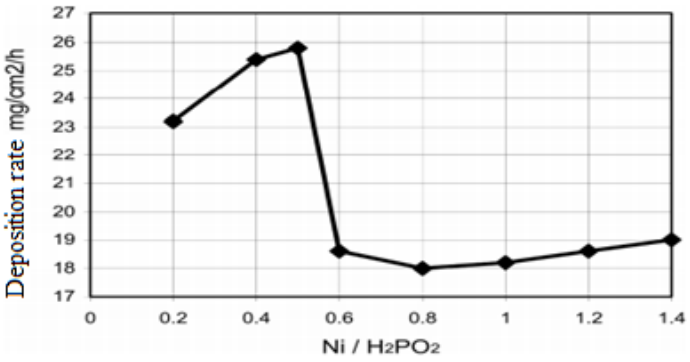


Figure 3.7 Dependence of deposition rate in an acetate-containing solution on the Ni_2^+/ H_2PO_2−ratio [60]

3.2.2. Properties of Electroless Ni-P Process

Nickel-phosphorus coating's microstructure and composition directly changes the characteristic of coating. Phosphorus content in Ni-P coatings with a phosphorus ratio varying between 1 and 13% is the main factor affecting the properties of the coating. By and large, as-coated nickel phosphorus deposits are homogenous, hard, and wear and corrosion resistant. Table 3.4 demonstrates the properties of coating according to phosphorus content [61].

Table 3.4 Coating properties according to phosphorus content [62]

Phosphorus content	**1 - 4%**	**7 - 9%**	**10 - 12%**
Structure	crystalline		amorphous
Physical Properties			
Thermal expansion coefficient (µ/m.K)	13	12	11
Density (g/cm^3)	8.5	8.1	7.9
Mechanical Properties			
Tensile strength (N/mm^2)	200	800 - 900	750 - 900
Internal stress (over steel substrate) (N/mm^2)	-10	±5	±5
Hardness HV	0.5	0.7	~1.5
Chemical Properties			
Acid resistance	low	medium	good
Other Properties			
Solderability	very good	good	medium

3.2.2.1 Hardness

Electroless nickel-phosphorus coatings are known for their hardness property that can increase upon exposure to heat treatment. Hardness is most commonly conceived as easily determined and useful in featuring the surface contact response of different types

of engineering materials [64]. As hardness is directly related to crucial properties for the deposit like wear and abrasive resistance, this parameter has been broadly studied in electroless Ni-P deposition. Phosphorus content, heat-treatment temperature, and period of heat treatment are the most effective factors for the hardness of deposition [65].

3.2.2.2 Heat Treatment

Hardness of the Ni-P coatings are significantly affected by post heat treatment process. In fact, achievement of high hardness values by means of suitable heat treatment is a remarkable property of the electroless Ni-P coatings. This lays out excellent erosion and wear resistance. The phosphorus content of the bath defines the parameters of the heat treatment such as time and temperature. When it is in the single-phase region (below 4,5 or 11%), just one reaction, in which phase β or γ transforms to α and PNi_3, occurs. This phase transformation takes place at 330 - 360°C for high phosphorus and 400°C for low phosphorus content bath solutions [66]. Nevertheless, for medium content phosphorus, another transformation (β transforms to A nickel) occurs at 250 - 290°C, and this causes thin particles to precipitate during the coating process. Figure 3.8 below demonstrates the effect of heat treatment temperature on the hardness of the coating. In addition, lots of sources have reported that the maximum hardness of the coating is obtained when heat treatment is applied at 400°C for an hour [47, 58].

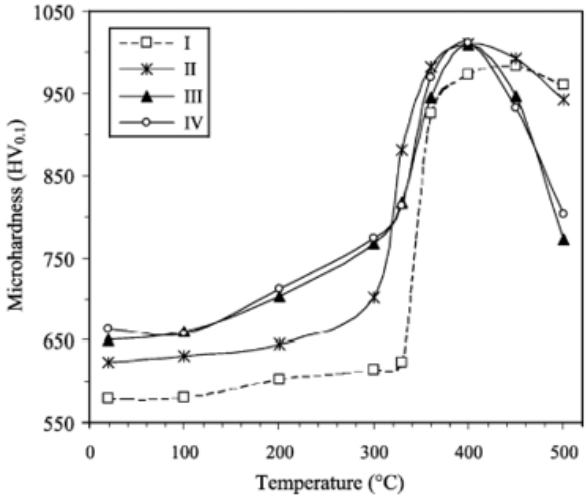


Figure 3.8 Hardness for different temperatures at 1h (wt. % P) I: 12%; II: 8.8%; III: 6.7%; IV:6,3% [66]

3.2.2.3 Adhesion Properties

Coatings with poor adhesion do not provide effective protection. In general, adhesive potential of electroless nickel coatings is superior to the nickel electrodeposition method. This is due to the existence of a stronger metal-to-metal bonding during the electroless deposition. However, in the case of coating non-ferrous alloys such as magnesium and aluminum, the adherence of the electroless nickel coatings to the substrate is sometimes weak. Hence, the studies on adhesion is mainly concentrated in using one of these alloys as substrates [65].

Plating with a rich adhesion ensures effective protection. Generally, the electroless nickel plating is superior to the nickel electroplating method according to adhesion properties. The presence of stronger metal to metal bonding throughout the deposition process in the electroless plating accounts for this strength. Nevertheless, when non-ferrous alloys such as aluminum and magnesium are used as substrate material, the adherence of the nickel to substrate may sometimes be low. Adhesion of electroless deposition on substrates such as copper, iron, nickel, and their alloys is better than the electroplating nickel. This adhesion can be reinforced with heat treatment [65]. Furthermore, the zincating process increases the adhesion of substrate to nickel in electroless nickel coatings for lots of substrates such as titanium and magnesium [67].

3.2.2.3 Tribological Behavior

3.2.2.3.1 Test Methods

Tribo-testers are employed in different configurations to evaluate the tribological properties of the electroless Ni-P coatings such as friction and wear behavior. As can be seen in Figure 3.9, some of these configurations are block-on-disc, pin-on-disc, ball-on-plate, and roller-on-plate. Often, the coated plate is tested against the harder counterface. Various tribo-test parameters are used to measure the performance of the electroless nickel coating: applied load, sliding distance, sliding velocity, and test durability. Tribological tests are carried out in both dry and lubricant-used environments. Different lubricants can be used here to evaluate the suitability of the lubricant according to the electroless coating deposit [65].

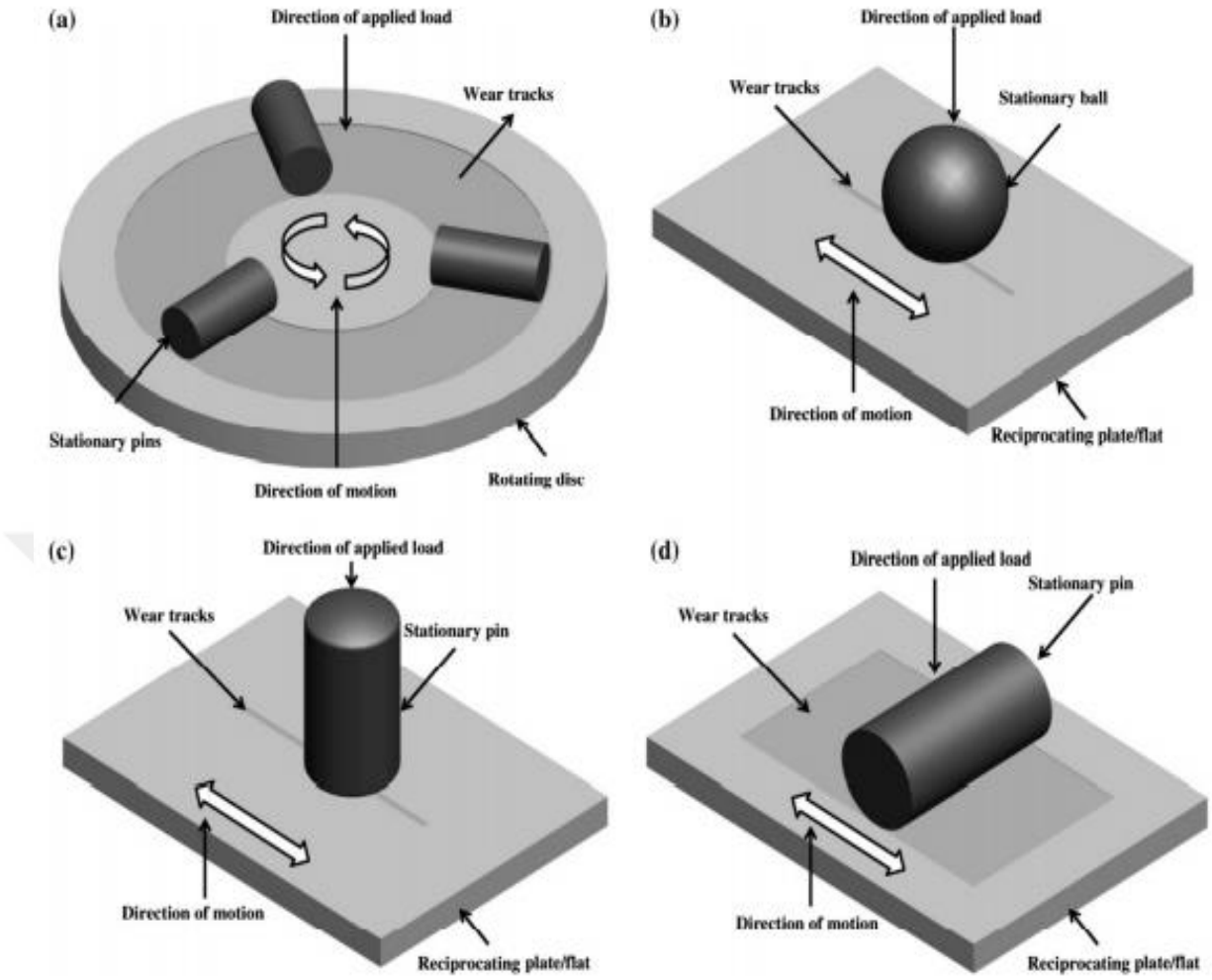


Figure 3.9 Common tribo-testing methods (a) Pin-on-disc, (b) Ball-on-plate, (c) Pin-on-plate, (d) Roller-on-plate [68]

3.2.2.3.1 Wear Resistance

One of the features that make the electroless nickel phosphate coatings unique is their superior wear resistance. The correlation between wear resistance and surface hardness has been theoretically proven. On the other hand, the wear behavior of a surface is affected by many variables such as surface morphology and the nature of the stresses applied. The wear resistance of the electroless nickel coatings depends not only on the phosphorus content but also on the properties of the heat treatment applied. As discussed in the previous sections, the hardness is mostly present in coatings with a

phosphate ratio of 4%, and it decreases as the phosphorus ratio increases. The same conclusion applies to the wear resistance properties [35, 47].

Figure 3.10 shows the relationship between wear resistance and phosphorus. The harder it is, the lower the weight loss due to wear. Figure 3.11 indicates the relationship between heat treatment temperature and wear resistance.

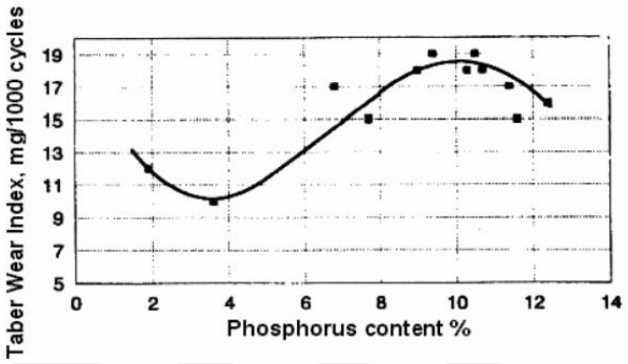


Figure 3.10 Effect of P content on wear resistance [66]

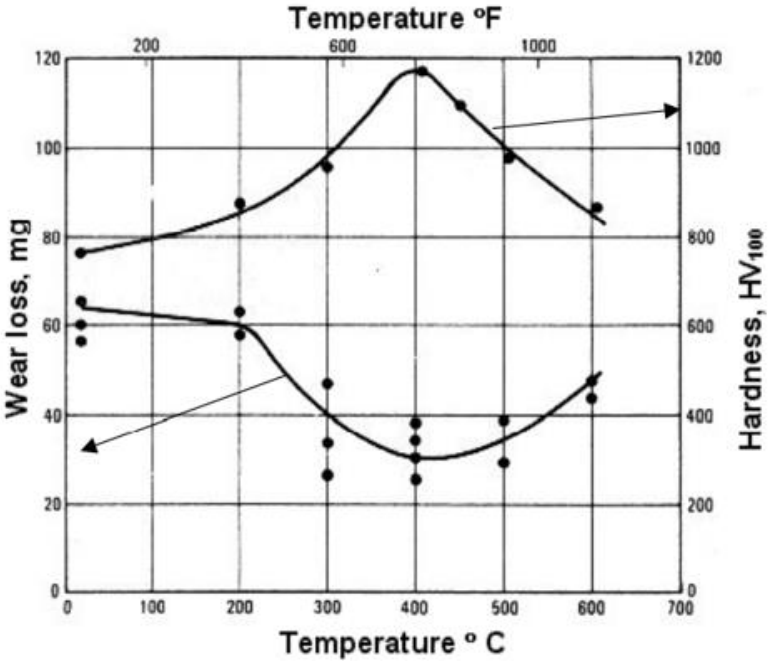


Figure 3.11 Effect of heat treatment on the wear resistance [47]

3.3 Electroless Composite Coatings

Composite electroless nickel coatings is the practice of adding particles to the coating solution to improve certain properties of the coating or to add a new property. These functional particles are evenly distributed throughout the nickel matrix, which is firmly bonded on the substrate. This unique dispersion and bond make composite electroless nickel coatings more durable and long-lasting than other wear and lubrication alternatives. Almost any particle can form a composite with the electroless nickel coatings as long as it can withstand bath conditions and its size is suitable. Compared to traditional composite coating techniques, the electroless nickel composite coatings offer many advantages such as deposit quality, excellent tribology, and large homogeneity. The process occurs when the particle collides and accumulates on the surface of the workpiece to be captured by the electroless matrix [43, 47].

3.3.1 History of Electroless Composite Coatings

The idea of improving such properties as hardenability, wear resistance, and corrosion resistance by adding second phase particles to the electroless nickel plating baths has led to studies on electroless nickel composite coatings. Efforts to produce such precipitates initially resulted in decomposition of the bath. Since the fine particles cause the surface area of the electroless plating bath to increase 700 - 800 times, initially decomposition appears in the electroless composite plating baths. However, this problem was solved with the help of suitable stabilizers and surfactants, so the electroless composite coating method was implemented successfully [65]. The particle added the electroless nickel plating process is based on the Odekerken's work in 1966 [69]. Since then, various electroless Ni-P composite coatings have been successfully co-deposited using micro and nano sized particles.

3.3.2 Bath Composition

Common components of the electroless plating baths are nickel ions, hard particles, reducing agents, and other materials that support the coating. The electroless composite coating process is similar to the traditional reduction technique, but it involves suspended particles. The components used in electroless composite coatings,

and their properties are indicated in Table 3.5. The efficiency of the co-deposition process depends on bath chemistry, operating conditions, and the nature of the particles. The inclusion of particles that improve the properties of the electroless coating is related to the growth of the deposit surrounding the coating; there is no molecular bond between the Ni-P matrix and the co-deposited particles. Particle selection depends on the type of surface to be coated and the properties to be developed. Some particles used in the electroless composite coatings are nitrides, oxides, carbides, and carbon-based particles [65].

Table 3.5 Electroless composite coating bath components and functions [65]

Component	Function	
Metal ion	Provides source of metal	STANDARD
Reducing agent	Provides source of electron to reduce metal ions	
Complexants	Prevents Ni-P precipitation	
Accelerators	Activates the reducing agent and increases deposit	
Buffers	Controls the pH	
Stabilizers	Prevents the bath decomposition	
Hard Particles	Fosters to desired composite coating	COMPOSITE COATINGS
Surfactants	Increases the surface wettability	

3.4 Graphene

Carbon, which is widely found from the earth, is also the only element with isomers from 0 to 3 dimensions. The carbon element with atomic number 6 is in group 4A of the periodic table. Its electronic configuration is $1s^2$ $2s^2$ $2p^2$ and has four valence electrons [70].

Carbon atoms are covalently bonded to each other and show three different bonds, sp1, sp2, and sp3, depending on the number of electrons. When these bonds are examined, with sp1, 2 bonds and carbon atoms in each atom form a linear geometry, with sp2, 3 bonds in each atom and carbon atoms form a triangular geometry with sp3, 4 bonds in each atom, and carbon atoms form a pyramid geometry with each other [70].

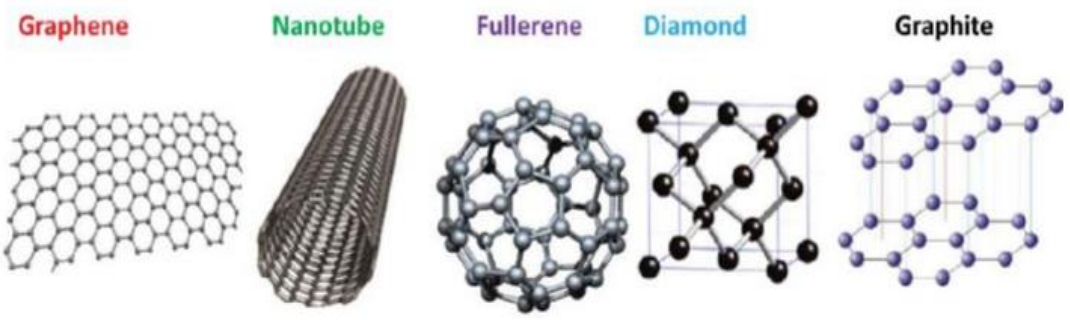


Figure 3.12 Carbon allotropes [71]

Graphene was first introduced at the University of Manchester in 2004 by Prof. Dr. Andre Geim and Prof. Dr. Konstantin Novoselov [72]. It enabled the emergence of a new unknown material class.

Carbon is called nanostructures thanks to its 0-dimensional (0D) and 1-dimensional (1D) structures at nanometer levels allotropes of carbon shown in Figure 3.12. Graphene has a very important place in nanostructures. Graphene is a layer of carbon atoms one atom thick. However, graphene is the two-dimensional form of hexagonal structures formed by carbon atoms arranged in a honeycomb shape. As can be seen in Figure 3.12, fullerenes with a 0-dimensional (0D) structure were formed by the

spherical arrangement of carbon atoms. Carbon nanotubes with a 1-dimensional (1D) structure can be defined as a cylindrical roll-like form of graphene. Graphite is the structure formed by overlapping graphene layers [70].

Graphene is a honeycomb-shaped hexagonal structure of carbon atoms, and it is a good example that pencil tips that we use frequently today are made of graphene layers. Graphene consists of a transparent carbon layer with an atomic width. For this reason, it conducts heat and electricity well [72].

Graphene is the thinnest material known in the market. It has extraordinary properties such as good thermal conductivity, high mobility of electrons, 2-dimensional very narrow lattice structure that prevents even minimal atoms from passing through, and its structure remains unchanged even at high temperatures [73].

3.4.1 Properties of Graphene

The graphene has superior properties [72 - 74] as summarized following:

Electrons travel through graphene as if they had no weight. In this way, electrons can behave like photons in graphene and their speed can reach as high as 800 km per second. Compared to silicon, the speed in graphene is 100 times higher.

In addition to being the thinnest structure discovered in the market, graphene is also the material with the highest mechanical properties. It is on average 100 times stronger than steel, which is widely used today.

Graphene is a material with high electrical and thermal conductivity. Graphene is a better conductor compared to diamond.

Even the smallest atom cannot pass through graphene, which has a very tight arrangement. In addition to this feature, graphene can easily shape and the surfaces of materials in different forms can be easily coated with graphene.

In addition, some of the properties of graphene is shown in Table 3.6.

Table 3.6 Properties of graphene [75]

Property	Value
Dimension	2
Tenacity	Flexible, elastic
Hybridization	Sp2
Experimental SSA(m2/g)	1500
Electrical Conductivity(S/cm)	2000
Thermal Conductivity (W/m. K)	4840-5300

3.5 Titanium and Titanium Alloys

3.5.1 General Properties of Titanium

In 1791, when mineralogist and chemist William Gregor was working in a place called Karakum near Menachan Valley in Cornwall, he discovered titanium, a metal whose origin he could not determine, and named this metal "mechanite" after being inspired by its location. Four years later, German chemist Martin Heinrich Klaproth proved that this metal is a new element. Because this element is difficult to extract from the soil, in Greek mythology it was looked like Titans imprisoned under the earth, and Martin Heinrich Klaproth named the element titanium [76].

It is not possible to separate titanium from carbon, which requires a difficult and expensive process to be extracted from ores by normal heating. Pure titanium was first prepared by Matthew A. Hunter in 1910 by heating sodium with $TiCl_4$ at 700 - 800 ^oC (Hunter process) [77].

Finally, Wilhelm Kroll developed the Kroll process between 1938 – 1940 years, in which titanium tetrachloride was reduced with magnesium in a protective atmosphere, thus demonstrating that titanium could be extracted commercially. Kroll is recognized

as the father of the titanium industry. The method is the most used in titanium production even today. After the US Mining Bureau demonstrated the commercial viability of the Kroll method in 1946, the US Armed Forces began to deal with titanium. After the Second World War, titanium-based alloys were soon adopted as key materials for aircraft engines. Its properties such as high melting point, low density, and corrosion resistance have increased its use in military and space industries in a short time. Today, aviation is still the major consumer of titanium and its alloys, while other markets such as architecture, chemical processing, medicine, power generation, and transportation are gaining increasing acceptance [76, 78].

While the use of titanium first started aerospace industry, over time, it started to spread to many areas due to its superior properties. While it is used in aerospace applications due to its lightness and high strength, it has become an indispensable material in the chemical industry and marine applications with its good corrosion resistance. On the other hand, it has been accepted in biomedical applications (orthopedics and dentistry) due to all three features. Titanium, which has been increasingly important for the last 60 years, is among the most commonly used metallic materials in the world; It ranks fourth after iron and magnesium. Titanium has a low density of 4.5 g / cm^3 and a high melting temperature of 1660 ºC. The strength of titanium alloys is approximately 2.5 times that of aluminum alloys and is the same as some alloy steels [79].

Despite all these positive properties, titanium is insufficient in engineering applications where moving contact occurs due to its friction and wear properties. Energy and material loss occurs in applications where titanium is used as a result of friction and severe wear-up to adhesion. As a result of abrasion, the oxide structure that provides corrosion resistance deteriorates and severe corrosion occur as well as abrasion. It has been clearly demonstrated that surface modification techniques should be applied to improve the friction and wear properties of titanium [80, 81].

3.5.2. The Classification of Titanium Alloys

The hexagonal crystal structure of pure titanium in allotropic character at room temperature (RT), called α-phase, transforms into a volume-centered cubic structure called β-phase at 882°C. α -transformation temperature called for the temperature

which in all alloys in α-phase, temperature above it when alloys entirely in phase called as β-transformation temperature. Between these two transformation temperatures, there are both α and β phases in the microstructure of the material [82].

The most important alloying element of titanium is aluminum, which is among the α-stabilizers (elements that stabilize the α phase). The transition elements oxygen, nitrogen, and carbon also belong to the group of elements that stabilize the α phase, and they raise the conversion temperature. There are two groups of elements that stabilize the β phase by lowering the transformation temperature. The first of these is β b-isomorph elements, e.g., Mo, V, and Ta are much more important due to their much higher solubility in titanium and are completely soluble in this phase. The second is β-eutectic elements and even very low volume fractions of these, e.g., Fe, Mn, Cr, Co, Ni, Cu, Si and H can cause the formation of intermetallic compounds. Sn and Zr elements, on the other hand, are called neutral elements because they dissolve in the α and β phases, although they are used in the α-phase [52, 76].

These elements have low solubility in the α phase and lower the conversion temperature. These β-isomorphic group elements must be incorporated into the alloy, both to stabilize the phase and to reduce or prevent the formation of intermetallic compounds seen in high temperature use.

Generally, titanium alloys are classified as α, α + β and β alloys and further subdivided into near-α and metastable-β alloys. This is schematically summarized in a three-dimensional phase diagram consisting of two-phase diagrams with an α- and a β-stabilizing element respectively shown in Figure 3.13. According to this scheme, α alloys consist of alloys commercially pure (cp or CP) titanium with only α-stabilizing and / or neutral elements. If too little β-stabilizer is added, it is called near-α alloy. The group of near-α alloys is followed by α + β alloys, which contain 5 to 40 percent β-stabilizers by volume, and this group is the most widely used group of titanium alloys. If the ratio of-stabilizing elements is increased to a level where no longer transforms into martensite upon fast quenching, the alloys are still in the biphasic domain and metastable β class alloys are reached. It should be noted that these alloys can still yield

an equilibrium volume fraction of more than 50%. Finally, single phase β alloys mark the end of the alloying scale of conventional titanium alloys [76].

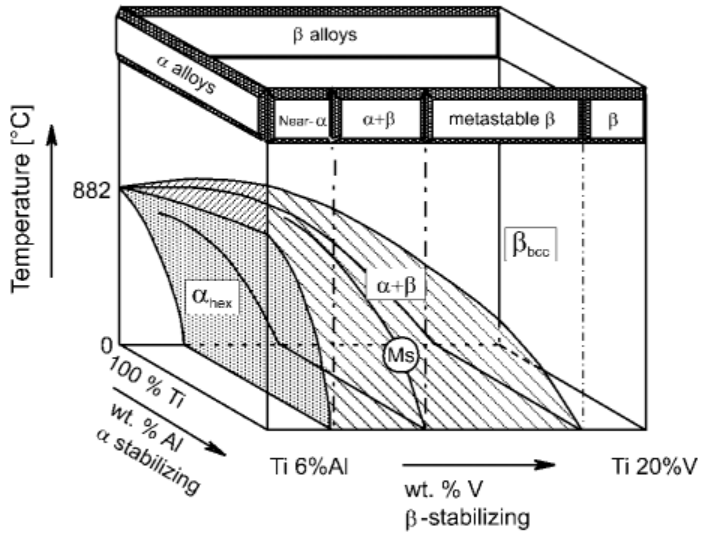


Figure 3.13 Three-dimensional phase diagram to classify Ti alloys [76]

The properties of titanium alloys change depending on the volumetric ratio and distribution of α and β phases in the structure. Compared with α phase β, it can be said that it has higher resistance to plastic deformation, has lower ductility, its mechanical and physical properties are anisotropic, its diffusion rate is approximately twice the diffusion rate β, and exhibits higher creep resistance. The density of aluminum, the most important α stabilizing element, is about half that of titanium. Therefore, although heavier elements such as vanadium and molybdenum are used in α alloys, α alloys are lighter. α alloys generally have medium strength. α + β alloys can have high strength, while semi-stable β alloys can have very high strength. However, β alloys that can reach very high strength values have to compromise their ductility for this property. While ductility is largely dependent on microstructure, β alloys can have ductility close to that of α and α + β alloys when precipitation hardening is not applied. Titanium's high oxygen affinity causes the formation of a very thin (in nm range) oxide layer on its surface even at RT. The reason for the high corrosion resistance of titanium-based materials is this oxide layer formed on the surface. The corrosion resistance of α alloys

is higher than β alloys. This is due to the presence of oxygen that stabilizes the α phase [84]. A classification according to the alloy condition can be made as follows [83].

Unalloyed-commercial purity titanium: Commercial purity titanium, which is preferred in cold working environments, has high corrosion resistance, but its strength is lower than alloyed titanium.

α-phase alloys: These alloys containing elements such as Al, known as α-phase stabilizers, and neutral elements such as Sn (such as Ti5Al-2.5Sn) show properties close to pure titanium, but unlike they have a good tensile strength up to 300 ° C. They are preferred in cold working environments.

Near α-phase alloys: They contain high amounts of α-phase stabilizers such as Al, O, as well as low amounts of-phase stabilizers such as Mo, V (such as Ti-8Al-1Mo-1V). They show properties close to α-phase titanium, but they can also be used in environments with operating temperatures up to 400 - 520 ° C.

α + β phase alloys: They contain α and β-phase stabilizers. Ti-6Al-4V, the most used and oldest titanium alloy, is included in this group. These low-density materials retain their strength and corrosion-resistant properties up to high temperatures.

β-phase alloys: They contain high amounts of β-phase stabilizers. High hardness and strength, cold formability are its general characteristics. Although their operating temperatures are higher than α + β phase alloys, they can find new areas of use (metal matrix composites and steam turbine power plants, etc.)

Ti-6Al-4V, the first alloy produced and developed in the United States at the Illinois Institute of Technology for aircraft structural applications in the 1950s; It is an α + β titanium alloy with properties such as high strength, high fracture toughness, low density, superior biocompatibility, and excellent corrosion resistance. Ti-6Al-4V is a light but strong alloy and saves weight in highly loaded structures, so it is extremely suitable for jet engines, gas turbines, and many airframe components [3 - 6]. This alloy currently accounts for more than 50% of all titanium use in the world and is the most widely used titanium alloy. Up to date, no titanium alloy has surpassed the dominant position of Ti-6Al-4V alloy containing 6% aluminum and 4% vanadium. The

aerospace industry accounts for more than 80% of this use, with its next largest application being medical prostheses accounting for 3% of the market, followed by the automotive, marine, and chemical industries. Chemical content and physical and mechanical properties of Ti-6Al-4V alloy are shown in Table 3.7 [76, 82].

Table 3.7 Physical-mechanical properties and chemical contents of Ti-6Al-4V [85]

Physical and Mechanical Properties		**Element Contents**	
Density [g/cm3]	4,42	Al	6.0%
Melting Range [°C±15°C]	1649	V	4.0%
Specific Heat [J/kg. °C]	560	N	0.05%
Volume Electrical Resistivity[ohm.cm]	170	C	0.1%
Thermal Conductivity[W/m.K]	7,2	H	0.0125%
Tensile Strength [MPa]	1000	Fe	0.3%
Elastic Modulus [GPa]	114	O	0.2%
Hardness [Rockwell C]	36		

Despite the superior properties of titanium and its alloys, these materials are insufficient in environments with friction and wear. Adhesive wear resistance of titanium alloys is low because titanium exhibits very strong adhesion to the counter material during sliding. The reason for this is that titanium is ductile and chemically reactive. The friction coefficient, which is not constant during sliding, reaches very large values. Plastic deformation increases with adhesion in the actual contact area on the area where the asperities touch.

Titanium has poor tribological properties due to its crystal structure, electron arrangement, and lack of lubricants. The surface of titanium is extremely reactive because it has an electron arrangement with a low-value d-band character. On the other

hand, despite the SDH (metals with this structure normally have good friction properties and the ideal tight-pack ratio is 1.633), the ideal tight-pack ratio of titanium is 1.588. As a result of this situation, the pyramidal and prismatic slip planes as well as the base plane are also encouraged to slip, and ductility and plastic deformation increase with the increase of slip systems. Old-style lubricants, which are successful in most metals, are insufficient for titanium because of the low thermal conductivity of titanium alloys.

3.6 A Brief Review on Graphene Reinforced Nickel Matrix Composite Coatings

Graphene was introduced in 2004 and started to be the subject of studies. Graphene, which has been studied many times since its discovery, exhibits different properties from traditional materials, and thanks to these properties, it has been used as a reinforcement element in many composite materials. The first studies on graphene reinforced nanocomposites started in 2008 [86]. In this context, studies on graphene-reinforced nickel matrix nanocomposite materials, which are a part of this new and developing subject, are examined in this section.

Hu et al. reported [87] in 2012 that they used the electroless coating method for the first time for the synthesis of Ni/Graphene sheets. Ni-graphene sheet was synthesized from graphene oxide sheets by autocatalytic coating method in $NiSO_4$ solution using $NaBH_4$ as reducing agent. The microstructure of the synthesized Ni/graphene composites is shown in the Figure 3.14 a-d. In Figure 3.14-a, meso and micropores were formed on the surface of Ni-graphene sheets. EDS analysis of the region marked in Figure 3.14-a is illustrated in Figure 3.15-b. Au peaks occurring in the EDS analysis were due to Au-coating deposited on Ni/graphene sheets prior to SEM analysis. Mass fractions of Ni, O, and C elements were found as 55.4%, 38.4%, and 6.2%, respectively. Higher zoom SEM images and corresponding EDS analyzes are shown in Figures 3.14-c and 3.14-d, respectively. From Figure 3.14 we can conclude that; Although the Ni accumulation rate reached a high value of 55.4%, no aggregates were formed. Hu et al. [87] pointed out that the Ni/graphene composites they synthesized have the potential to be used as catalysts due to their porous structure, high specific

surface area, and uniform distribution of nickel particles on the surface of graphene sheets.

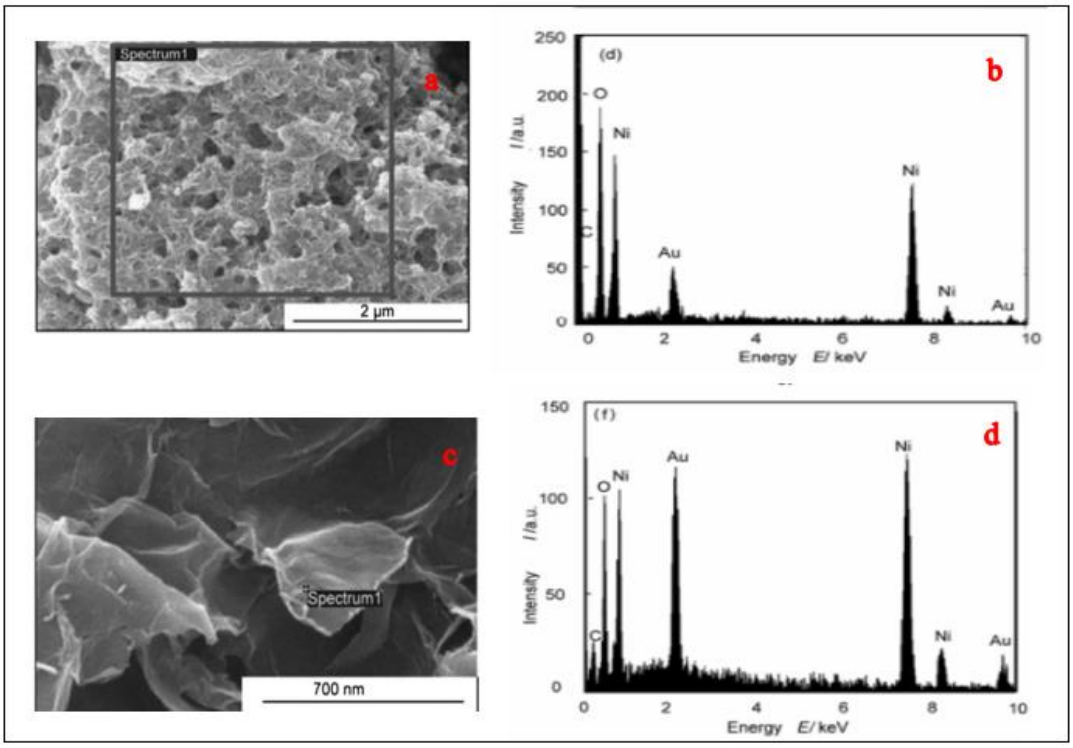


Figure 3.14 The microstructure of the synthesized Ni/graphene composites, a) SEM image of Ni-graphene sheet, b) EDS of marked region in image a, c) Higher magnification of Ni-P graphene sheets, d) EDS of marked region in image c.

Kumar et al. [88] coated a graphene-reinforced nickel composite film on a mild steel plate by the electrodeposition method. The surface morphologies of the prepared nickel and graphene reinforced nickel coatings are shown in Figure 3.15a and b respectively. In the figure, there is a uniform deposited microstructure image all over the pure nickel-plated higher grain size substrate. However, in the composite coating with the added graphene, a shiny, smaller grain size and less hillocks microstructure appears. Moreover, it was revealed that the graphene adsorbed on the substrate during composite micrograph film deposition inhibited crystal growth and increased the nucleation sites for nickel reduction, resulting in a fine-grained and robust arrangement of nickels in the composite coating. The study also reported that graphene supplementation improves corrosion resistance and micro hardness.

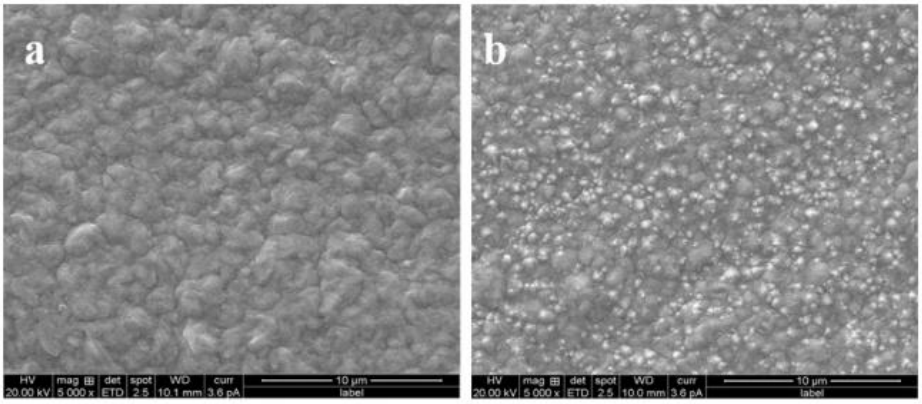


Figure 3.15 Microstructure of coating, a) Nickel coating b) Graphene reinforced nickel plating

Kuang et al. [89] obtained nickel/graphene composite by adding suspended graphene oxide into nickel sulfamate solution by the electrophoresis method. They produced a successful nickel-based graphene composite by electrochemical reduction of graphene oxide layers and Ni+2 ions containing 0.12 wt.% graphene. They investigated the thermal conductivity of composites produced using the laser flash method. As a result, the thermal conductivity of the composite coating increased by 15% compared to the pure nickel coating. In addition, the hardness values of the composites are 4 times higher than the pure coating. Reduced graphene sheets appreciably affected the Ni growth's preferred orientation in composite coatings and boosted the properties of composites.

Yu et al. [90] coated 06Cr25Ni20 stainless steel samples used for glass casting with graphene reinforced electroless nickel phosphate composite film. During the coating process using 0.04 g/l graphene reinforcement, after coating was carried out in the coating solution for 20 minutes, the experimental setup was subjected to vibration with ultrasonic vibration intermittently for 2 hours, and the coating process was completed. XRD analyzes of reinforced and non-reinforced samples subjected to heat treatment after coating are shown in the figure. In Figure 3.16 a, FCC nickel peak at 45 degrees (111) was observed in both coatings, while a C (110) peak at 29 degrees was observed in Gr-Ni-P coating. Both amorphous and crystalline structures were observed in both coatings. Figure 3.16 b shows the XRD patterns of the coatings after heat treatment,

with narrower and higher density peaks for both coatings. This shows the phase transformation of the heat treatment from amorphous to crystalline for both coatings. After heat treatment, nickel (200) became the most intense peak at 52 degrees and bcc Ni3p revealed new peaks. The C peak remained the same after heat treatment, indicating that there was no chemical reaction between Ni-P and Gr during crystallization. The average grain sizes were calculated with the Debye-Scherrer formula, which was 47.2 nm for Ni-P coating and 32.8 nm for Gr-Ni-P composite coating, which can be interpreted as the mechanical properties of Gr-Ni-P improved. In addition, homogeneous distribution of graphene in the coating was ensured by ultrasonic excitation. Results reported that graphene reinforcement imparted 8% more stiffness and 8.2% more Young's modulus to the electroless Ni-p coating

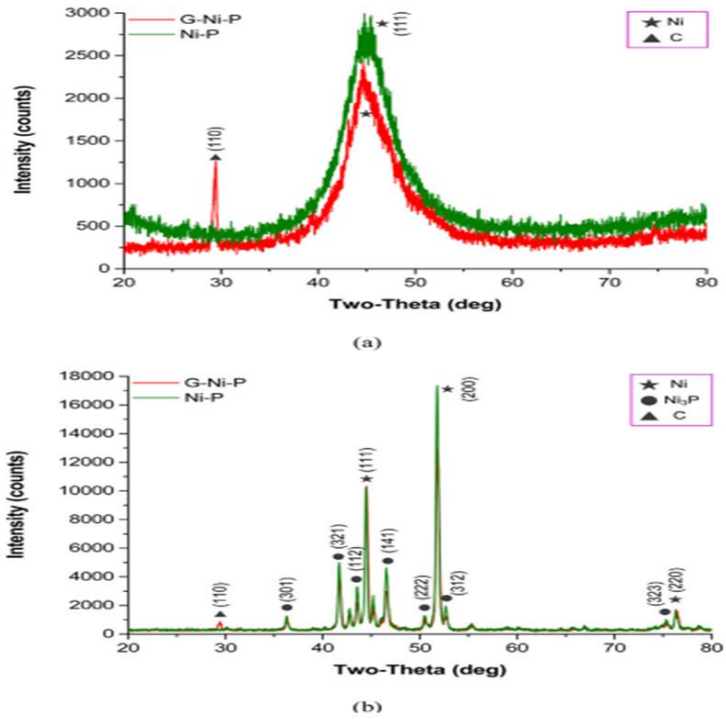


Figure 3.16 XRD patterns of Ni-P and G-NiP coating: a) Co-deposited, b) Heat-treated

Mindivan et al. [91] produced nickel and graphene nano-plate (GNP) reinforced Ni-based coatings using direct current (DC) using Watts-type coating bath method. St 37 steel was used as the substrate for the electroplating and GNP (0.3 g/l) was used as the reinforcement material with a lateral thickness of about 5 nm and a thickness of about

5 - 8 nm. Elemental, morphological, and phase evaluations were carried out using EDS, SEM, and XRD analyses and the wear-hardness behavior of the coatings was investigated. As a result, it was found that the GNP reinforcement thinned the grain structure of the nickel matrix, the GNP was homogeneously distributed in the structure, and the GNP reinforcement reduced the surface roughness. Finally, it was found that the composite coating, produced in DC current type, has a more compact structure and offers lower wear rate and higher hardness compared to pure nickel coating

CHAPTER 4

EXPERIMENTAL METHOD

As mentioned previously that the electroless coatings are superior to other methods due to their economy, homogeneous distribution, and easy application. In recent years, there has been significant amount of research on improving the properties of the electroless nickel-phosphate coatings with nanoparticle reinforcement. It improves the wear, toughness, and corrosion resistance. In this study, optimum conditions such as bath temperature, nanoparticle amount, heat treatment temperature were investigated to produce coatings for the electroless nano composite coatings.

4.1. Preparation of the Experiment Setup

The coating process was carried out by immersing the samples, whose surface cleaning processes were completed, into the prepared coating solutions. The coatings were made in a 600 ml glass beaker, in a setup built on a magnetic stirrer with temperature and speed control. The experimental setup was placed in a fume hood for the environment and ambient temperature.

The effects of heat treatment and graphene nanoparticle amount parameters on the microstructure and mechanical properties of graphene reinforced electroless nickel phosphate coatings were investigated.

4.1.1. Preparation of Substrates

Ti-6Al-4V titanium substrates were used in this study. All the substrates have 50 x 50 x 2 mm dimensions at the beginning of the processes. Figure 4.1 demonstrates the photograph and microstructure of substrates.

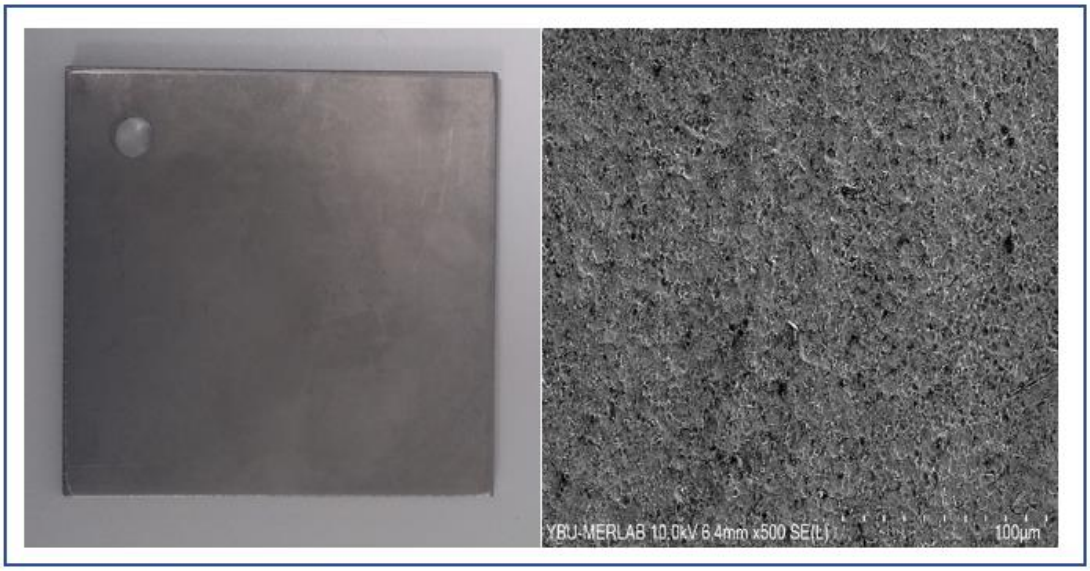


Figure 4.1 Ti-6Al-4V substrate and microstructure of the substrate

Oil, oxide, hydrocarbon, and similar impurities on the substrates cause the coating not to adhere well to the substrate and to achieve the desired properties. For this reason, surface preparation processes were applied before the coating process in order to ensure that the substrate surface was clean enough.

Titanium and its alloys are quite difficult to coat because, due to their thermodynamic behavior, they tend to form a passive and tenacious oxide layer [53]. The section in which the substrate cleaning procedures are explained includes various procedures to eliminate the oxide layer. However, it regenerates so quickly that forming the coating before the oxide layer blocks the access to nickel ions is quite complex. If the electroless nickel coatings are applied on dirty or oxidized surfaces, their properties will not be as desired. Zincating is one of the methods for using to prevent oxide layers before the coating process. Surface preparation, activation and avoidance of oxide layer processes applied for titanium alloy substrates are as follows, respectively.

1. Cleaning with acetone and rinsing in distilled water.

2. Soaking in 6% HF solution for 30 seconds to ensure the surface activity of the titanium substrates and to remove the oxide layer for the autocatalytic reduction process to take place.

3. Zincating for 90 seconds in order to prevent the formation of the oxide layer on the titanium. The Zincate layer acts as a good base and activator for electroless coating.

Surface preparation processes are shown in Figure 4.2 a, b, and c respectively.

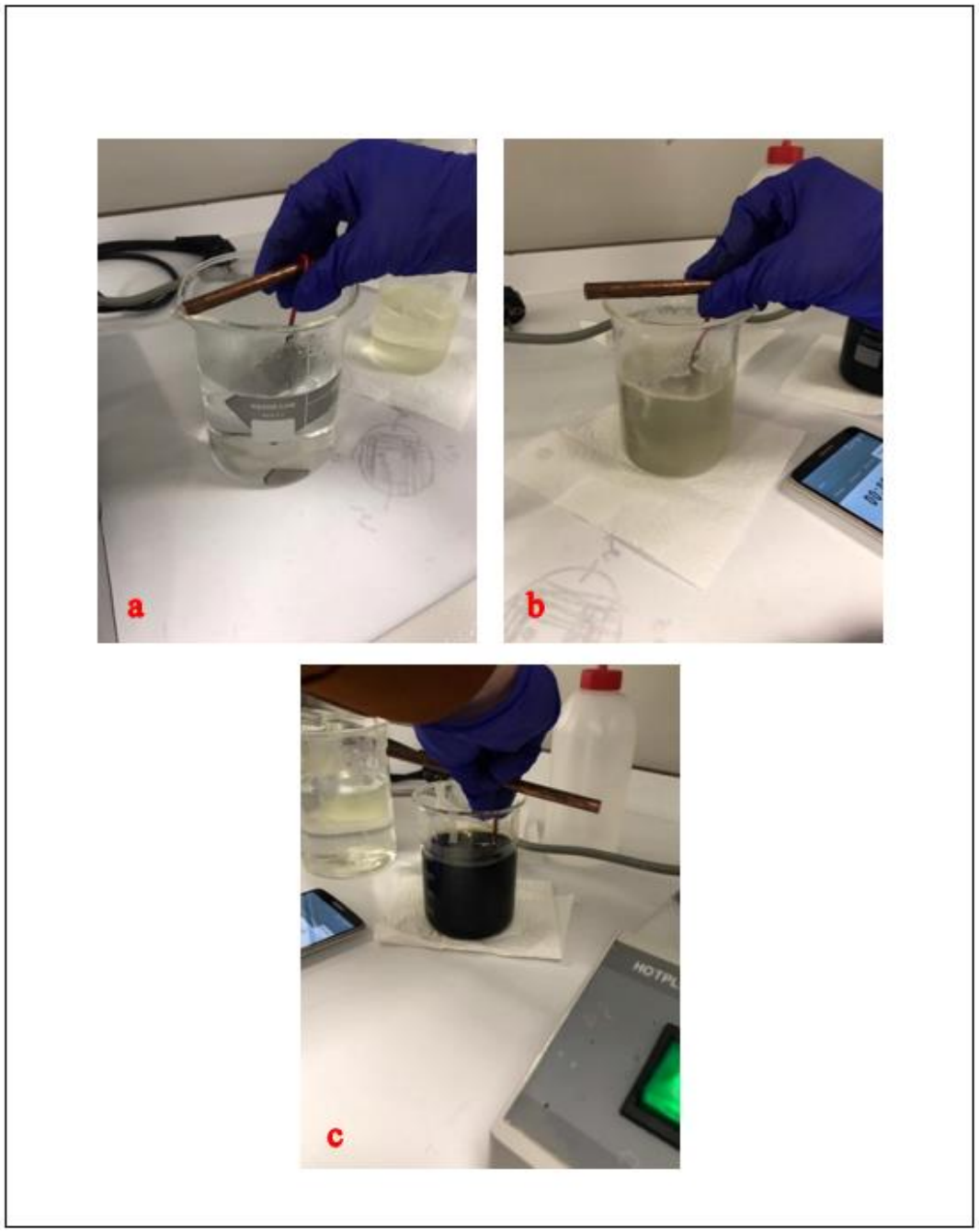


Figure 4.2 Surface preparation of substrate a) Cleaning, b) Soaking, and c) Zincating

4.1.2 Preparation of Graphene-Reinforced Electroless Ni-P Coating Bath

For the preparation of graphene reinforced electroless nickel phosphate bath, 500 ml of distilled water, 30 ml of A and 50 ml of component B, and 0.1 g/L surfactant (SDS) were added to ensure homogeneous mixing of nano powders into a 600 ml beaker. 2 g/L graphene were added to the bath realize the composite electroless coating. The properties of graphene nanoparticles with an average radius of 1.5 μm are chosen. Electroless nickel phosphate graphene coating bath was mixed with an ultrasonic homogenizer for 1 hour in order to prevent the nano powders from clumping and collapsing during the coating process. Then, the bath solution taken on the heater was mixed continuously with a magnetic stirrer and heated up to the optimum temperature of 90 - 92°C, and it was made ready for the coating process.

The coating process was carried out in this way for both the electroless plating bath of the graphene-reinforced Ni-P; After the bath solution reached the optimum temperature, the samples, whose pre-cleaning processes were completed, were immersed in the bath solution. Ti-6Al-4V substrates, which were kept in the bath solution for 1 hour in order for the coating process to take place, were removed from the coating bath at the end of the period and left to dry in pure water for rinsing. A thermometer was used to maintain the temperature of 90 - 92 degrees throughout the process, and a magnetic stirrer was used to ensure homogeneous mixing.

4.2 Experimental Processes Applied to the Samples After Coating Process

4.2.1 Heat Treatment

In order to see the effect of heat treatment on each prepared sample, it was divided into 2 cm wide pieces with a metal cutter. After cutting and deburring, the samples, oiled with acetone and alcohol, are ready for heat treatment.

It was heat-treated for 1 hour at 450 degrees in an argon atmosphere heat treatment furnace and then the samples were left to cool. Substrates which put in the heat furnace for heat treatment are shown in Figure 4.3.

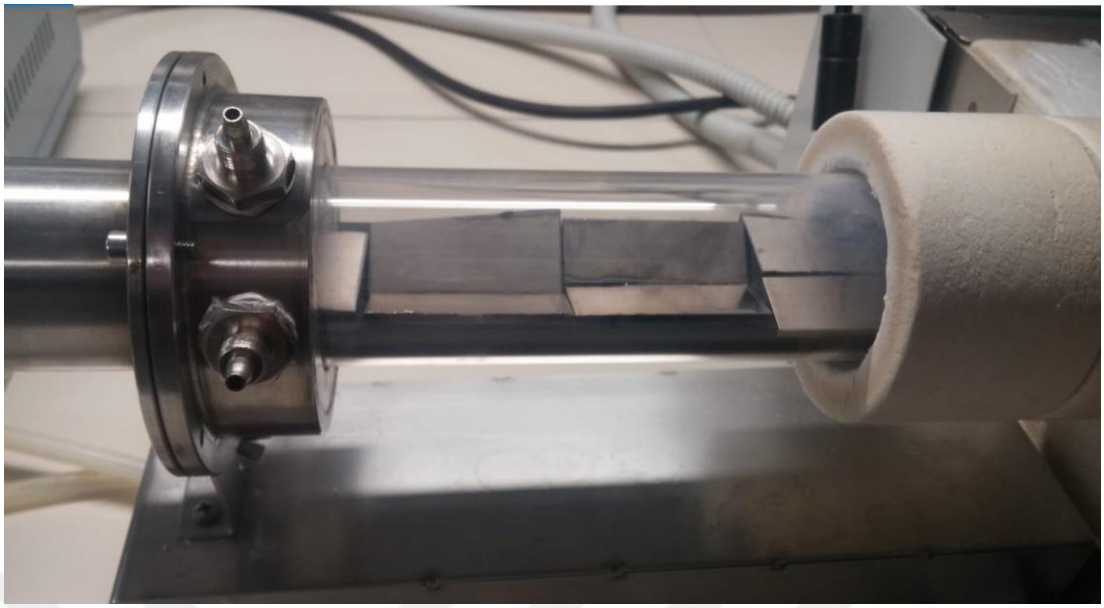


Figure 4.3 Heat treatment of substrates

4.2.2 Abrasion Test

The wear and friction tests of the coated samples were carried out in the linear (reciprocating) module of the UTS Tribometer T30M-HT wear test device. The wear tests are based on the ball-on-plate tribo-testing configuration technique. The Figure 4.4 shows the schematic view of the UTS wear device and the reciprocating wear system. The working principle of the experimental setup is to examine the wear in pairs of friction elements in contact with each other and to determine the wear properties of metallic materials by calculating the amount of wear. The experiments were carried out at RT, in an oil-free environment, and each sample was cleaned with acetone before and after the experiment. Abrasion tests were performed according to ASTM G133-05 Standard Test Method for Linearly Reciprocating ball-on-Flat Sliding Wear test standard. The wear marks were further characterized by SEM and XPS tests. The test parameters are summarized as shown in the Table 4.1.

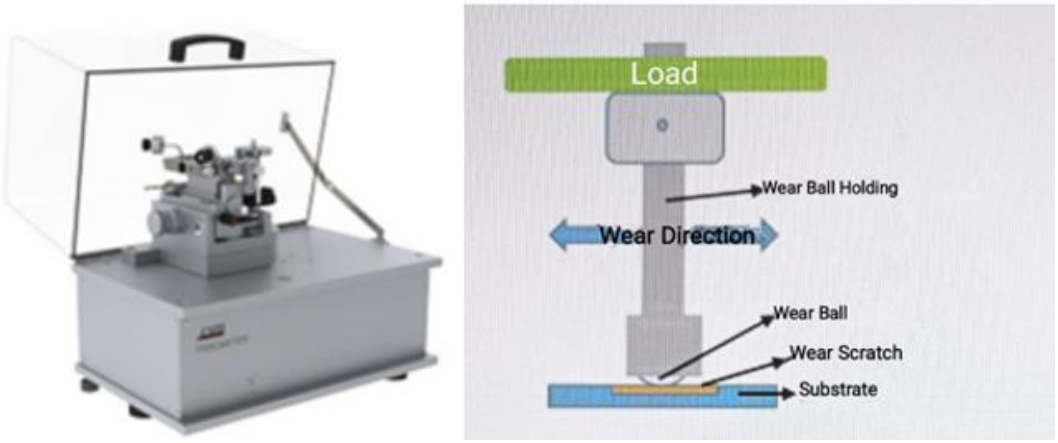


Figure 4.4 Device and schematic view of reciprocating wear mechanism [19]

Table 4.1 Wear test parameters

Load	1 N
Frequency	5 Hz
Stoke	10 mm
Sliding Distance	100 m
Sliding Speed	100 mm/s
Test Duration	16.7 min
Ball material	Alumina

4.3. Characterization of Coating Layer

4.3.1. Surface Preparation of Samples for Optical Microscope and SEM Analysis

Surface preparation processes for the optical microscope and scanning electron microscope (SEM) analyzes of the samples were carried out in the Powder Metallurgy Laboratory of the Mechanical Engineering Department of Gazi University. The samples were mounted on the Struers Citopress-1 brand mounting device shown in the Figure 4.5.a. Sanding was then carried out under running water using radial SiC sandpapers of 240, 600, 1000, and 1200, respectively. The working electrode was washed with running water, rinsed with distilled water, and dried with a dryer to prevent staining of the sample surfaces in the transitions between the SiC abrasives. Sanding and polishing process was done on the Struers Labopol-1 brand device shown in the Figure 4.5.b. Afterwards, the samples were polished with felt using 3 μm and 1 μm diamond suspensions. The polished samples were washed with distilled water and dried.



Figure 4.5 a) Mounting device, **b)** Sanding device

4.3.2. Coating Thickness Analysis

The measurement of the coating thickness of the samples was measured in the Leica CTR6000 microscope at Gazi University. Coating thickness measurements were performed by taking the average of 10 different measurements using the device's own scaling. The microscope used appears in the Figure 4.6.

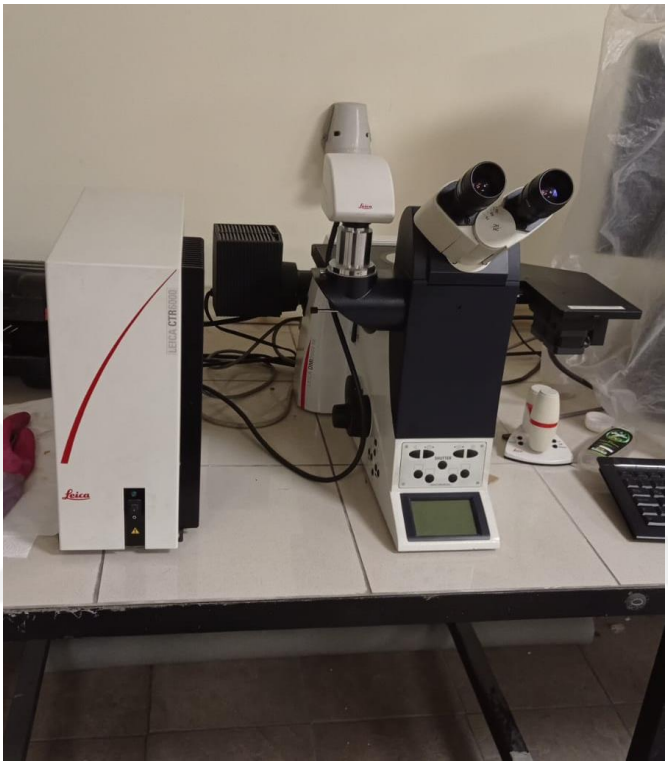


Figure 4.6 Coating thickness measuring device

4.3.3. Scanning Electron Microscopy (SEM) Analysis

The surface morphologies of the coated samples were characterized by Scanning Electron Microscope (Hitachi SU5000) in Ankara Yildirim Beyazit University (AYBU) Central Laboratory. The scanning electron microscope is shown in Figure 4.5. All examined samples were etched with 3% nitric acid and 97% ethyl alcohol solution before being taken into the microscope. During the SEM examination, the acceleration voltage of the scanning electron microscope was 10 kV. Ni-P-Gr coating structures obtained as a result of the experiment were compared with the literature. It has been observed how the grain structure (morphology) changes under different

conditions on the coating surface and wear marks. EDS analysis was also performed on the samples using the same device. In the EDS analysis, the ratios of the elements in the structure were examined.



Figure 4.7 SEM device

4.3.4. X-Ray Diffractometer (XRD) Analysis

X-Ray Diffractometer (XRD) is one of the analysis techniques that gives information about the crystallographic properties that reveal the phase structures of materials. In the XRD method, X-Rays with a very short wavelength are sent onto the material. Depending on the crystal direction and crystal structure, the refracted X-Ray reveals a diffraction pattern unique to the material. Using the patterns obtained, the average grain size of the grains that make up the material can also be calculated with the Debye-Scherrer equation in 4.1.

$$\textit{Debye-Scherrer Formula: } D = \frac{K\lambda}{\beta cos\theta} \textit{ [104]} \qquad (4.1)$$

Where D is crystal grain size (nm), K is constant (0.9), λ is the wavelength of the used X-Rays(Å), θ is diffraction angle, and β is the width of the X-Ray peak at half the intensity (rad) [104].

In this study, the XRD analysis was performed by scanning with Cu K alpha monochromator at a speed of 2 degrees/min. The wavelength of the beam is 1.54059Å. Analysis of the peaks by the XRD analysis was conducted with the help of computer software. The crystal structure characterization of the Ni-P-Gr coating layer produced in the study, the region where 2θ is between 10º and 110º, was investigated. In addition, the changes in the crystal structure caused by the addition of graphene were investigated with the help of XRD.

4.3.5. X-Ray Photoelectron Spectroscopy (XPS) Analysis

X-Ray Photoelectron Spectroscopy (XPS) analyzes were taken on both the normal sample surface and wear marks. Before starting the analysis, ion beam etch was done. This process is performed in order to clean if there is 10 nm thick pollution, oxidation, etc. from the surface. While looking for nickel, carbon, phosphate, and oxygen in the analyzes on normal surfaces, aluminum, which is the ball material used during wear, was also added to the analysis in the analyzes on the wear marks.

XPS is the study of the energy distribution of electrons emitted from the surface by exposure to X-Ray bombardment. In principle, all electrons can be studied, from the fundamental to the valence levels. In this respect, the technique differs from ultraviolet photoelectron spectroscopy, in which only valence electrons can be studied. XPS is a technique used to perform chemical analysis of the surfaces of a material. It is based on the principle of measuring the kinetic energy of the scattered electrons of atoms or molecules on the examined surface. This technique is used to analyze elements, inorganic compounds, metal alloys, semiconductors, polymers, catalysts, glass and ceramic samples, paints and inks, and medical prostheses. At the same time, XPS analysis gives information about the amount of oxide in graphene and whether solvents can be removed [92].

4.3.6 Raman Spectroscopy Analysis

Graphene reinforced samples surfaces, and wear marks were analyzed using Raman Spectroscopy. Changes in the structure of graphene found in wear traces during wear were investigated. Raman analysis was performed using the Jasco brand and NRS-

4500 model Raman spectrometer. The Raman spectrometer device used is seen in Figure 4.6.

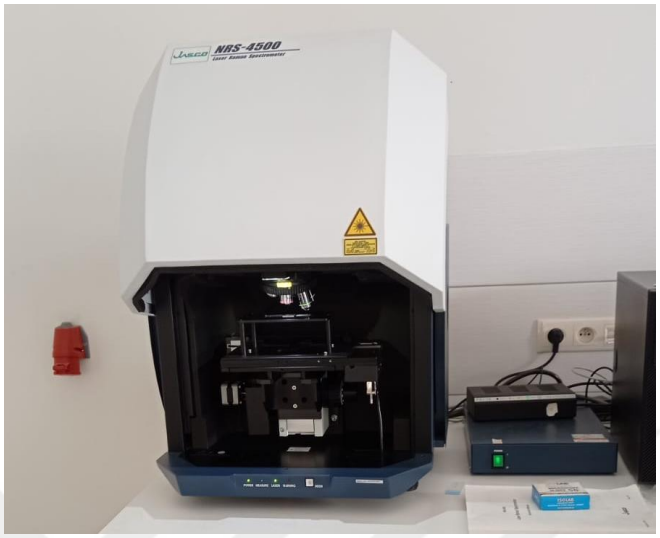


Figure 4.8 Raman spectrometer device

4.3.7 Microhardness Analysis

Microhardness studies were carried out for the obtained nano composite coatings, and a load of 200 grams was applied for 15 seconds in the measurements made on the Matsuzawa HWMMT-X3 brand device. The hardness values were read from the traces obtained with the help of the software in the device. At least 5 measurements were applied to each sample and the averages were recorded as the Vickers hardness value. Microhardness device can be seen in Figure 4.7.



Figure 4.9 Microhardness test device

CHAPTER 5

RESULTS AND DISCUSSION

Ni-P coating and Ni/Gr composite coatings improve tribological properties. However, titanium alloy Ti-6Al-4V has a restricted usage area due to its weak tribological properties. Therefore, it was chosen as the substrate in the present study. Owing to the superior corrosion and mechanical properties of graphene, the tribological properties have been found to have improved with the increase in the amount of graphene nanoparticles reinforced into the structure. Graphene-reinforced Ni matrix composite coatings were produced to see the effects of the above-mentioned properties and the results were compared. In the production of graphene nanoparticle-reinforced Ni matrix composite coatings, coating bath and coating conditions were used while creating the pure Ni-P coating. In these studies, the electroless Ni-P coating bath was composed of 2 g/L graphene nanoparticles together with 0.1 g/L sodium dodecyl sulfate (SDS) particles. In line with other studies in the relevant literature, the coating bath temperature was kept between 90 - 92°C.

Studies in the literature report that heat treatment in electroless nickel coatings causes significant changes in the properties and structure of the coating. Moreover, hardness and wear resistance, particularly in these coatings, can be increased by applying heat treatment. The related literature also reports findings that the highest hardness and mechanical properties occur in Ni-P and Ni-B coatings between 350 - 450 °C temperatures. Hence, a heat treatment temperature of 450 °C was specified for all the coatings, and the heat treatment process was carried out in a tube furnace. To prevent the formation of oxide layers on the surface of the coatings during the heat treatment and to remove the oxide layers that may have formed during the coating, the coatings were subjected to the 450 °C heat treatment for 1 hour in an argon atmosphere.

5.1 Structural Analysis

5.1.1 SEM Analyses

In the electroless nickel plating, nickel grains are nucleated first at the beginning of the plating process. These nuclei act as catalysts and create reactions. Owing to Nickel nuclei, which transport the electrons that occur as a result of the reactions that take place, elements such as phosphorus or boron are reduced in the structure of the reducing agents and nickel. In this autocatalytic process, after the formation of nickel nuclei, nickel phosphorus grows on these nuclei and forms clump structures. These clumps, which then coalesce and grow towards the interface between the substrate and the coating bath, turn into nodules. When the electroless coating process is completed, a nodular-grown nickel phosphorus coating is obtained.

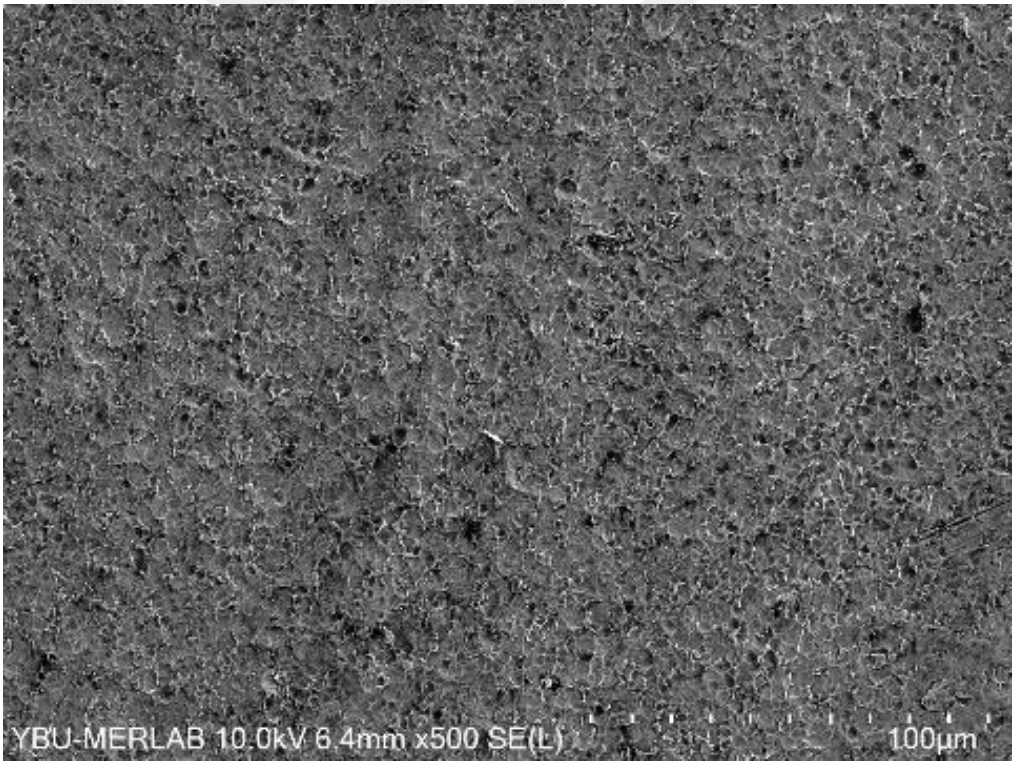


Figure 5.1 SEM analysis of Ti-6Al-4V substrate

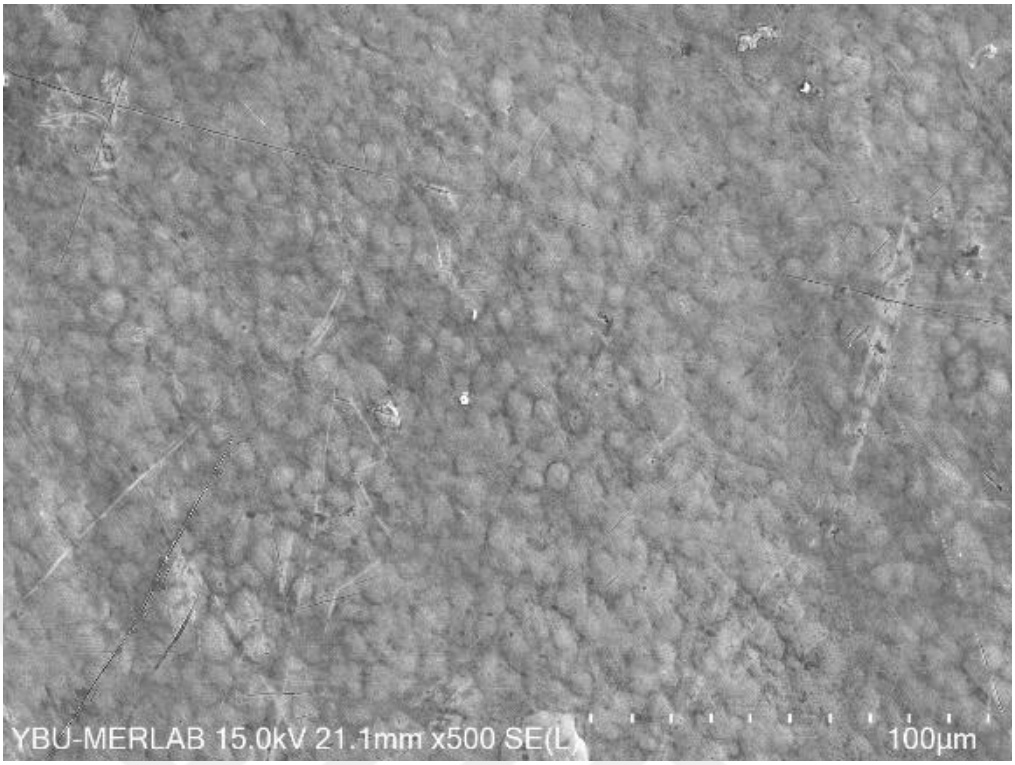


Figure 5.2 SEM analysis of a Gr-Ni-P composite coating

Figures 5.1 and 5.2 display the SEM images of the uncoated Ti-6Al-4V substrate and graphene reinforced nanocomposite coating, respectively. The microstructure of the Ti-6Al-4V alloy consists of a coaxial α phase and a small amount of intergranular β phase [98]. This microstructure of the titanium alloy substrate, as seen in Figure 5.3, was completely changed by coating by the electroless coating method, as a result of which a new non-porous and crack-free microstructure was obtained. Thus, the above-mentioned formation mechanism of the nickel phosphate coating was realized, and a homogeneously deposited nodular microstructure was successfully obtained. This nodular microstructure is known to be characteristic of nickel phosphate coating [65].

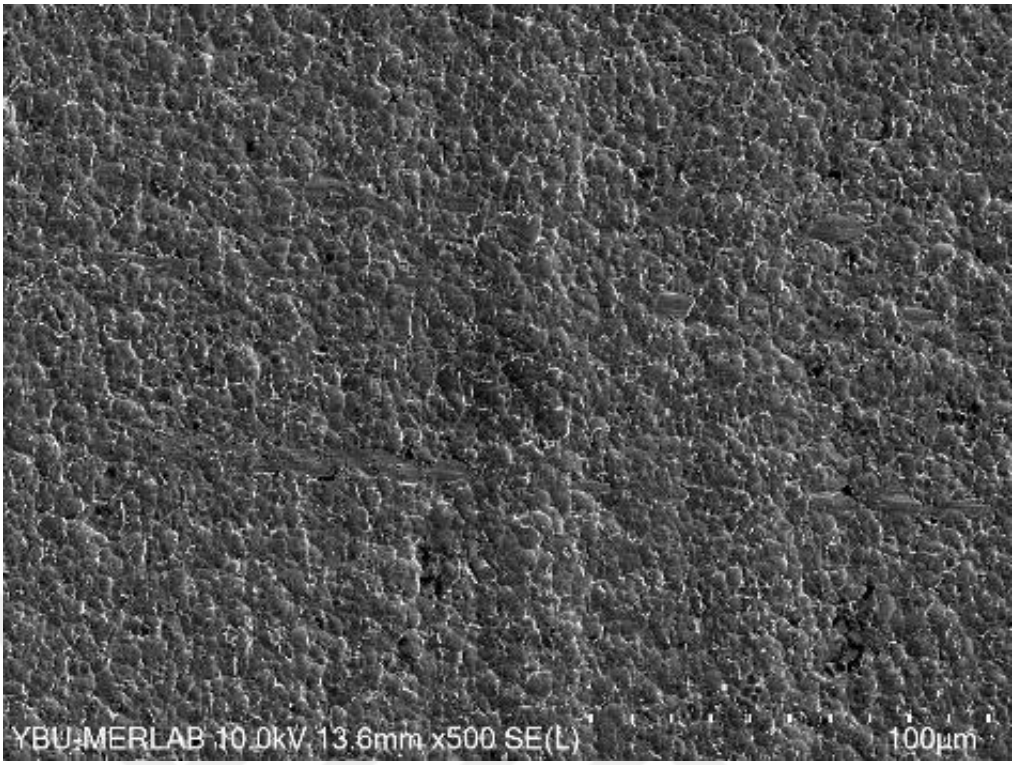


Figure 5.3 SEM analysis of heat-treated Ti-6Al-4V substrate

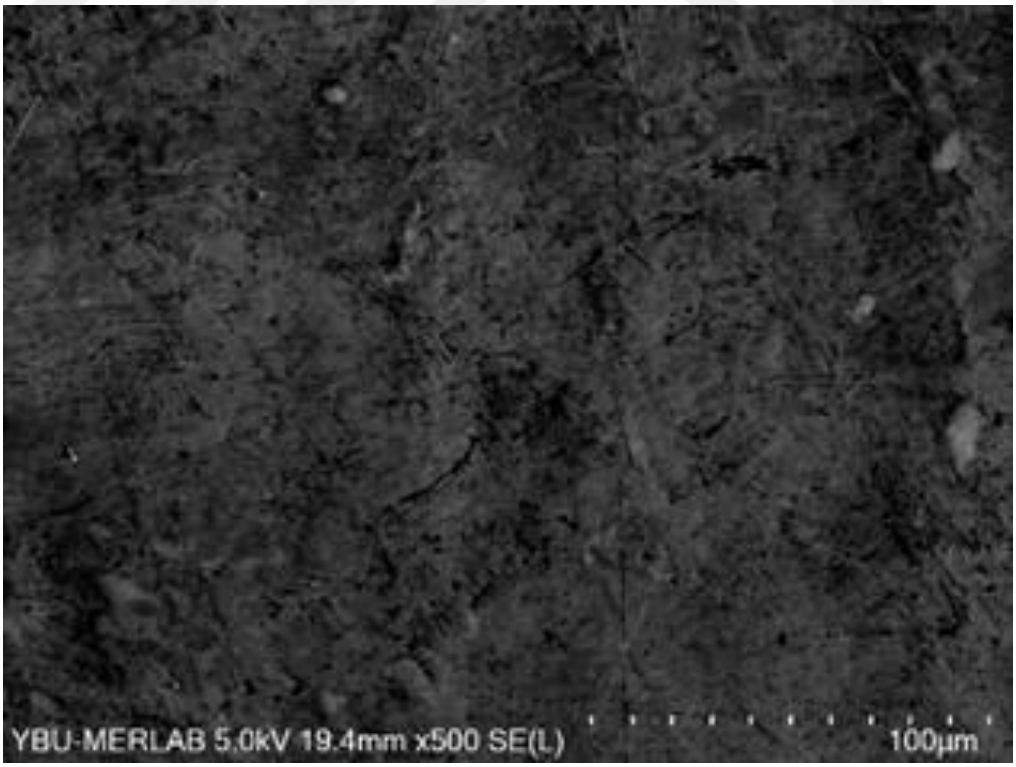


Figure 5.4 SEM analysis of heat-treated composite

A 450°C heat treatment was applied to the samples to examine the effect of heat treatment on the graphene reinforced nickel composite coating. The SEM images of the heat-treated titanium alloy substrate and composite coating are shown in Figures 5.3 and 5.4, respectively. In the heat-treated titanium alloy, while the ratio of titanium increased, the α and β phase shapes have reduced. Heat treatment causes significant changes on the mechanical and microstructural properties of the nickel phosphate coating [56]. With the heat treatment, the nodular structure of the composite coating changed, the bumps in the structure disappeared and a smoother structure was obtained.

Parallel to the common practice in the literature [99], EDS analysis was conducted to determine the elements and their ratios in the structure. Figures 5.5 - 8 display images of the EDS analyses of the surface of uncoated, heat-treated uncoated, composite coated, and heat-treated composite coated samples, respectively. In Figures 5.5 and 5.6, heat-treated and non-heat-treated samples without the electroless coating are displayed. Figure 5.5, displaying the EDS analysis of the uncoated sample, manifests that the elements belonging to the Ti6Al4V alloy, which is the substrate material, are present. These analyses contain elements of titanium, aluminum, vanadium, and carbon. However, in Figures 5.6 and 5.7, in the electroless nanocomposite coating, the alloying elements have been replaced by the nanocomposite coating elements Ni, P, and carbon.

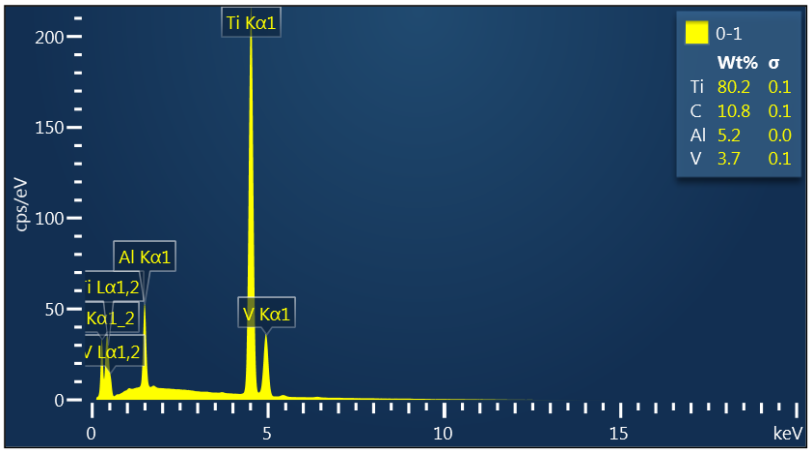


Figure 5.5 EDS analysis of a Ti-6Al-4V sample

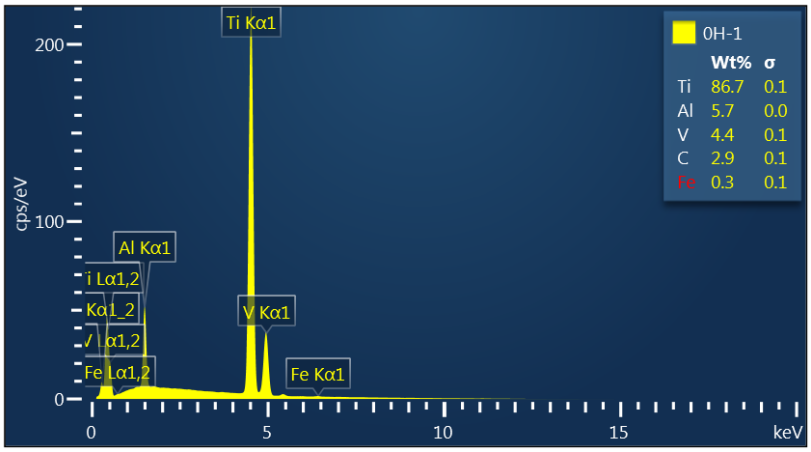


Figure 5.6 EDS analysis of a heat-treated Ti-6Al-4V sample

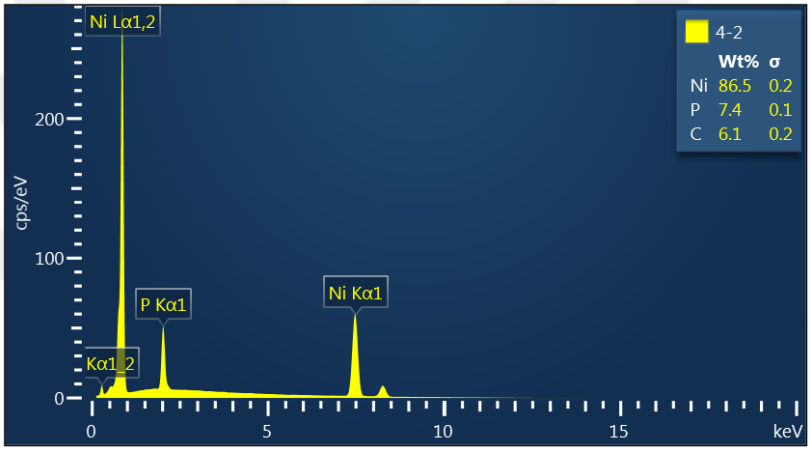


Figure 5.7 EDS analysis of a composite coated sample

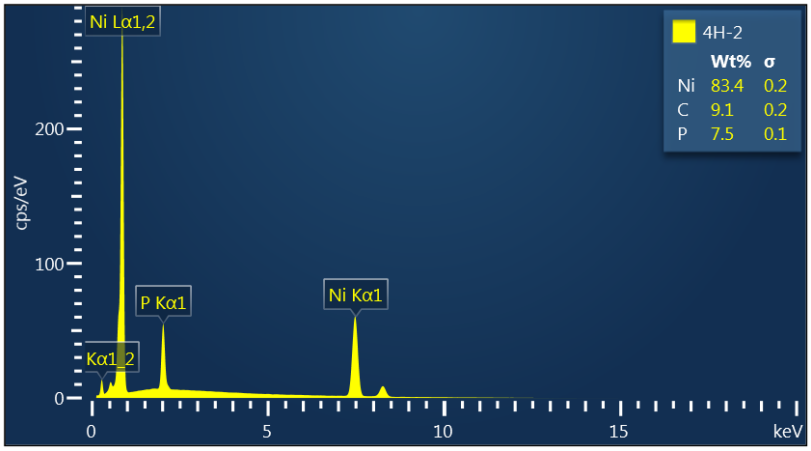


Figure 5.8 EDS analysis of a heat-treated composite sample

The elemental analysis of the effect of heat treatment on the uncoated sample can be observed in Figures 5.5 and 5.6. Accordingly, the carbon ratio of pure Ti-6Al-4V substrate decreased with the effect of heat treatment, while the ratios of the other elements increased. On the other hand, the images from the elemental analysis of composite coating and heat-treated composite coating are shown in Figures 5.7 and 5.8, where an increase in the amount of carbon and phosphorus and a decrease in the amount of nickel in the heat-treated sample can be observed. The change in the carbon ratio is more striking in the uncoated sample when compared to that in the composite sample.

5.1.2 XRD Results

Heat treatment has a significant effect on hardness and similar properties in the electroless nickel phosphate coatings. The reason for this effect is the large microstructural effects that occur on the microstructure during heat treatment of the electroless nickel phosphate coatings. Ni-P coatings have an amorphous crystal structure. As known, amorphous materials are metastable and turn into a stable phase when heated to certain temperatures [65]. This is called the transformation of the amorphous structure to the crystalline phase. Figures 5.9 and 5.10 show the XRD plots of the uncoated pure sample and the composite coating, respectively. The crystal structure of the uncoated sample in Figure 5.9 is found have turned into an amorphous crystal structure after the composite coating process as can be seen in the blue graph in Figure 5.10. A careful examination of the XRD pattern of electroless nickel-phosphate-graphene coating shows that amorphous and crystalline structures coexist, and a broad peak exists in the face-centered cubic (F.C.C) Ni (111) at the point where two-theta (2θ) equals 45 deg. The XRD image of the graphene-reinforced composite coating after heat treatment turned into a crystalline structure, as seen in red in Figure 5.9; that is, a phase change from amorphous to crystalline had occurred.

On the other hand, the average grain sizes were calculated for each sample using the Debye-Scherrer formula, and the mean crystalline dimensions of the pure and composite samples were found to be 38.52 and 30.98, respectively. The shrinkage of the grains in the material increases the amount of grain boundary in the unit volume,

causing the material to become stronger [93]. In this case, it can be interpreted that the strength of the graphene-reinforced nickel matrix composite coating is higher than that of the uncoated sample.

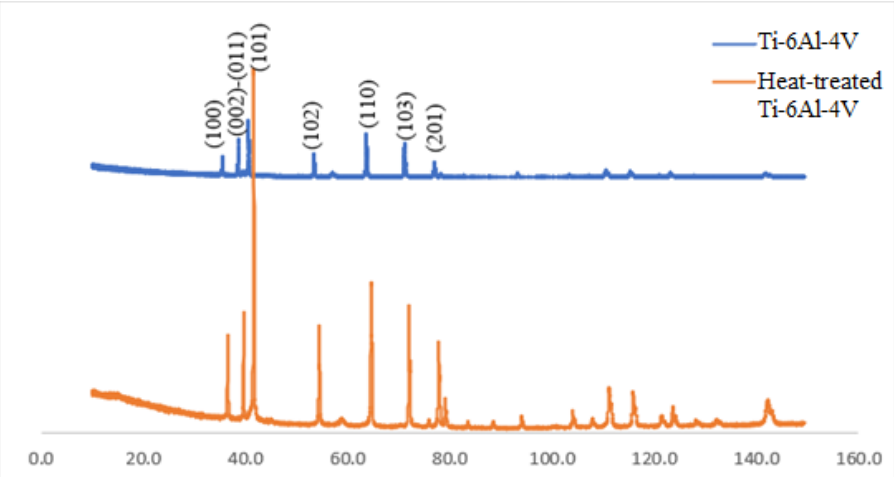


Figure 5.9 Ti-6Al-4V XRD patterns

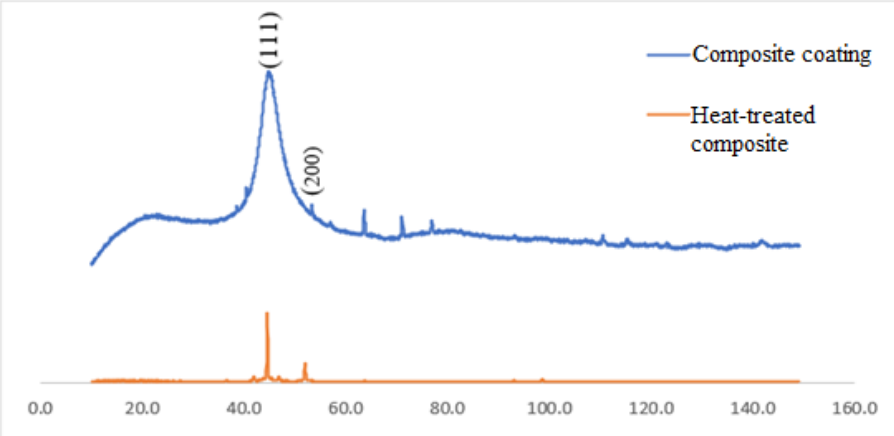


Figure 5.10 Nanocomposite coating XRD patterns

5.1.3. Coating Thickness Results

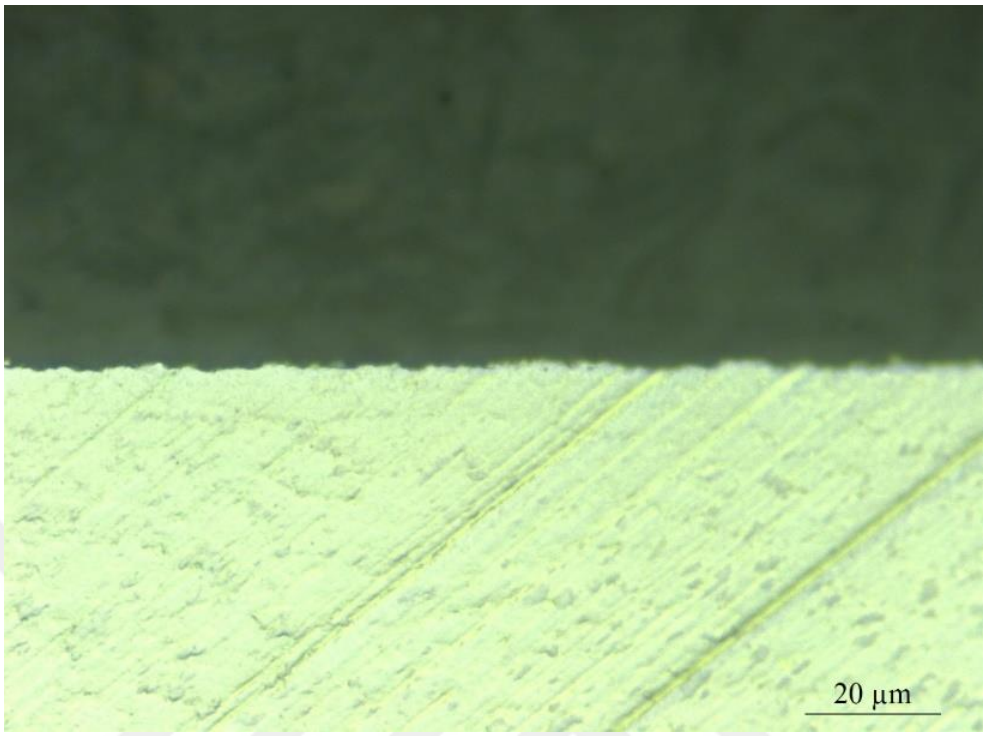


Figure 5.11 A section of Ti-6Al-4V substrate

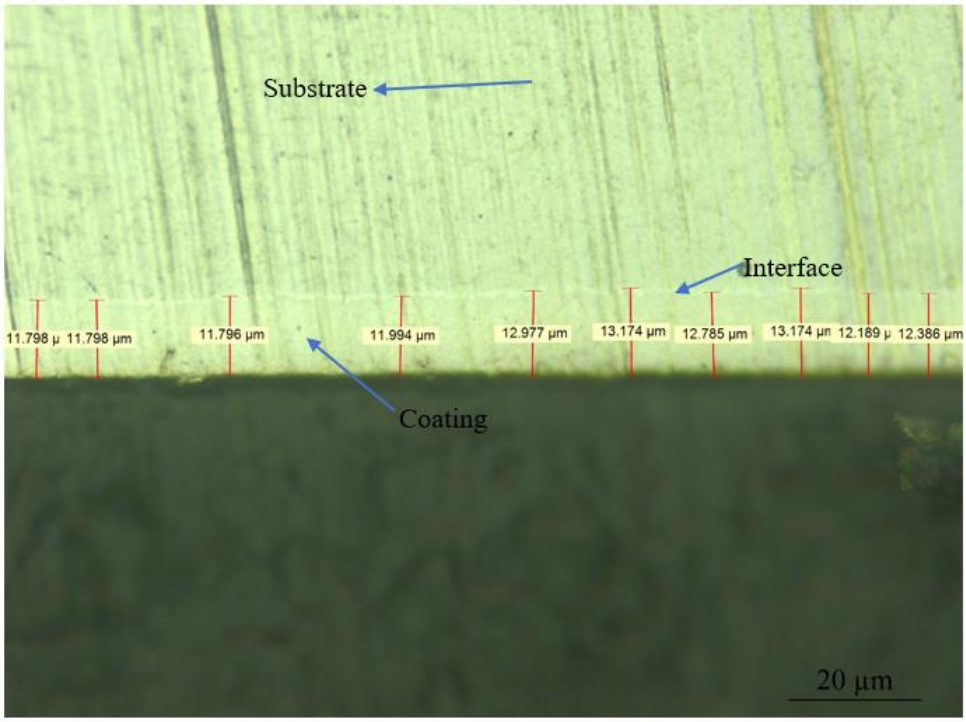


Figure 5.12 A section of Ni-P-Gr coating

Sections were taken from the uncoated and composite coated samples, and the coating thicknesses were measured by using a microscope. These sectional images are displayed in Figure 5.11 and Figure 5.12 for the titanium alloy substrate and the nanocomposite coating, respectively. In Figure 5.12, the substrate, the substrate-coating interface, and the coating are clearly visible. It can be seen that the interface lies homogeneously on the substrate. Since the electroless coating process takes place in the bath solution, it is known that a homogeneous coating thickness is obtained regardless of the substrate shape, and Figure 5.12 supports this information [34, 35]. On the other hand, with the use of the microscope's own scale, ten different measurements were taken on the coating. These measurements yielded a coating thickness of 12.47 μm. In a study by Meshram et al. [105], Ni-P and Ni-P-Gr coatings were successfully deposited on the substrate via the electrodeposition method for 1 hour. As a result, the coating thickness for Ni-P coating was approximately 3.30 μm, while the coating thickness was found to be approximately 7 μm for each ratio with graphene reinforcement at different ratios. Graphene added to the Ni-P matrix provides more surface area for the reduction of nickel-phosphorus, which may increase the deposition rate leading to the observed increase in the thickness of the graphene-reinforced coatings [105]. Although the coating time of this study is the same, the reason for obtaining higher coating thickness than that in Meshram's study can be explained by the addition of graphene at a higher rate. As a matter of fact, the volume of graphene entering the structure increases due to the increase in the graphene added to the bath composition by weight [19]. Likewise, Yasin et al. [106] applied graphene-reinforced Ni-P coating at different rates with the electrochemical coating technique in their study and obtained the maximum coating thickness at the maximum graphene ratio (0.4 g/L).

5.1.4 XPS Results

Figures 5.13 and 5.14 show the XPS analysis and wear scratch of the coated sample, respectively. The Ni2p spectrum of graphene-reinforced nickel nanocomposite coating is characterized by a highly intense bond at 853.3 eV. This peak could be related to the Nickel [94, 95]. The chemical state of graphene is sp2, and the binding energy of this chemical state is approximately 284 eV [96]. Detailed images of the XPS peaks are shown in the graphs labelled as a, b, c, and d in Figure 5.15. Accordingly, the C1s peak was observed at approximately 284 eV in graphs a and b. On the other hand, in graphs c and d, the Ni2P spectrum is observed at about 854. These peaks indicate the presence of nickel and graphene in XPS analysis. In addition, the Al2p peak belonging to the counter material Al_2O_3 was searched on the wear marks during the analyses, but none was not found. This can be interpreted as the hardness of the coating being lower than that of the wear ball.

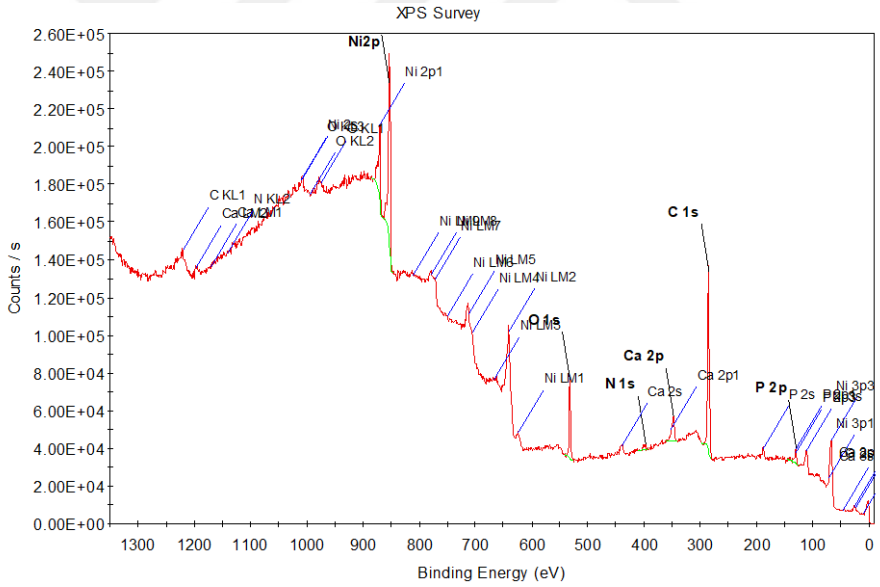


Figure 5.13 Composite coating XPS

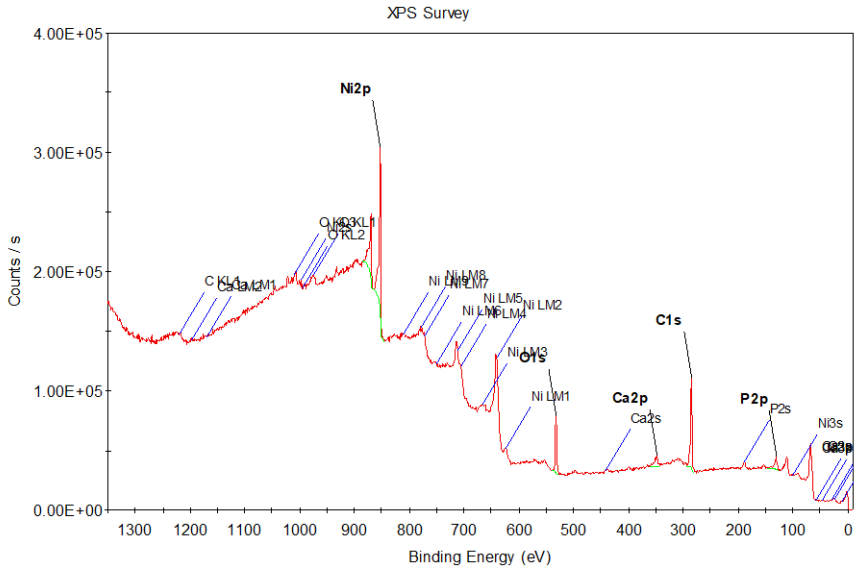


Figure 5.14 Composite coating wear scarf XPS

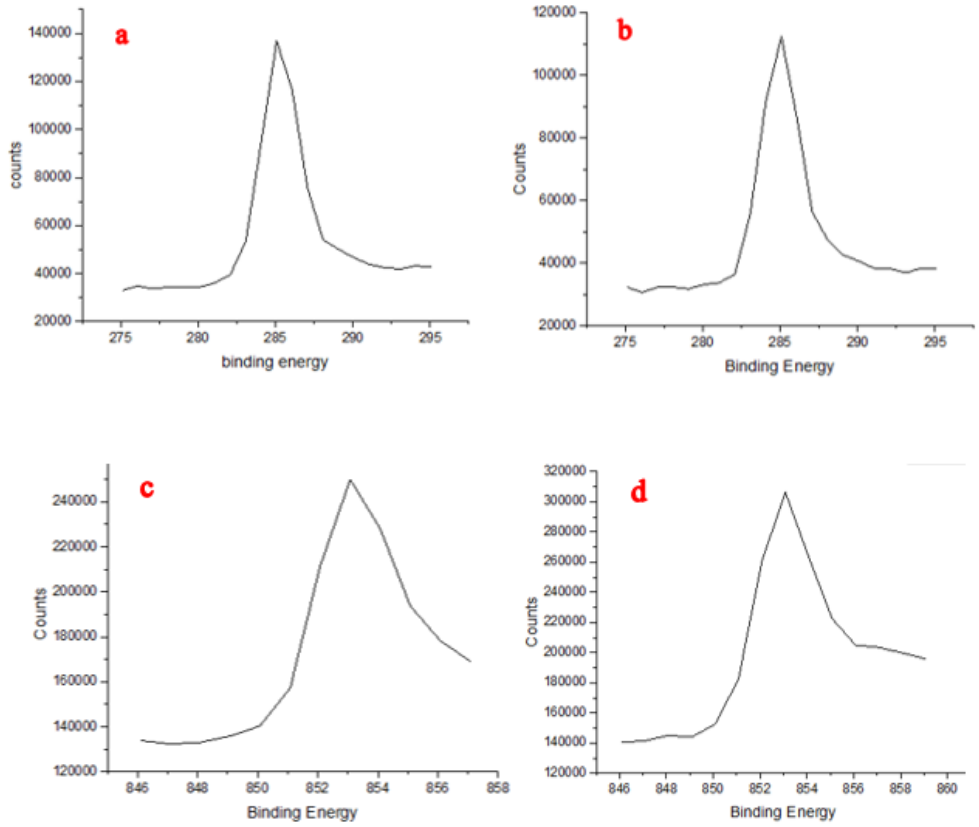


Figure 5.15 C1s and Ni 2p3/2 regions of high-resolution XPS spectra obtained with carbon and Ni in the Ni-graphene nanocomposite coating: a) C1s on surface b) C1s on scratch c) Ni2p on surface d) Ni2p on scratch.

5.1.5 Raman Spectrum of Composite Coating

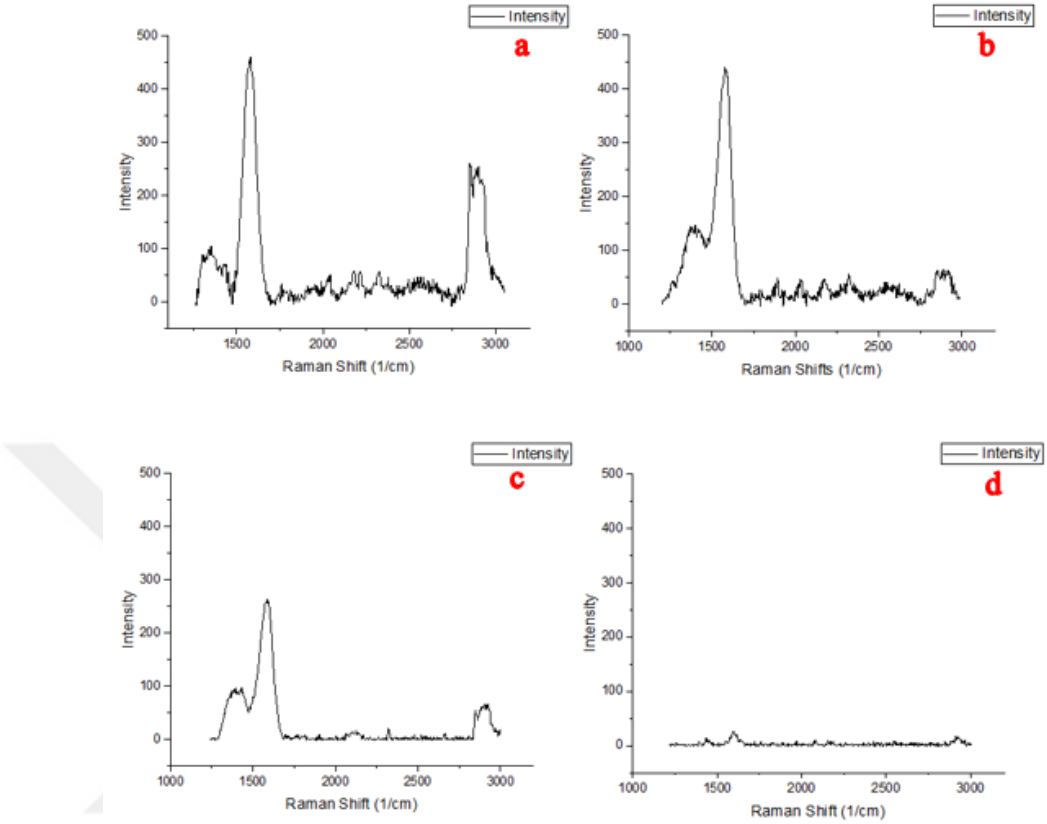


Figure 5.16 Raman spectroscopy of composite coating: a) Coated surface b) Coated scratch c) Coated heat-treated surface d) Coated heat-treated scratch

Raman spectroscopy, which plays an important role in the structural characterization of graphite materials, provides important information about graphene defects and stacking. With the Raman spectrometry, graphene can be clearly distinguished from graphite. The main features in the graphite/graphene Raman spectrum are represented by the D, G, and 2D peaks. A G peak at about 1580 cm^{-1} and a 2D peak at about 2700 cm^{-1} are observed in the graphite samples. The 2D tape of graphite is observed to always have a shoulder of approximately 2650 cm^{-1}, and this shoulder represents graphite. The D band is located at approximately 1330 cm^{-1} and is indicative of the defects in the sample [101 - 103]. Figure 16 shows the Raman spectra of a-d graphene-reinforced composite coatings. As can be seen in the figure, each sample has a D peak at approximately 1370 cm^{-1}, a G peak at 1590 cm^{-1}, and a 2D peak at 2790 cm^{-1}, and

there is no shoulder at the 2D peak in any of the samples. The Raman spectra obtained from the composite coatings confirmed that graphene has been successfully reinforced into nickel-phosphorus obtained by the electroless coating method. The samples without heat treatment are shown in Figures 5.16 a and b, which shows that the intensity of the D and 2D peaks increased with the effect of wear. This situation can be interpreted as the increase in defects with wear. On the other hand, Figures 5.16 c and d show the results obtained on the surface and wear marks of the samples after the heat treatment. The densities at all peaks decreased with the effect of heat treatment and approached zero with the effect of abrasion. Graphite formation has occurred, and the graphene peak has decreased with the increasing temperature during abrasion. Graphite, which increased further with the heat treatment, caused the graphene peak to take a minimum value with the temperature formed when abrasion was applied to the heat-treated sample. As a result, graphite is one of the most widely used lubricants [107], and it can be deduced that the lubricating property increases with the increase of graphite peak with heat treatment and wear.

5.2 Tribological Behavior of the Substrates

5.2.1 Microhardness Measurement Results

The hardness of the produced samples was measured by using the Vickers hardness test method. Five different hardness measurements were made for each sample. Average hardness values are shown in Figure 5.17. Accordingly, while the average hardness values were 327.96 HV for the alloy, the hardness increased to 359.14 HV with the effect of heat treatment. With graphene-reinforced Ni-P coating via electroless coating process, the hardness of the substrate increased by about 34%, which increased to approximately 73% with heat treatment. This is in line with the studies in the literature [88, 90, 91, 108].

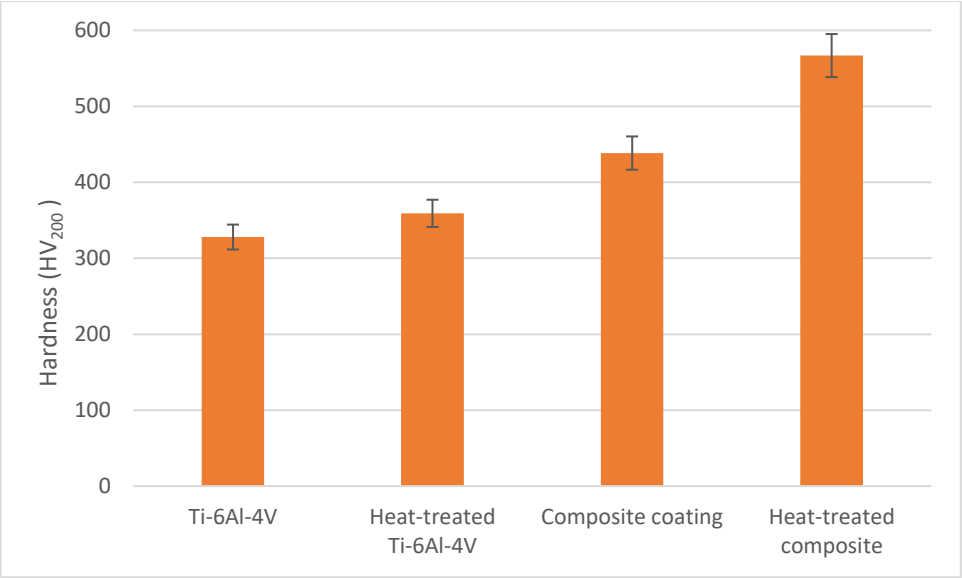


Figure 5.17 Average microhardness values

The mechanisms for strengthening metals and their alloys are stress hardening, grain boundary strengthening and grain size reduction, dispersion hardening, solid solution hardening, crystal orientation and aging. However, in nanocomposite coatings, hardness is gained by grain boundary strengthening and grain size reduction, crystal orientation and dispersion hardening mechanisms [109].

On the other hand, many studies in the literature reported that the addition of the second phase increases the microhardness, which is attributed to the second phase particles providing grain refinement and charge transfer [110]. Moreover, the related literature reports that the graphene added to the nickel matrix increases the hardness [88, 90, 91, 108, 111]. That is, graphene-reinforced Ni-P coating provides better wear properties than Ni-P coating with the electroless coating method to improve the wear properties of the titanium alloy substrate. Mindivan et al. [91]. attributed the increase in hardness to the incorporation of graphene into the face-centered cubic (fcc) nickel lattice. The presence of graphene nanoparticles entering the fine-grained metal matrix prevents the easy movement of dislocations, increases the resistance to plastic flow, and the inherent high strength of graphene provides a higher degree of hardness [112]. In addition, the increase in hardness due to graphene reinforcement is a result of the

dispersion strengthening mechanism, and this behavior is consistent with the previously published literature [111].

Heat treatment significantly changes the hardness of the electroless nickel phosphorus coating [47, 58]. As a matter of fact, while the average hardness of the nanocomposite coating was 438.52HV, it increased by approximately 29% with the effect of heat treatment and became 566.9HV. When these results are compared with the XRD plots, it can be concluded that the reduction in crystal size by heat treatment increases the hardness.

5.2.2 Wear Mechanisms

After the wear, SEM images, shown in Figures 5.18 a-b and 5.19 a-b, were examined. It was observed that sliding lines parallel to the ball had occurred with the effect of plastic deformation during the sliding process of the ball on all wear trace surfaces; that is, abrasive wear was found to have occurred. In Figure 5.18, illustration a represents a SEM image before heat treatment, while illustration b is the heat-treated sample. Partial debris is also visible on the wear surface in Figure 5.18 a. The cause of the spills is the formation of cracks as a result of fatigue on the sample surface or just below this surface during the sliding process, and then the particles that break off around the crack [97]. It is seen in illustration b that these adhesive wear marks formed in illustration a are reduced by heat treatment. Surface hardness affects the formation of the adhesive bond. As the surface hardness increases, the deformation under load will decrease and the surface film layer will be more resistant to damage. As a result, the adhesive bond between surfaces will weaken and adhesive wear will decrease [113]. The increase in the hardness of the titanium alloy with the effect of heat treatment proves that the amount of adhesive wear in Figure 5.18 b is less than that in 5.18 a.

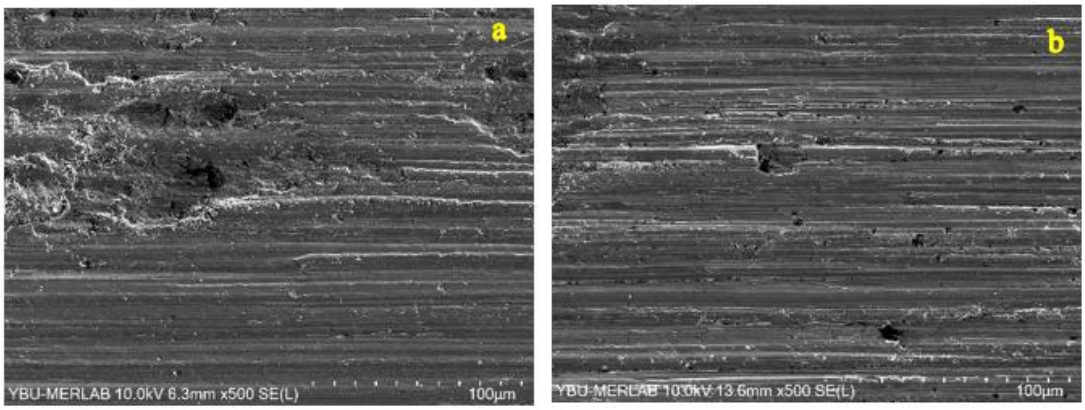


Figure 5.18 Wear traces of Ti-6Al-4V substrates a) Non-heat-treated and b) Heat-treated.

The stresses created on an object with a load exerted by another object form cracks under the surface as the surface below rises above the tensile strength of that object. When these cracks under the surface progress and reach the surface, the surface particles are released in the appearance of shells. This method of wearing is known as "delamination". When the wear surface is examined in Figure 5.19 a, as it can be understood from the wear microstructure, plastic deformation occurred as a result of the forces acting on the part surface, and this caused the formation of microcracks. This type of wear, in which the coating is detached from the surface in layers, also shows delamination as described above. However, traces of wear due to abrasive wear can also be observed. However, the dominant wear mechanism in the untreated nanocomposite coating is delamination. Abrasive wear resistance decreases with increasing hardness [114], which proves the change in the dominant wear mechanism in composite pavement in Figure 5.19. The change in the wear mechanism is expected when compared to the hardness results. Figure 5.19 b shows the microstructure of the heat-treated composite coating. Compared to Figure 5.19 a, the microstructure is found to have changed significantly as mentioned previously. With the effect of the heat treatment, the structures in the composite coating that were broken off in layers were replaced by grooves and microcracks. These grooves, which occur in parallel with the abrasive ball during wear, show that abrasive wear mechanism is the dominant wear mechanism. In other words, with heat treatment, the dominant wear mechanism has become abrasive instead of delamination. Figure 5.20 shows the SEM photograph of the heat-treated composite material at higher magnification. As can be seen here,

although the loads occurring on the sample surface during wear caused cracks with plastic deformation, these cracks could not progress and break the layer. Accordingly, it can be deduced that heat treatment increases the wear resistance of the coating. Considering the hardness results, the wear resistance is higher in the heat-treated composite coating, where maximum hardness is achieved, and it is normal for the wear to occur in this way.

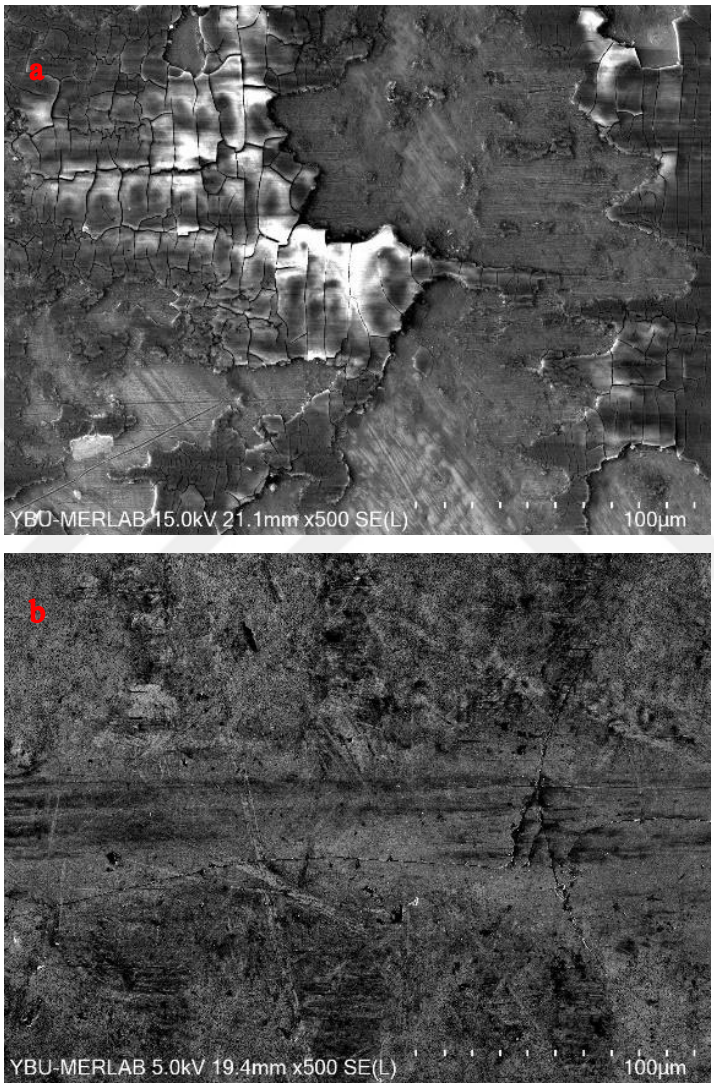


Figure 5.19 Wear traces of composite coating substrates: a) Non-heat-treated and b) Heat-treated

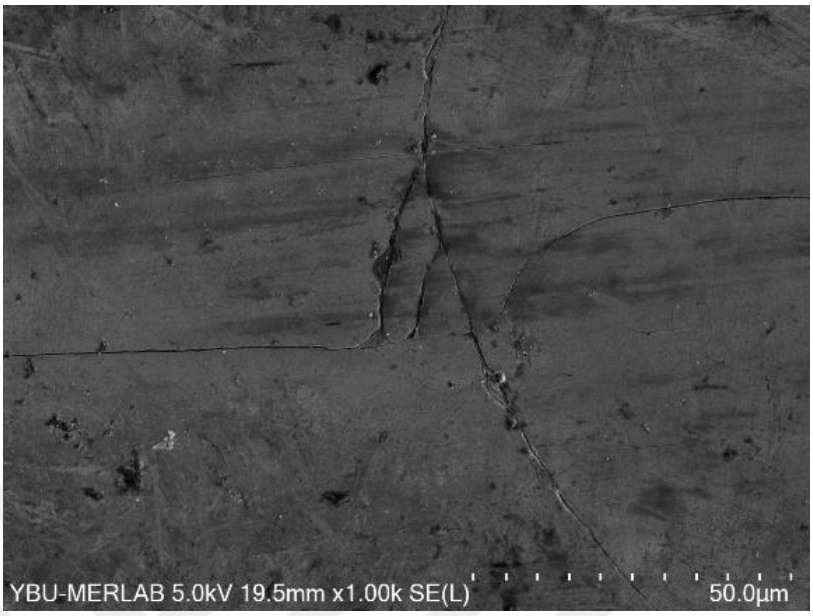


Figure 5.20 High magnification SEM photograph of heat-treated composite wear mark

Aydın [115] produced Ni-P-Gr coatings with the electrodeposition method in his master's thesis and observed in the wear mechanism that graphene reduced the amount of adhesive wear and the wear track size of the wear ball. In Figures 5.18 a and 5.18 b, parallel corrugated structures formed by the abrasive in the uncoated sample were seen in a large area in the uncoated sample, while they were formed in a smaller area in the composite coating, in Figures 5.19 a and 5.19 b. The ball contact surface is observed to have reduced. This can be interpreted as the sample showing greater resistance to the abrasive. In other words, due to the lubricating property of graphene, the graphene-reinforced composite coating and heat treatment seem to increase the wear resistance of the titanium alloy substrate. The same result was observed when compared with the Raman Spectroscopy results.

5.2.3 EDS Analysis of Wear Scratches

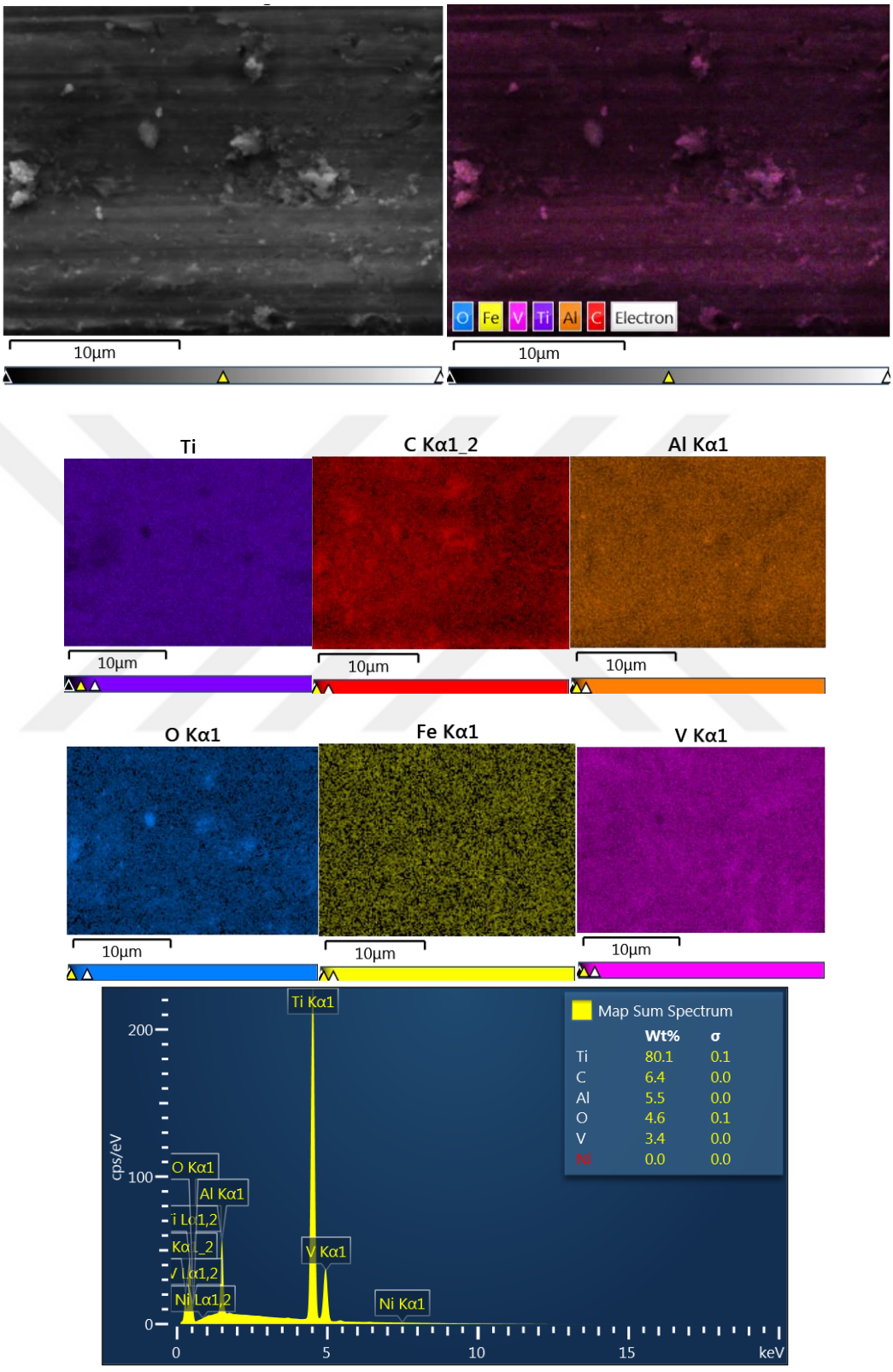


Figure 5.21 EDS mapping of a non-heat-treated Ti-6Al-4V sample

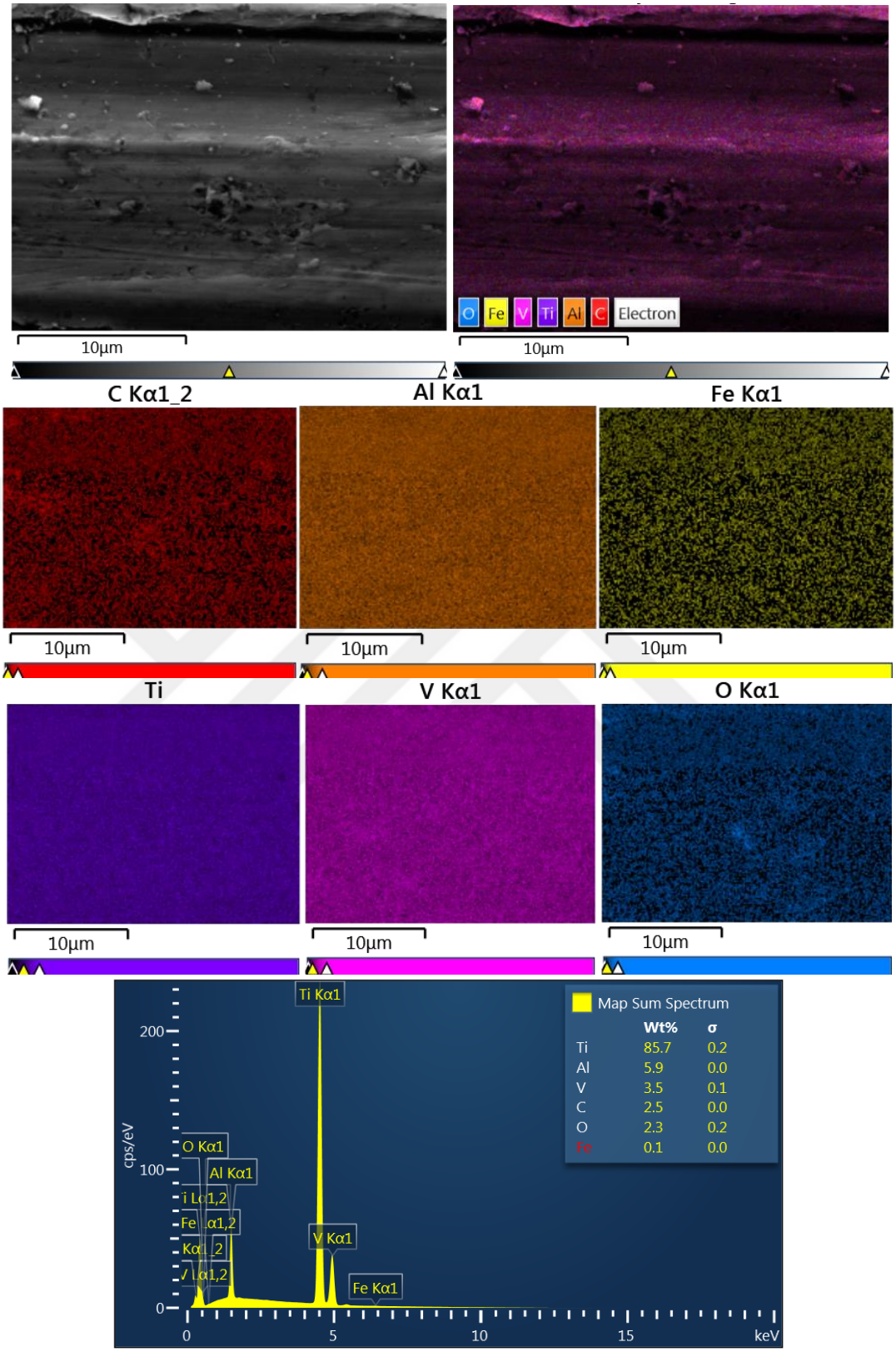


Figure 5.22 EDS mapping of a heat-treated Ti-6Al-4V sample

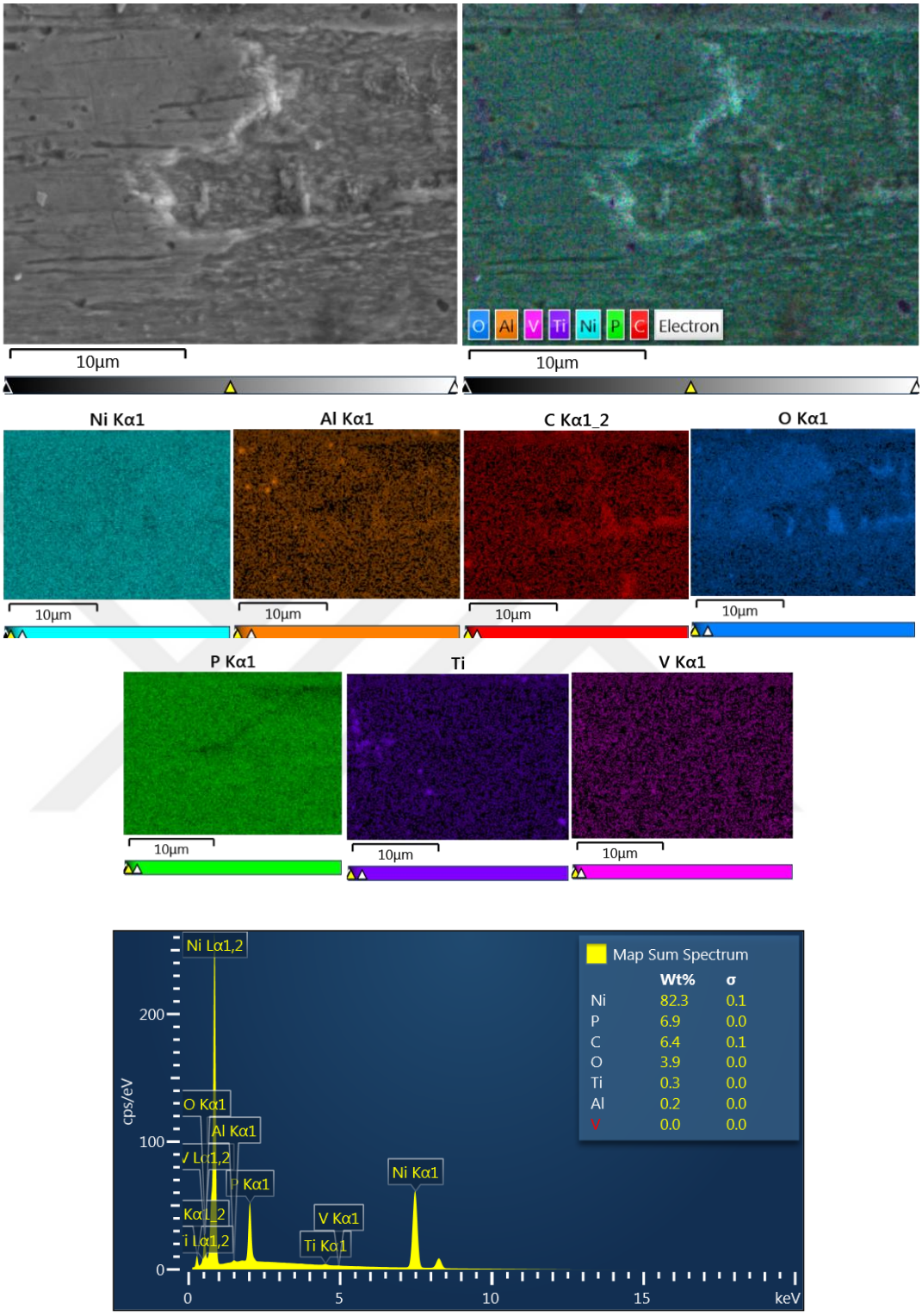


Figure 5.23 EDS mapping of a non-heat-treated composite sample

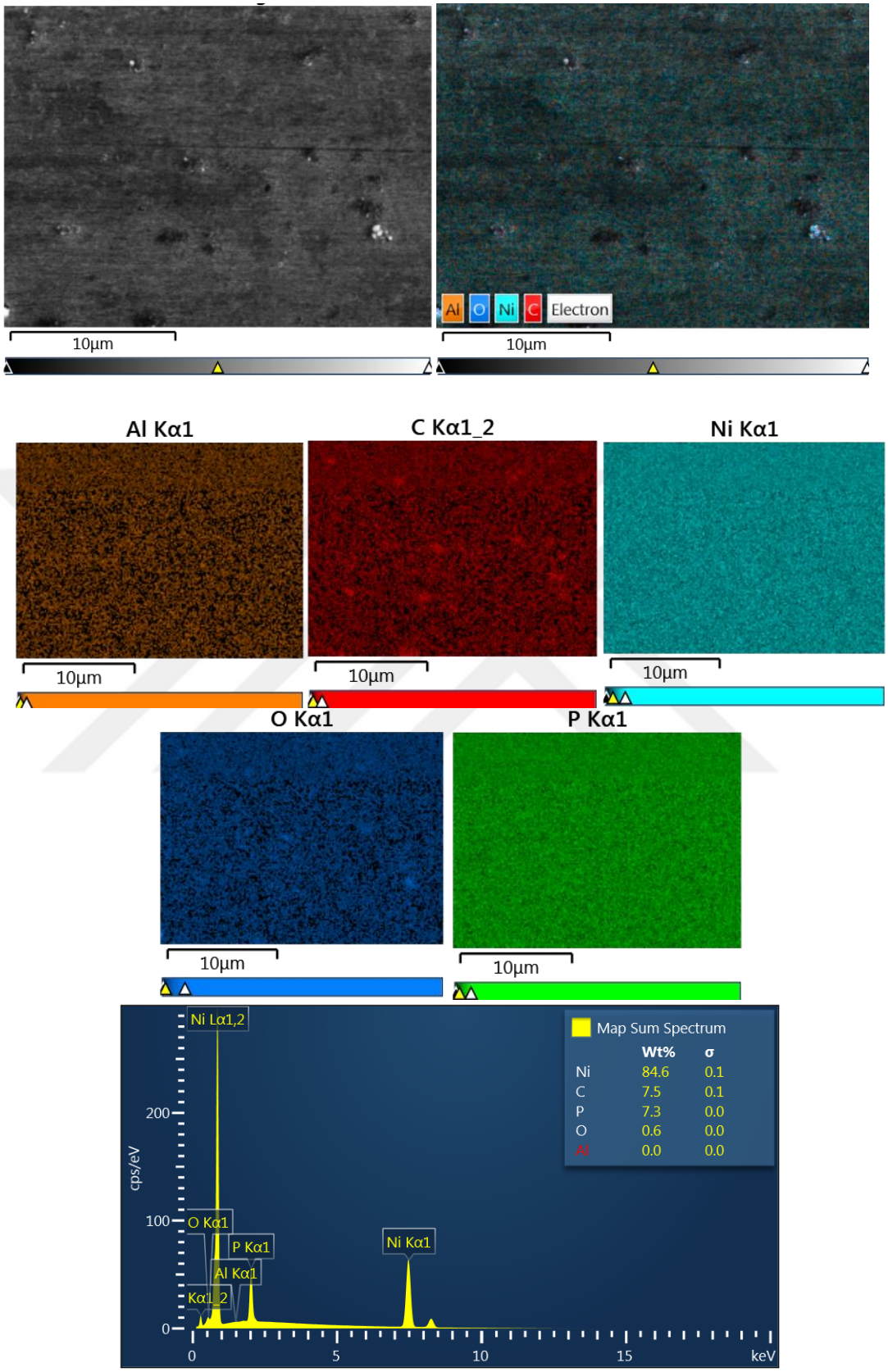


Figure 5.24 EDS mapping of a heat-treated composite sample

By means of EDS analysis, the elements in the structure and the ratios of the elements in the structure were determined. In similar studies in the literature, the elements in the structure and their amounts were also determined by EDS analysis [103]. Figures 5.21-24 demonstrate the results of the EDS mapping analysis of the samples. An examination of all the figures revealed that the nickel and phosphate elements were homogeneously distributed in the structure. The carbon element seen in the structure was due to the graphene particles added to the bath solution. The oxygen ratio in the uncoated samples in Figures 5.21 and 22 decreased in the composite coatings in Figures 5.23 and 24. This can be explained by the decrease in oxygen affinity of titanium due to the coating [84]. The presence of alloy elements in the EDS map analysis on the non-heated composite coating in Figure 5.23 and their absence in Figure 5.24 can be explained by the fact that the delamination type wear mechanism mentioned in the SEM analysis is not visible in the heat-treated sample. The presence of alloy elements here is an indication that the layers have been removed from the coating as a result of delamination because these elements did not appear in the EDSs taken from the surface.

5.2.4 Wear Scratch Widths

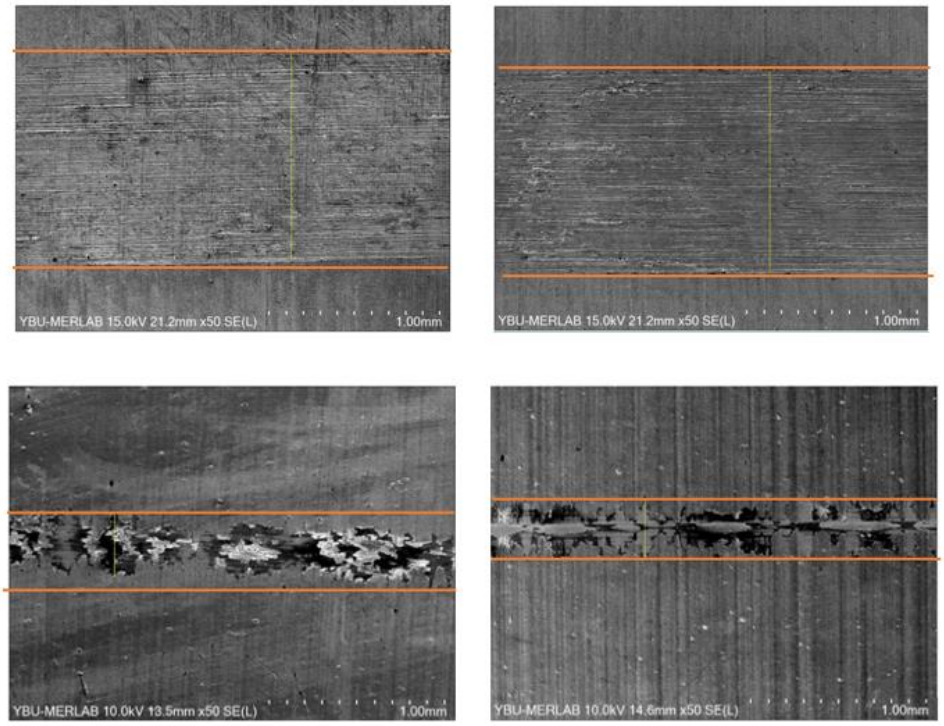


Figure 5.25 SEM morphologies of the wear tracks of substrates: a) Ti-6Al-4V b) Heat-treated Ti-6Al-4V c) Composite coating d) Heat-treated composite coating.

The trace widths of the SEM images of the wear marks were measured using the ImageJ software program. Trace widths are displayed in Figure 5.25 between a-d. The trace width was measured as 1.226 mm in the pure sample without coating, and heat treatment was decreased to 1.127 mm for the heat-treated pure sample. Especially with the graphene reinforcement, which is known to increase wear resistance, the visibly reduced trace width was measured as 0.367 mm in the untreated composite, while it slightly reduced to be 0.342 mm with the effect of heat treatment. Studies by Mindivan et al. [91] Algül et al. [108] in which nickel-phosphorus graphene was produced by the electrocoating, revealed that the width of the wear scar would be less than the substrate material as the amount of graphene increased plastic deformation and width of wear marks on the nickel-graphene composite coating surface are reduced because the composite coating increases hardness and graphene has solid-lubricating properties [71].

5.2.5 Specific Wear Rates

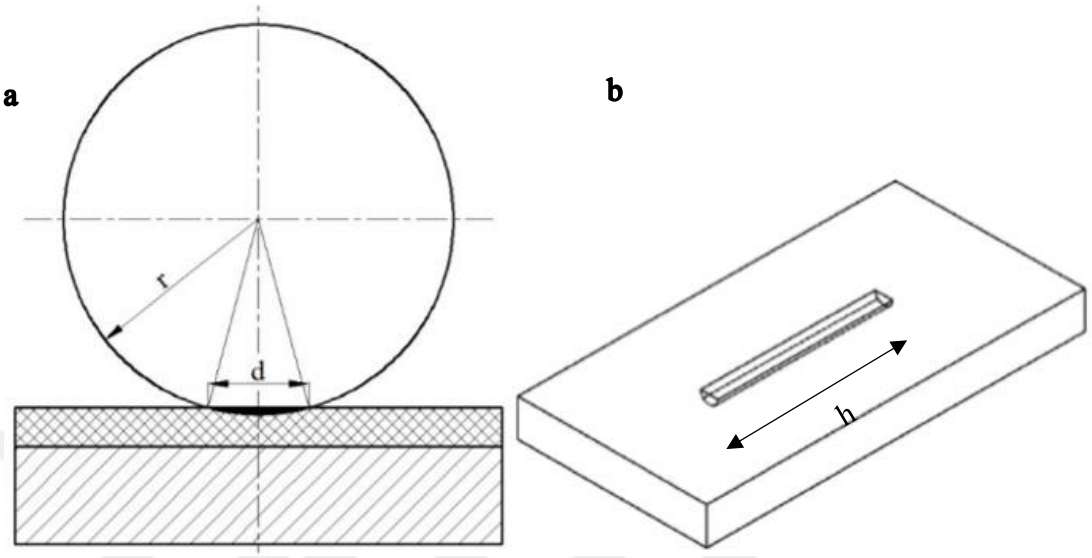


Figure 5.26 The wear scar generated by reciprocating sliding motion of the ball on a flat specimen; a) 2D view of the wear scar [116] b) 3D view of the wear scar [117].

Wear volume loss was calculated using geometric formulas from the schematic images shown in Figure 5.26. In the figure, r represents the radius of the abrasive ball, d represents the scratch width, and h represents the stock of wear test. After calculating the wear volume loss, the specific wear rate was calculated using the formula 5.1,

$$W_r = \frac{W}{NL} \text{ [116]} \tag{5.1}$$

where W_r is the specific wear rate in $mm^3/(Nm)$, N is the normal load in N, L is the sliding distance in m, and W is the calculated wear volume mass in mm^3.

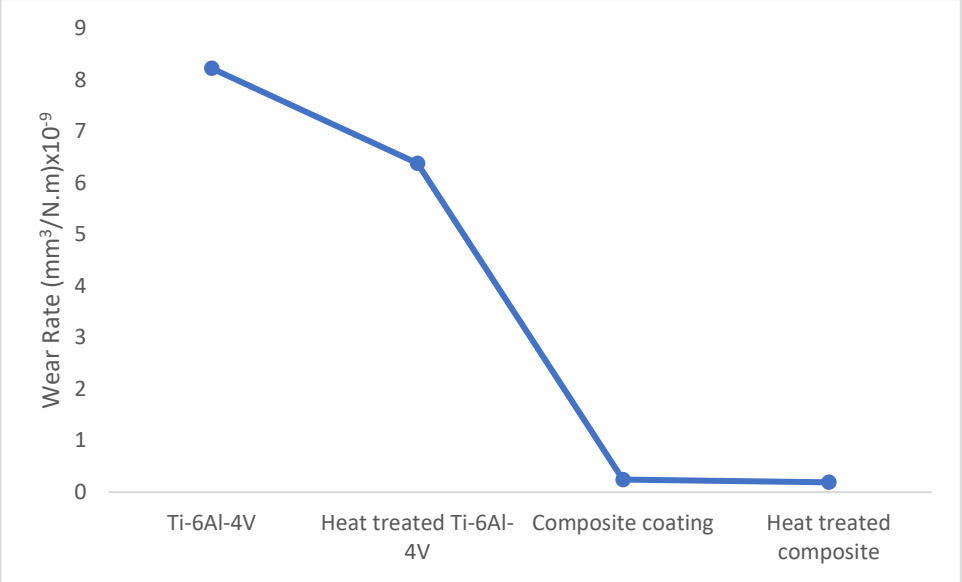


Figure 5.27 Specific wear rates

The specific wear rate of each sample is shown in Figure 5.27. The calculated wear rates were 8.22, 6.38, 0.24, and 0.19 ($x10^{-9}$) mm^3/Nm respectively. The specific wear rate for the titanium alloy was reduced by about 22% with the effect of the heat treatment. With the graphene-reinforced nickel phosphorus coating of Ti-6Al-4V, the wear rate was reduced by approximately 98%. In addition, the heat treatment had a negative effect on the wear rate of the coated sample, and a 21% reduction was achieved in the wear rate. Figure 5.27 proves that the wear resistance of the heat-treated nanocomposite coating is higher than all the other samples. This highest wear resistance under multiple passes with the abrasive ball is a direct result of achieving higher hardness compared to other specimens. On the other hand, Algül et al. [108], in their research, examined how the wear rates changed with graphene reinforcement and reported that graphene reduces wear loss as in the results of this study. As mentioned in the Raman Spectroscopy results, the graphene reinforced nanocomposite coating has a solid-lubricating effect, so the reason for the increase in wear resistance is that graphene prevents direct contact between the abrasive ball and the nickel matrix.

CHAPTER 6

CONCLUSION

In this thesis, graphene-reinforced nickel phosphorus (Gr-Ni-P) nanocomposite coatings were successfully produced on Ti-6Al-4V substrates using the electroless coating method. The nanocomposite coatings produced with the use of optimum parameters were subjected to abrasion, and heat treatment and their microstructure and tribological properties were examined by various tests. The produced coatings were analyzed using the SEM, the XRD, and the XPS methods.

As originally targeted in this study, Gr-Ni-P coating improved the tribological properties of the titanium alloy and increased its wear resistance. The following results were obtained:

1. The Gr-Ni-P coating was successful. The microstructure of titanium alloy turned into a nodular structure. In addition, a 12.47 μm coating thickness was achieved on titanium alloy substrates.
2. With the coating process, the substrate surface turned into an amorphous structure. Then the phase transformation occurred with the effect of heat treatment on the crystal structure, the structure of the coating turned into a crystal structure again.
3. Using the Debye-Scherrer equation, the average crystallite sizes were calculated with the data obtained from the XRD analysis. The value was 38.52 nm for the uncoated sample and 30.98 nm for the coated sample.
4. In the XPS analysis, binding energies of approximately 284 eV and 853 eV were obtained, revealing the presence of Gr and Ni in the coating structure, respectively.
5. The Raman spectrometer analyses revealed that the lubricating property increased with the effect of the heat treatment. In addition, the heat generated by the wear also increased the lubricating properties.

6. The microhardness results revealed that hardness was the highest in the coated sample with the heat treatment.
7. The microstructure and wear scar widths of the wear scars were investigated. It has been observed that heat treatment has a positive effect on wear in both the coated and the uncoated structures. The dominant wear mechanism is adhesive and abrasive in the uncoated samples, while delamination in the coated samples. It was observed that there was a higher degree of effect of wear in the uncoated samples. The lowest wear scar width was obtained in the heat-treated graphene-reinforced nanocomposite coating.
8. The EDS mapping analysis shows that a homogeneous deposition was obtained on the coating.
9. The wear rate of the Ti-6Al-4V substrate is approximately 98% higher than that of the heat-treated nanocomposite coating. The highest wear resistance has been obtained in the heat-treated nanocomposite coating.

REFERENCES

[1] Eker A. Metal Matrisli Kompozitler ve Üretim Yöntemleri, Master Dissertation, Yıldız Teknik Üniversitesi. 2010

[2] Kaya, B. Nano Kompozit Kaplama, Master Dissertation, İstanbul Teknik Üniversitesi. 2005

[3] Mindivan F., Aydın K., and Mindivan H., Elektrolitik Kaplanmış Nikel/Grafen Kompozit Kaplamaların Üretimi ve Karakterizasyonu, Nevşehir Bilim ve Teknoloji Dergisi, *8*, 29-36, 2019

[4] Gao X, Yue H, Guo E., Mechanical properties and thermal conductivity of graphene reinforced copper matrix composites, Powder Technology, *7*, 301:601, 2016

[5] Imam, M.A., and Fraker, A.C., Titanium alloys as implant materials, in medical applications of titanium and it's alloys, Philadelphia, 1996

[6] Nishida, Y. "Introduction to Metal Matrix Composites", Springer Japan, 2013

[7] Agarwal, B.D., Broutman, L.J., Analysis and performance of fiber composites, John Wiley & Sons, A.B.D., 1980

[8] Kalemtaş, A., Metal matrisli kompozitlere genel bir bakış, Putech&Composites, 22, 18-30, 2014

[9] Ölmez, C., Grafit/Al2O3 Takviyeli Alüminyum Metal Matris Kompozitlerin Frezelenmesinde Takım Aşınmalarının İncelenmesi, Master Dissertation, İnönü Üniversitesi. 2020

[10] Hull, D., An Introduction to composite materials, Cambridge University Pres, England, 71-79, 1992

[11] Kaczmar, J. W., Pietrzak, K., Włosiński, W., The production and application of metal matrix composite materials. Journal of materials processing technology, 106(1-3), 58-6, 2000

[12] Takei, T., Hatta, H., Taya, M., Thermal expansion behaviour of particulate–filled composites 1: Single and multi–reinforcing phases, Mat. Sci. Eng. A, A131, 133- 143, 1991

[13] Couturier, R., Ducret, D., Merle, P., Disson, J.P., Joubert, P., Elaboration and characterization of a metal matrix composite: Al/AlN, J. Eur. Ceram. Soc., *17*, 1861–1866, 1997

[14] Daniel, B.S.S., Murthy, V.S.R., Murty, G.S., Metal– ceramic composites via in–situ methods, J. Mater. Process. Technol., *68*, 132–155, 1997

[15] Hou, Q.H.M., Koczak, M., Feasibility of aluminum nitride formation in aluminum alloys, Mater. Sci. Eng. A, 195, 121, 1995

[16] Kornmann, X., Polimer Layered Silcate Nanocomposites, EMP, Dübendorf, Switzerland, 44-56, 2001

[17] C. ha, S. I., Kim, K. T, Arshad, S. N., Mo, C. B., Hong, S. H., Extraordinary Strengthening Effect of Carbon Nanotubes in Metal-Matrix Nanocomposites Processed by Molecular-Level Mixing, Advanced Materials, *17*, 11, 1377–1381, 2005

[18] Kaya, B. Nano Kompozit Kaplama, Master Dissertation, İstanbul Teknik Üniversitesi. 2005

[19] Karslıoğlu, R. Karbon Nanotüp Takviyeli Nikel-Kobalt Kaplamaların Geliştirilmesi, doctoral dissertation, Sakarya Üniversitesi. 2014

[20] Goh, C. S., Wei, J., Lee L. C., Gupta, M., Development of novel carbon nanotube reinforced magnesium nanocomposites using the powder metallurgy technique, Nanotechnology, 17(1):7,2006

[21] Kallip K., Babu N.K., AlOgab K.A., Microstructure and mechanical properties of near net shaped aluminium/alumina nanocomposites fabricated by powder metallurgy, J Alloys Compd, 714:133-43, 2017

[22] Chen,W., Yang, T., Dong, L.,Elmasry, A., Song, J., Advances in graphene reinforced metal matrix nanocomposites: Mechanisms, processing, modelling, properties and applications, Nanotechnology and Precision Engineering, *3*,189–210, 2020

[23] Lima C.R.C., Guilemany J.M., Adhesion improvements of Thermal Barrier Coatings with HVOF thermally sprayed bond coats, Surf Coat Technol, 201(8):4694-701, 2017

[24] Yin S., Zhang Z., Ekoi, E.J., Wang, J.J., Dowling, D.P., Nicolosi, V., Lupoi, R., Novel cold spray for fabricating graphene-reinforced metal matrix composites, Mater. Lett. *196*, 172-175, 2017

[25] Champagne V.K., Helfritch D., Leyman P., Grendahl S., Klotz B., Interface material mixing formed by the deposition of copper on aluminum by means of the cold spray process, J Therm Spray Technol, *14*(3):330–335, 2005

[26] Ajayan P.M., Schadler L.S., Braun P.V., Nanocomposite science and technology, Weinheim, Wiley-VCH, 2003

[27] Ebrahimi,F, Bourne, G.R., Mechanical properties of nanocrystalline nickel produced by electrodeposition, Nanostructured Mater. 11 ,343-350 ,1999

[28] Tao, S., Li, D.Y., Tribological, mechanical and electrochemical properties of nanocrystalline copper deposits produced by pulse electrodeposition Nanotechnology., 17, Dec,2005

[29] Al-Falahi, L., Graphene Reinforced Silver Nanocomposite by Electrodeposition for Electrical Contact Materials, Master Dissertation, Yıldırım Beyazıt Üniversitesi, 2018

[30] Zhang, B., Impact Parameters and Deposition Rate, Amorphous and Nano Alloys Electroless Depositions, 323-381, 2016

[31] Maharana, H., Surface Modification of Copper by Electro-codeposition, National Institute of Technology, Rourkela, 2017

[32] Brenner A, Riddell GE. Inventors: Nickel plating by chemical reduction. US2532282; 1950

[33] Schlesinger M, "Modern electroplating" 5th edn. John Wiley & Sons Inc, 2010

[34] Riedel, W., Electroless Nickel Plating, Metals Park, Ohio: ASM International, 1991

[35] Çakır, A. F. Akımsız Nikel Kaplamalar ve Uygulamaları, Yüzey İşlemler, 98, 76-83, 2001

[36] Shahin, G. E., Comparison of Electroless Nickel & Functional Chromium. In SUR/FIN 2009 Technical Conference. Louisville, KY, USA, 2009

[37] Zhang, Q., Wu, M., and Zhao, W., Electroless nickel plating on hollow glass microspheres, surface & coatings technology, 2005

[38] Prasanta S., Suman K.D., Tribology of electroless nickel coatings – A review, Material and Design 32, 4, 1760-1775, 2011

[39] Chen, B.H., Hong, L., Ma, Y., Ko, T.M., Effects of Surfactants in an Electroless Nickel-Plating Bath on the Properties of Ni-P Alloy Deposits, Ind. Eng. Chem. Res., 2668-2678, 2002

[40] Gawrilov, G.G., "Chemical (Electroless) Nickel Plating." Redhill, UK: Portcullis Press, 1979

[41] Barnstead, M. *Electroless Nickel Plating*, Retrieved 25 February 25, 2022, from Electroless Nickel Plating | Products Finishing (pfonline.com). 2011

[42] Dadvand, N., Investigation of the Corrosion Behaviour of Electroless Nickel-Boron and Nickel-Phosphorus Coatings in Basic Solutions, Doctoral Thesis, Metallurgical Engineering at Dalhousie University, Halifax, Nova Scotia, 2002

[43] Mallory, G. O. and Hadju J. B. , Electroless plating: fundamentals and applications, American Electroplaters and Surface Finishers Society, New York, USA ,1990

[44] Barnstead, M. and Morcos, B., Electroless Nickel Plating, Products Finishing Directory, MacDermid, Inc. CT, USA 2010

[45] Martyak, N., McCaskie, J., Speciation in electroless nickel solutions, Plating and Surface Finishing, 83, 62–66, 1996

[46] Wang, X. C., Cai, W. Bin, Wang, W. J., Liu, H.T., Yu, Z.Z., Effects of ligands on electroless Ni–P alloy plating from alkaline citrate–ammonia solution, Surface and Coatings Technology, 168, 300–306, 2003

[47] Baudrand, D.W., Electroless Nickel Plating. In ASM Metals Handbook Volume 5 - Surface Engineering, 954–1009, 1994

[48] Palaniappa, M., Seshadri, S.K., Friction and wear behavior of electroless Ni–P and Ni–W–P alloy coatings, Wear, 265, 5, 735-740, 2008

[49] Sotskaya N.V., Ryabinina E.I., Kravchenko T.A., Shikhaliev K.S., Kinetics of electroless plating of Ni–P alloys with organic additives containing –S–S-fragments, Prot. Met., 39, 3, 250-254, 2003

[50] Shusheng Z., Han K., Cheng L., The effect of SiC particles added in electroless Ni–P plating solution on the properties of composite coatings, Surf Coat Technol, 202, 12, 2807-2812, 2008

[51] Osifuye CO., Electrochemical corrosion resistance of electroless plated mild steel, Master Dissertation, Department of Chemical, Metallurgical & Materials Engineering, Tshwane University of Technology, Pretoria, South A, 2014

[52] Difference between elecro and electroless plating. (n.d). Retrieved from https://www.classicplating.com/En.html

[53] Şahin, F. Akımsız Nikel- Fosfor Kaplanan Ti-6Al-4V Alaşımının Aşınma Davranışının İncelenmesi, Master Dissertation, Eskişehir Osmangazi Üniversitesi, Turkey, 2016

[54] Krishnan, K. H., S. John, K. N. Srinivasan, J. Praveen, M. Ganesan and P. M. Kavimani, An overall aspect of electroless NiP depositions - A review article, Metallurgical and Materials Transactions A 37 (6): 1917–1926, 2006

[55] Cheng, Y. H., Zou, Y., Cheng, L., Liu, W., Effect of complexing agents on properties of electroless Ni-P deposits. Materials Science & Technology, 24, 4, 457-460, 2008

[56] Taheri, R., Evaluation of electroless nickel-phosphorus (electroless nickel) coatings, PhD thesis, University of Saskatchewan, 2003

[57] Fields W., Zickearff J.R., Electroless, Publication of ASM committee on ENplatting, 1984

[58] Reidel W., "Electroless Nickel plating", ASN International, 1997

[59] Halimoğlu, Ş. Sodyum borhidrür indirgeyicisiyle akımsız metal kaplamaların incelenmesi, Master Dissertation, İstanbul Teknik Üniversitesi. 1998

[60] Taheri, R. Evaluation of electroless nickel-phosphorus (electroless nickel) coatings, PhD thesis, University of Saskatchewan, 2003

[61] Davis, R.J. "Nickel, cobalt and their alloys "USA: ASM International, 2000

[62] Kanani, N., Chemische Vernicklung: Nickel-Phosphor-Schichten Herstellung-Eigenschaften -Anwendungen. Germany: Leuze, 2007

[63] Parkinson, R. Properties and applications of electroless nickel, Nickel Development Institute. NiDL Technical Series No. 10081, 1997

[64] Keong, K. G., Sha, W., Malinov, S., Hardness evolution of electroless nickel–phosphorus deposits with thermal processing, Surface and Coatings Technology 168(2): 263–274, 2003

[65] Delaunois F., Vitry V., Bonin L., Electroless Nickel Plating Fundamentals to Applications, CRC Press, 2020

[66] Duncan, R. N., Metallurgical structure of electroless nickel deposit, plating and surface finishing, Plating and Surface Finishing 83(11), 65–69, 1996

[67] Hino, M., Murakami, K., Mitooka, Y., Muraoka, K., Furukawa R., Kanadani, T., Effect of zincate treatment on adhesion of electroless NiP coating onto various aluminum alloys, Materials Transactions 50(9), 2235–2241, 2009

[68] Zahid, R., Masjuki, H. H., Varman, M., Mufti, R. A., Kalam M. A., Gulzar, M., Effect of lubricant formulations on the tribological performance of self-mated doped DLC contacts: A review, Tribology Letters 58(2): 32. 2015

[69] Agarwala, R.C., Agarwala V., Electroless Alloy/Composite Coatings: A Review, Sadhana, 28, 475-493, 2003

[70] Yeğen, F.I., Grafen Şeritler. Master Dissertation, Ankara Üniversitesi, 2011

[71] Tiwari, S.K., Kumar, V., Huczko, A., Oraon, R., Adhikari, A.D., Nayak, G.C., Magical Allotropes of Carbon: Prospects and Applications, Crit. Rev. Solid State Mater. Sci., 41, 4, 257–317, 2016

[72] Altıntaş, A. Alümina ve Grafen Tozlarının Vakum Altında Yüksek Frekanslı İndüksiyon Sistemiyle Sinterlenmesi, Master Dissertation, Celal Bayar Üniversitesi, 2017

[73] Baykal, M. A. Karbon Grafen Şeritlerdeki Kusurların Analizi. Master Dissertation, Gebze Teknik Üniversitesi, 2016

[74] Şenel, M. C., Gürbüz, M., Koç, E. Grafen takviyeli alüminyum matrisli yeni nesil kompozitler, Mühendis ve Makina Dergisi, 56, 669, 36 – 47. 2015

[75] Raccichini, R., Varzi, A., Passerini, S., Scrosati, B., The role of graphene for electrochemical energy storage, Nat. Mater., *14*, 3, 271–279, 2015

[76] Peters, M., Hemptenmacher, J., Kumpfert J., Leyens, C. (Ed.),” Structure and Properties of Titanium and Titanium Alloys”, ISBN: 3-527-30534-3, Wiley VCH, 2003

[77] Titanium (n.d). Retrieved from https://tr.wikipedia.org/wiki/Titanyum

[78] Bardes, B.P., Metals Handbook, Volume 3 Properties and Selection: Stainless Steels, Tool Materials and Species-Purpose Metals Titanium and Titanium Alloys, 352, 9th ed., ASM, 1980

[79] Tanrıöver, K., Taşçı, A., Titanyum Alaşımlarının Isıl İşlemi, Makine Magazin, 58, 1997

[80] Brunette, D.M., Tengwall, B., Textor, M., Thomsen, P., Titanium in Medicine, Springer Verlag, Heidelberg. 2001

[81] Long, M. and Rack, H.J., Titanium alloys in total joint replacement- a materials science perspective, Biomaterials, 19, 1621-1639, 1998

[82] Gerhard W., Rodney B., Collings E.W., "Materials Properties Handbook - Titanium Alloys" ASM International, 2007

[83] Ensaroğlu, C., Çakır, M.C., Titanyum ve alaşımlarının işlenebilirlik etüdü,Mühendis ve Makina 546, 46, 2005

[84] Akagündüz, E. Isıl işlem görmüş Ti6Al4V alaşımının yüzey özelliklerinin mikroyapı ve yüzey çizilme dayanımları açısından incelenmesi, Master Dissertation, Gebze Yüksek Teknoloji Enstitüsü Mühendislik ve Fen Bilimleri Enstitüsü, 2008

[85] Işık B., Kentli A., The prediction of surface temperature in drilling of Ti6Al4V, Archives of metallurgy and materials, 2014

[86] Cengiz, Ö. Grafen Takviyeli magnzyum kompozitlerin üretimi ve karakterizasyonu, Master Dissertation, 19 Mayıs Universitesi, Samsun, 2018

[87] Hu Q.-H., Wang X.-T., Chen H., Wang Z.-F., Synthesis of Ni/ graphene sheets by an electroless Ni-plating method, New Carbon Mater., 27, (1), 35–41. 2012

[88] Kumar C. M. P., Venkatesha T. V., Shabadi R., Preparation and corrosion behavior of Ni and Ni–graphene composite coatings, Mater. Res. Bull, 48, (4), 1477–1483, 2013

[89] Kuang D., Xu L., Liu L., Hu W., Wu Y., Graphene-nickel composites, Applied Surface Science, 273, 484-490, 2013

[90] Yu, Q., Zhou t., Jiang Y., Yan X., An Z., Wang X., Zhang D., Ono T., Preparation of graphene-enhanced nickel-phosphorus composite films by ultrasonic-assisted electroless plating, Aplied Surface Science, 435, 617-625, 2018

[91] Mindivan F., Aydın K., Mindivan H., Elektrolitik kaplanmış Nikel/Grafen Kompozit kaplamaların üretimi ve karakterizasyonu, Nevşehir Bilim Ve Teknoloji Dergisi, 8, 29-36, 2019

[92] Engelhard M.H., Droubay T.C., Du Y., X-Ray Photoelectron Spectroscopy Applications, Encyclopedia of Spectroscopy and Spectrometry, 3, 716-724, 2017

[93] Tane sınırları (n.d). Retrieved February 25, 2022, from https://muhendishane.org/kutuphane/malzemelerin-mekanik-davranisi/tane-sinirlari/

[94] Zhang W., Li Y., Zeng X., Peng S., Synergetic effect of metal nickel and graphene as a cocatalyst for enhanced photocatalytic hydrogen evolution via dye sensitization. Sci Rep 5,10589, 2015

[95] Johra F.T., Lee J.W., Jung W.G., Facile and safe graphene preparation on solution-based platform, J Ind Eng Chem, 20, 2883–2887, 2014

[96] Binding energy of graphene (n.d). Retrieved February 25, 2022, from https://www.jp.xpssimplified.com/elements/carbon.php

[97] Xu Z. Q., Zhang, X., Shi, W., Zhai, K., Yang, Tribological properties of TiAl matrix self-lubricating composites containing multilayer graphene and Ti3SiC2 at high temperatures, Tribol. Trans, 58, 1131–1141, 2015

[98] Brunelli, K., Dabala, M., Magrini, M., Diffusion treatment of Ni–B coatings by induction heating to harden the surface of Ti–6Al–4V alloy, Materials Chemistry and Physics, 115, 467-472, 2009

[99] Yang, Y.Y., Preparation of Ni-Co Alloy Foils by Electrodeposition, Advances in Chemical Engineering and Science, 1(2):27–32, 2011

[100] Ferrari, A.C., Meyer, J.C., Scardaci, V., Casiraghi, C., Lazzeri, M., Mauri, F., Piscanec, S., Jiang, D., Novoselov, K.S., Roth, S., et al. Raman spectrum of graphene and graphene layers. Phys. Rev. Lett. 97, 2006

[101] Ferrari, A.C., Raman spectroscopy of graphene and graphite: Disorder, electron-phonon coupling, doping and nonadiabatic effects. Solid State Commun., 143, 47–57, 2007

[102] Vidano, R.P., Fischbach, D.B., Willis, L.J., Loehr, T.M. Observation of raman band shifting with excitation wavelength for carbons and graphites. Solid State Commun. 39, 341–344, 1981

[103] Su, F., Liu, C., Guo, J., Huang, P., Characterizations of nanocrystalline Co and Co/MWCNT coatings produced by different electrodeposition techniques. Surface and Coatings Technology, 217:94-104, 2013

[104] Scherrer equation (n.d). Retrieved February 25, 2022, from https://en.wikipedia.org/wiki/Scherrer_equation

[105] Meshram, A.P., Kumar, M.K.P., Srivastava, C., Enhancement in the corrosion resistance behaviour of amorphous Ni-P coatings by incorporation of graphene, Diamond & Related Materials, 105,107795, 2020

[106] Yasin, G., Khan, M.A., Arif, M., Shakeel, M., Hassan, T.M., Khan, W.Q., Korai, R.M., Abbas, Z., Zuo, Y., Synthesis of spheres-like Ni/graphene nanocomposite as an efficient anti-corrosive coating; effect of graphene content on its morphology and mechanical properties, Alloy and Compounds, 755, 79-88, 2018

[107]Triboloji (n.d) Retrieved February 25, 2022, from https://tr.wikipedia.org/wiki/Triboloji

[108] Algul H., Tokur, M., Ozcan, S., Uysal, M., Cetinkaya, T., Akbulut, H., Alp A., The effect of graphene content and sliding speed on the wear mechanism of nickel–graphene nanocomposites, Applied Surface Science, 359, 340-348, 2015

[109] Sohrabi, A., Dolati, A., Ghorbani, M., Monfared, A., Stroeve, P., Nanomechanical Properties of Functionally Graded Composite Coatings: Electrodeposited Nickel Dispersions Containing Silicon Micro and Nanoparticles, Journal of Metarials Processing Technology, 121 (3), 497-505, 2010

[110] Shi, L., Sun, C., Gao, P., Zhou, F., Liu, W., Mechanical properties and wear and corrosion resistance of electrodeposited Ni–Co/SiC nanocomposite coating, Applied Surface Science, 252(10), 3591–3599, 2006

[111] Rana, A.R.K., Farhat Z., Preparation and tribological characterization of graphene incorporated electroless Ni-P composite coatings, Surface & Coatings Technology, 369, 334-346, 2019

[112] B.M. Praveen, T.V. Venkatesha, J. Electrodeposition and properties of Zn–Ni–CNT composite coatings, Alloys Compd. 482, 53-57, 2009

[113] Özdin, K. Alüminyum Esaslı SiC Takviyeli Kompozitlerin Üretimi ve Aşınma Özelliklerinin Araştırılması, Doctoral Dissertation, Gazi Üniversitesi Fen Bilimleri Enstitüsü, Turkey, 2006

[114] Karabaşoğlu, M., Aşınma Deney Cihazı Tasarımı ve İmalatı, Master Dissertation, Sakarya Üniversitesi Fen Bilimleri Enstitüsü, Sakarya, 10, 14, 16-18, 29-38, 2008

[115] Aydın, K. Improvement of surface properties of low carbon steel with graphene content composite coating, Master Dissertation, Seyh Edebalı University, Turkey, 2019

[116] Zeng, Q., Erdemir, A., Eryılmaz, O., Ultralow Friction of ZrO2 Ball Sliding against DLC Films under Various Environments, Applied Sciences, 7, 938, 2017

[117] Sharma, S., Sangal, S., Monda K., On the optical microscopic method for the determination of ball-on-flatsurface linearly reciprocating sliding wear volume, Wear, 300, 82-89, 2013

CURRICULUM VITAE

PERSONAL INFORMATION

Name Surname : Hatice GÜNDÜZ

EDUCATION

High School : Demetevler Mimar Sinan Lisesi (2008-2012)
Bachelor's degree : Ankara Yıldırım Beyazıt University (2013-2018)
Master's degree : Ankara Yıldırım Beyazıt University (2018-2022)

TOPIC OF INTEREST

- Nanotechnology
- Coatings

PUBLICATION

Hatice Gündüz, Fahrettin Öztürk, Ramazan Karslıoğlu, Effect of Graphene Addition and Heat Treatment on Microstructure and Tribological Properties of Ni-P Electroless Coating, VI. International Scientific and Vocational Studies Congress – Engineering (BILMES EN 2021), 23-26 December 2021, TURKEY,